ABRUPT CLIMATE SHIFTS IN THE WESTERN TROPICAL TO SUBTROPICAL ATLANTIC REGION DURING THE LAST GLACIAL

Dissertation zur Erlangung des
Doktorgrades der Naturwissenschaften
am Fachbereich Geowissenschaften
der Universität Bremen

vorgelegt von

Gerrit Heil

Gutachter:
Prof. Dr. Gerold Wefer
Prof. Dr. Michael Schulz

Bremen, März 2006

“Don't believe anybody or anything, but always challenge existing knowledge – that's science.”

(Wolfgang van Berk)

Acknowledgements

First of all, I want to thank the Lord for giving me ideas, motivation and tenacy for this thesis and for guiding the path. I am on the quest.

The basic idea for this thesis was provided by my primary PhD supervisor Dr. Helge Arz. This work benefited greatly from suggestions by and discussions with Helge and his scientific partner Dr. Frank Lamy. Many thanks to both of you for helping improving this thesis.

Prof. Dr. Gerold Wefer, my main supervisor in Bremen, provided short, precise suggestions for improving the manuscripts. I am grateful for his support and his review of this thesis as well as the extraordinary training possibilities and the internationality at the RCOM. Furthermore, I thank Prof. Dr. Michael Schulz for providing the second review of this thesis and various “shipboard modeling discussions”.

A special word of thanks goes to Prof. Dr. Peter deMenocal, who introduced me into Mg/Ca thermometry and provided great support with discussions and personal issues during my stays at Lamont – and probably spent the biggest burger I ever had.

There are many people from the various working groups at the RCOM, Lamont, the GFZ and from the Gary Comer Foundation who helped improving this thesis and life beyond science. Many thanks to all of you, especially to Ulrich Alt-Epping, Dr. Steve Barker, Jop Brijker, Cristiano Chiessi, Dr. Thomas Felis, Phillip Franke, Dr. Henning Kuhnert, Iris Kristen, Olga Kwieczin, Dr. Helen McGregor, Dr. Stefan Mulitza, Dr. André Paul, Dr. Carsten Rühlemann, Regine daRocha, Leopold Peña, Rik Tjallingii, Xianfeng Wang and the Lamont soccer team. Furthermore, thanks to many people of the scientific community for providing stimulating ideas during various conferences and workshops as well as for providing datasets.

Very special thanks to everybody who helped with labwork during this thesis. This includes Martha Bryan, Dr. Barbara Donner, Dr. Walter Hale, Dr. Camille Levi, Dr. Monika Segl and my famous HiWis Filiz Afsar, Regine daRocha, Alex Engeler, Daniela Hitschel, Ulrike Marx, Friederike Schmidt-Schierhorn and Viola Stratmann.

The most important support came from my wife, who suffered many months and nights of loneliness while I was working on this thesis somewhere in the world. Thanks for giving me heart, room, structure and time – and for some urgent labwork. Many thanks also to all my other family members for supporting this thesis in many ways, especially to my parents, my grandmother and my brother.

This work was generously funded by the Gary Comer Foundation. Many thanks to Gary for trusting in all of us and to all Comer mentors and fellows for thriving conferences and discussions.

Table of contents

Acknowledgements v

1 Abstract 1

2 Introduction 5

2.1 Motivation and Scientific Objectives 5

2.2 Study area 8

2.2.1 Geographic and Geologic Setting 8

2.2.2 Oceanographic setting 11

2.2.3 Modern Climate 15

2.2.4 Paleoclimate 18

2.3 References Chapter 2 21

3 Material and Methods 25

3.1 Material and Overview of Methods 25

3.2 Radiocarbon dating 26

3.3 Stable Oxygen Isotopes 29

3.4 Stable Carbon Isotopes 31

3.5 Mg/Ca Ratios 35

3.6 X-ray Fluorescence Spectroscopy 37

3.7 References Chapter 3 38

4 Manuscripts 43

4.1 Outline of Manuscripts 43

4.2 Manuscript 1: Forcing of tropical South American precipitation during the last 63,000 years 45

4.3 Manuscript 2: Last Glacial millennial-scale changes in Atlantic Thermohaline Circulation and Northeast Brazilian precipitation 57

4.4 Manuscript 3: Extent of high northern latitude temperature forcing on millennial-scale precipitation changes in eastern South America 85

5 Discussion 109

5.1 References Chapter 5 115

6 Conclusions and Outlook 117

6.1 Conclusions 117

6.2 Outlook 118

6.3 References Chapter 6 121

1 Abstract

Millennial-scale climate oscillations of the last glacial hold great potential for analysing forcing and teleconnection mechanisms of global climate changes. These climate oscillations, called Dansgaard/Oeschger cycles, are primarily expressed as temperature variations in the high latitudes and as precipitation pattern changes in the tropics. Tropical precipitation pattern changes arise from shifts in the position of the Intertropical Convergence Zone, which are associated with hemispheric-wide reorganisations of the atmospheric circulation in the northern hemisphere. These, in turn, are driven by the pronounced millennial-scale temperature shifts in the high northern latitudes.

This study investigates the coupling mechanisms between high northern latitude temperature changes and shifts of the Intertropical Convergence Zone. Furthermore, it evaluates the impact of Intertropical Convergence Zone shifts on both the spatial extent of associated precipitation pattern changes and the amplitude of these precipitation shifts. As millennial-scale variations in high northern latitude temperatures are coupled to the rate of deep water production in the North Atlantic, this study also investigates the relation between changes in North Atlantic Deep Water production and shifts in tropical precipitation patterns.

This study is based on the analysis of marine sediment cores from the continental slope of the western tropical to subtropical South Atlantic off the East Brazilian coast. These archives provide proxy records of the hydroclimatic regime in Northeast to South Brazil and oceanographic conditions of the western tropical to subtropical South Atlantic during the last 74 kyrs. Proxies used in this endeavour include radiocarbon dating, foraminiferal stable isotope chemistry, magnesium-calcium thermometry and X-ray fluorescence spectroscopy. The results from the hydroclimatic proxy records have been combined with further tropical to subtropical South American precipitation records to evaluate the spatial extent of changes in hydroclimatic conditions.

The various South American precipitation records consistently indicate that the tropical South American climate system underwent significant millennial-scale reorganisations during the last glacial which were driven by shifts of the Intertropical Convergence Zone. The position of the Intertropical Convergence Zone, in turn, is dynamically coupled to variations in the meridional temperature gradient in the North Atlantic, which is primarily governed by high northern latitude temperature changes. Whereas the most prominent shifts of the Intertropical Convergence Zone occurred during special Dansgaard/Oeschger cycles known as Heinrich events, which are associated with massive temperature changes and pronounced decreases in

deep water production in the high-latitude North Atlantic, significant shifts of the Intertropical Convergence Zone can also be observed during other Dansgaard/Oeschger cycles.

The impact of Dansgaard/Oeschger cycle and Heinrich event high northern latitude temperature variations on the hydroclimatic regime of the South American tropics differs both in the spatial extent of Intertropical Convergence Zone shifts and corresponding precipitation pattern changes as well as in the amplitude of precipitation variations. Due to larger changes in the North Atlantic's meridional temperature gradient, Heinrich events are associated with more pronounced Intertropical Convergence Zone shifts than Dansgaard/Oeschger cycles. Therefore, the amplitude of precipitation changes is larger during Heinrich events in tropical South America. The impact of Intertropical Convergence Zone shifts on precipitation patterns diminishes with distance from the Intertropical Convergence Zone, i.e. precipitation records from equatorial regions are dominated by millennial-scale variations, whereas these are subordinate to changes of orbital timescale in southern tropical to subtropical regions. Through coupling of Intertropical Convergence Zone shifts to other atmospheric circulation systems like e.g. the South American Summer Monsoon, however, millennial-scale variations are also transferred to the South American subtropics. The amplitude of millennial-scale subtropical South American precipitation changes, however, is very low and suggests the impact of Intertropical Convergence Zone shifts may be limited to the tropics and northernmost subtropics in South America.

Oceanographic conditions of the western tropical Atlantic show millennial-scale changes which are coincident with the observed shifts in tropical precipitation patterns. Sea surface temperatures of the western tropical Atlantic, e.g., show pronounced changes during Heinrich events. The direction of these temperature changes, however, is antithetic during different Heinrich events. This study therefore demonstrates that, in contrast to the modern dependency of tropical South American precipitation patterns on western tropical Atlantic sea surface temperatures on seasonal to interannual timescales, changes in tropical sea surface temperatures do not alter South American precipitation patterns significantly on millennial timescales. The impact of variations in tropical sea surface temperatures on the hydroclimatic regime of South America is rather subordinate to that of changes in the North Atlantic's meridional temperature gradient.

Deep ocean conditions of the western tropical Atlantic clearly show cyclic millennial-scale variations which are coincident with shifts in tropical South American precipitation patterns. These variations in deep ocean conditions reflect changes in deep water production in the

North Atlantic, which are well-known to be associated with Dansgaard/Oeschger temperature cycles in the high northern latitudes. As high northern latitude temperature variations are mainly responsible for changes in the North Atlantic's meridional temperature gradient, and this, in turn, governs the position of the Intertropical Convergence Zone, this study provides evidence that variations in North Atlantic Deep Water production may amplify millennial-scale shifts of tropical precipitation patterns. Furthermore, coincident changes in western tropical Atlantic deep ocean conditions and tropical precipitation patterns provide a stratigraphic validation of the coincidence of millennial-scale changes in high northern latitude temperatures and tropical precipitation patterns.

2 Introduction

2.1 Motivation and Scientific Objectives

Climate models predict significant climate changes probably induced by human civilization to occur in the 21st century (IPCC, 2001). A reliable prediction of future climate change including an assessment of anthropogenic impacts, however, requires a thorough understanding of natural climate variability in the past (Alverson and Oldfield, 2000). Special attention thereby is paid to millennial-scale climate changes (so-called Dansgaard/Oeschger cycles) that occurred during the last glacial and, at least in part, were associated with global variations in climatic conditions (Broecker, 2005). As climate variations generally were more pronounced during the last glacial than during the Holocene (Bond et al., 1997), Dansgaard/Oeschger cycles hold great potential to analyse mechanisms causing and transmitting climate change (Broecker, 2003).

Whereas millennial-scale climate variations have been reported from many sites in Greenland (e.g. Grootes and Stuiver, 1997), the high to mid latitude North Atlantic (e.g. Bard et al., 2000; Bond et al., 1993) and Antarctica (e.g. Bender et al., 1994), few millennial-scale climate records are available from the tropics. These generally show precipitation shifts coincident with pronounced millennial-scale temperature changes in the high northern latitudes, which occur during so-called Heinrich events (e.g. Arz et al., 1998; Schulz et al., 1998; Wang et al., 2001; Fig. 1). Whereas these precipitation changes are caused by movements of the Intertropical Convergence Zone (ITCZ, e.g. Peterson et al., 2000), it is unclear what provides the teleconnection between temperature variations in the high northern latitudes and shifts in the position of the ITCZ. One hypothesis suggests a direct coupling of temperature changes in the high northern latitudes to hemisphere-wide reorganisations of the atmospheric circulation (e.g. Cane and Clement, 1999). The second hypothesis proposes a linkage of reorganisations of the Atlantic's Thermohaline Circulation (THC), which are well-known to coincide with the millennial-scale temperature variations in the high latitude North Atlantic (e.g. Bond et al., 1993), to tropical sea surface temperatures (SST), which, in turn, should be coupled to the position of the ITCZ (Broecker, 2003).

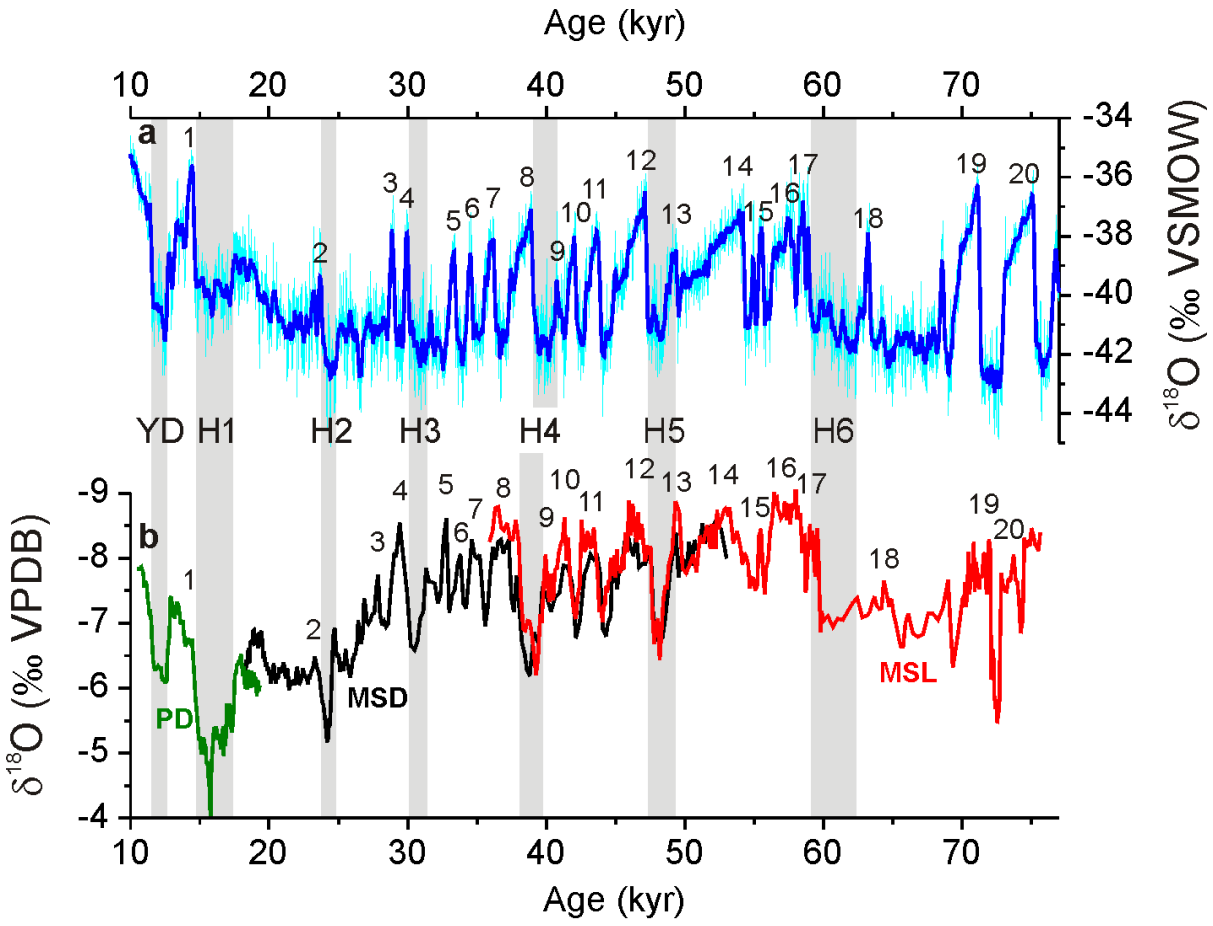

Figure 1: **a)** Temperature record from central Greenland (GRIP $\delta^{18}O$) compared to **b)** a monsoon intensity record from Southeast China (Hulu Cave stalagmite $\delta^{18}O$); Figure modified from Wang et al. (2001); data from Wang (2004)

The Hulu Cave record is composed of three single records from the stalagmites PD, MSD and MSL. Note the coincidence of temperature changes in Greenland and precipitation changes in China during Heinrich events (H1 to H6) and the Younger Dryas (YD) as well as during other Dansgaard/Oeschger cycles (numbers from 1 to 20 indicate Greenland Interstadials 1 to 20 in both the GRIP and the Hulu Cave record).

Besides the mechanisms underlying millennial-scale precipitation changes in the tropics, the spatial extent of these in the southern hemisphere is largely unknown. Some records from the northern tropics show precipitation shifts coincident with most of the millennial-scale temperature variations in the high northern latitudes (e.g. Peterson et al., 2000; Wang et al., 2001). In South America, precipitation records from equatorial Northeast Brazil indicate precipitation changes during Heinrich events and the Younger Dryas only (e.g. Arz et al., 1998; Behling et al., 2000; Fig. 2) and a precipitation record from South Chile (40°S) indicates precipitation shifts correlating to Antarctic rather than high northern latitude temperature changes (Kaiser et al., 2005).

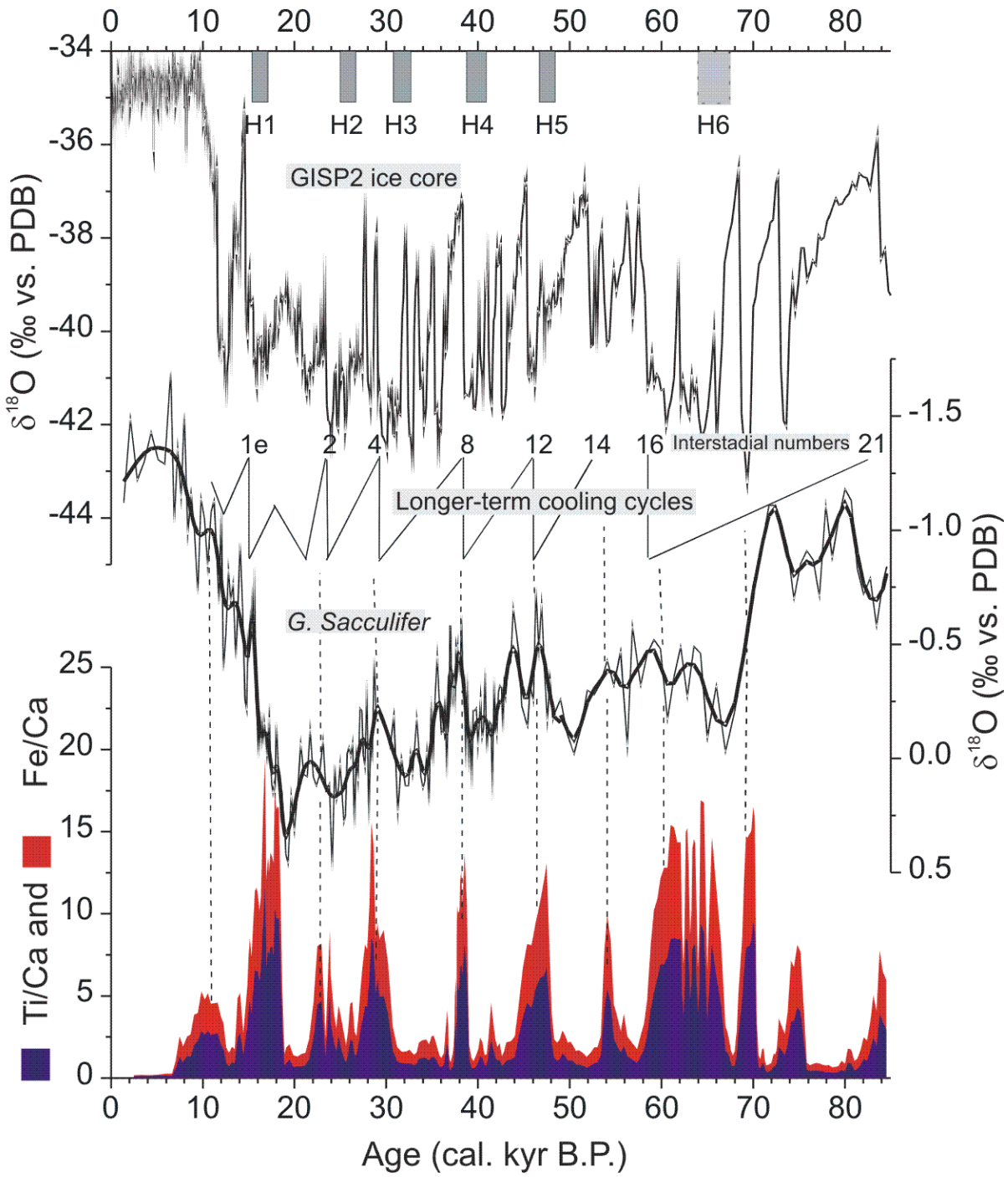

Figure 2: Comparison of the $\delta^{18}O$ record of the planktic foraminifer *Globigerinoides sacculifer* and the Ti/Ca and Fe/Ca record from the western tropical Atlantic twin sediment cores GeoB 3104/3912 to the $\delta^{18}O$ record from the Greenland ice core GISP2 (Grootes et al., 1993), the implied Greenland cooling cycles (Bond cycles, (Bond et al., 1993) and North Atlantic Heinrich events (age scale from Vidal et al., 1997; Figure from Arz et al., 1998)

Note the coincidence of wet events in Northeast Brazil (indicated by GeoB 3104/3912 Ti/Ca and Fe/Ca ratios) and cool periods in the North Atlantic during Heinrich events.

This study investigates the mechanisms causing millennial-scale precipitation changes in the South American tropics and the spatial extent of these changes. It is based on the analysis of marine sediment cores from the continental slope of the western tropical (off Northeast Brazil) and subtropical (off South Brazil) Atlantic. These provide centennial-resolution records of Northeast and South Brazilian precipitation, western tropical Atlantic SST and western tropical Atlantic deep ocean conditions. These records allow evaluating the mechanisms responsible for millennial-scale changes in tropical South American precipitation, tropical Atlantic SST and reorganisations of the Atlantic's THC. Furthermore, in comparison with other South American precipitation records they allow investigating the mechanisms governing the spatial extent of ITCZ shifts on millennial timescales.

2.2 Study area

2.2.1 Geographic and Geologic Setting

This study focuses on two regions, one of them comprising of the western tropical Atlantic and the adjacent Northeast Brazilian hinterland and the other one lying in the western subtropical South Atlantic and the adjacent South Brazilian hinterland (Fig. 3). The tropical investigation area extends from 4°S to 8°S and from 35°W to 41°W, whereas the subtropical one extends from 26°S to 28°S and from 46°W to 51°W. Additionally, this study includes a comparison to climate records from other sites in South America, which extend from 10°N to 28°S and from 77°W to 34°W, covering large parts of northern South America (Fig. 3). In this endeavour, a special focus lies on the East Brazilian coastal region and the adjacent western South Atlantic between 4°S and 28°S.

Geographically, South America can be subdivided in five main regions. Running from the southernmost to the northernmost tip of the continent, the Andes form its western margin. With 6963 m height, the Argentinean mountain Aconcagua forms the highest point of the Andes. There are two other main mountain systems in South America, the Guiana Highlands in the North (highest point: Pico da Neblina, 2994 m above sea level) and the extensive Brazilian Highlands in the East (highest point: Pico da Bandeira, 2890 m above sea level). The areas in between these mountain systems consist of the extensive, relatively flat River Basins of the Orinoco, the Amazon and the Paraguay/Paraná River system.

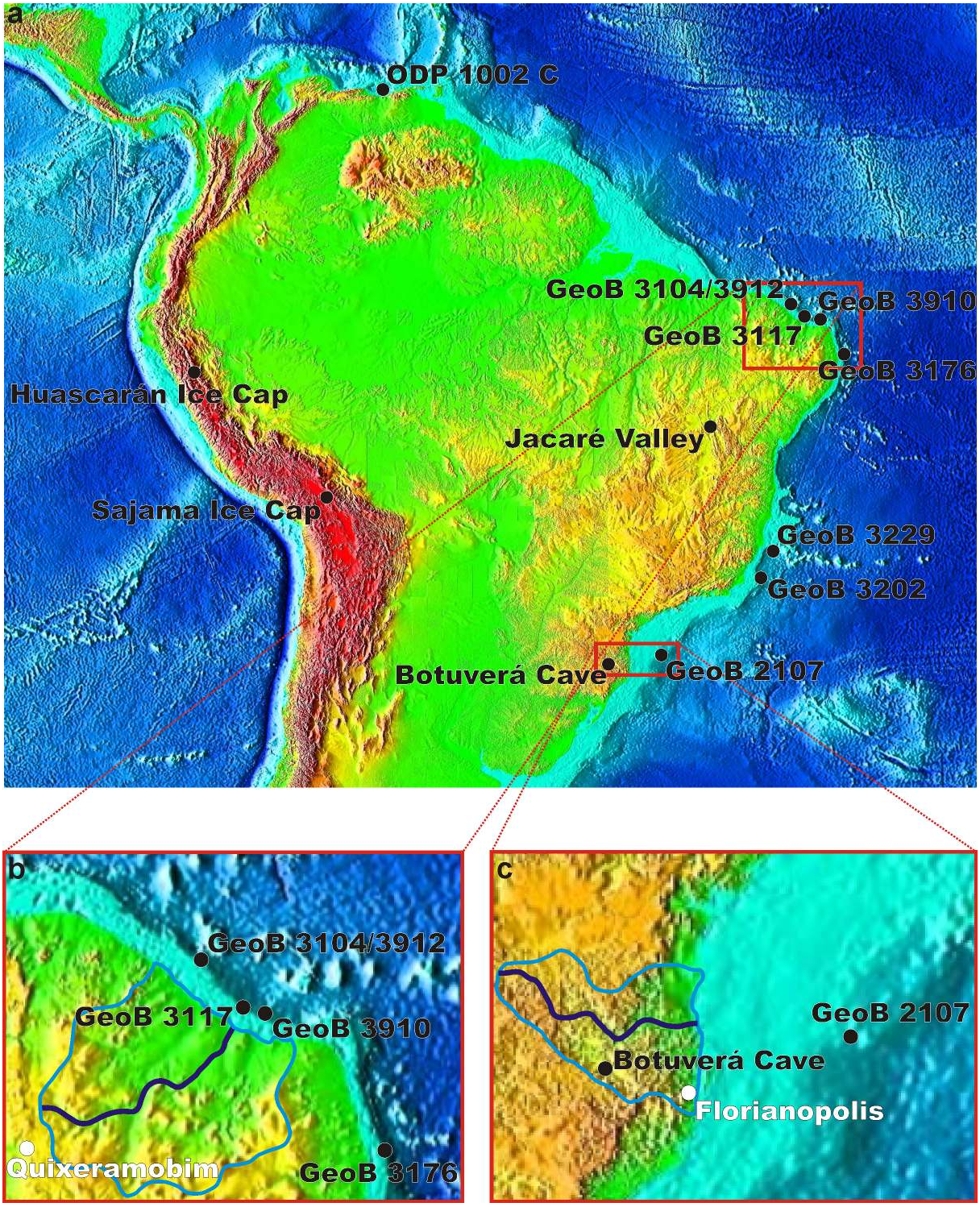

Figure 3: **a)** Geographic setting of South American records used in this thesis (red boxes indicate focus investigation areas); **b)** closeup of the Northeast Brazilian focus investigation area showing climate records and the catchment area of the Rio Piranhas, which drains the area; **c)** closeup of the South Brazilian focus investigation area showing climate records and the catchment area of the Rio Itajaí, which drains the area

Note the location of the climate stations Quixeramobim and Florianopolis, which are described in Fig. 7.

The terrestrial parts of the two focus investigation areas are situated at the northeastern and southern end of the Brazilian Highlands, respectively. The continental hinterland of the northern area is formed by the catchment area of the Rio Piranhas, which drains parts of the Northeast Brazilian states Ceará, Paraiba and Rio Grande do Norte (Fig. 3b). To the West, South and Southeast, it is confined by mountain chains of the Brazilian Highlands whereas it abuts on the Atlantic Ocean to the Northeast.

The continental hinterland of the southern focus investigation area is formed by the catchment area of the Rio Itajaí, which drains a large part of the South Brazilian State of Santa Catarina (Fig. 3c). To the west, the catchment area of the Rio Itajaí is confined by the Planaltos Residuais Sertanejos, which is the main mountain chain of the Brazilian Highlands in South Brazil. The northern and southern borders of this catchment area are formed by smaller mountain chains, whereas the Atlantic lies at its eastern margin.

The geology of the Brazilian Highlands is dominated by a Proterozoic to Paleozoic crystalline basement which is partly covered by Palaeozoic to Cenozoic sedimentary and volcanic rocks. The basement primarily consists of amphibolite to granulite facies metamorphics, granitoids, basalts and green schist facies metamorphics (Schobbenhaus et al., 1995). Phanerozoic sedimentary and volcanic coverings mainly include sandstones (often arenitic), claystones and basalts (Schobbenhaus et al., 1995).

The geologic setting of the two focus investigation areas resembles that of the Brazilian Highlands. The southern part of the catchment area of the Rio Piranhas is dominated by Proterozoic granitoids and gneisses and offers two small deposits of Cretaceous sandy conglomerates (Schobbenhaus et al., 1995). In the northern part of the catchment area, the granitoids and gneisses are covered by Cretaceous to Tertiary arenitic sandstones and conglomerates (Schobbenhaus et al., 1995). Fluvial and near-shore areas are covered by Holocene sands (Schobbenhaus et al., 1995). There are no significant deposits of carbonaceous material in the Rio Piranhas catchment area.

The lowlands and the coastal mountain chains of the Rio Itajaí's catchment area are made up by Proterozoic granitoids and silt- to sandstones which are covered by siliceous sands in the fluvial and near-shore areas (Rachwal and Curcio, 1994; Schobbenhaus et al., 1995). The mountain chains in the western part of the catchment area consist of Carboniferous to Permian sand- to siltstones and cherts with small limestone deposits (Schobbenhaus et al., 1995). Altogether, the catchment area of the Rio Itajaí is mainly made up by siliceous material and does not contain significant amounts of carbonaceous material.

2.2.2 Oceanographic setting

Between 3 and 16°S as well as 20 and 23°S, the western margin of the Atlantic ocean is characterized by a shallow (50 to 100 m deep) and relatively narrow shelf (30 to 50 km wide), which passes into a steep continental slope (Martins and Coutinho, 1981; Ponte and Asmus, 1978; Summerhayes et al., 1975). In between these areas, from 16 to 20°S, the shelf passes into the maximum 200 km wide carbonatic to basaltic Abrolhos Plateau. Around 21°S, the seamounts of the Vitoria-Trinidade Ridge extend approximately 700 km eastward into the Atlantic. From 23 to 28°S, the shelf widens and forms the Santos Plateau which is maximum 100 m deep and 200 km wide. South of 28°S, the shelf is about 80 km wide.

Whereas modern sedimentation on the inner shelf is dominated by coarse bioclastic carbonates, foraminiferal clay to ooze covers the outer shelf and the continental slope (Summerhayes et al., 1975). However, this does not apply to the areas of the shelf and continental slope situated off major rivers, which are dominated by terrigenous sediments. Whereas turbidites are only widespread on the middle and lower slope off Northeast and East Brazil, they also occur quite often on the upper slope in South Brazil (Kowsmann and de Ataide Costa, 1979).

The surface hydrography of the study area is dominated by the north and southward flowing South Atlantic western boundary currents, the North Brazil Current (NBC) and Brazil Current (BC, Fig. 4). Starting at around 10°S, both the NBC and the BC originate from the South Equatorial Current (SEC; Peterson and Stramma, 1990). The NBC starts as an undercurrent (North Brazil Undercurrent) with maximum transport volumes in about 100 to 200 m water depth and a weak surface current component (da Silveira et al., 1994; Schott et al., 1995; Stramma et al., 1995). Surface to thermocline conditions of the western tropical Atlantic are linked to the seasonal variability in trade wind intensity and the position of the ITCZ (Chang et al., 1997; Hastenrath and Merle, 1987; Richardson and Walsh, 1986; Stramma et al., 1995). During austral spring the southeast trades reach their maximum intensity and the SEC accelerates, deepening the mixed layer and the thermocline and accumulating salty, warm water masses off the South American continent (Johns et al., 1998). The opposite occurs during austral fall, when weak trade winds and reduced SEC intensity result in shallowing of the mixed layer and the thermocline and in surface water freshening and cooling (Johns et al., 1998). This results in a seasonally deepening mixed layer from 60 m depth in austral summer to autumn to 100 m depth in austral winter to spring (Hastenrath and Merle, 1987). Annual mean SST are 27.25 °C with a seasonal amplitude of 2 °C (Conkright et al., 2002) and

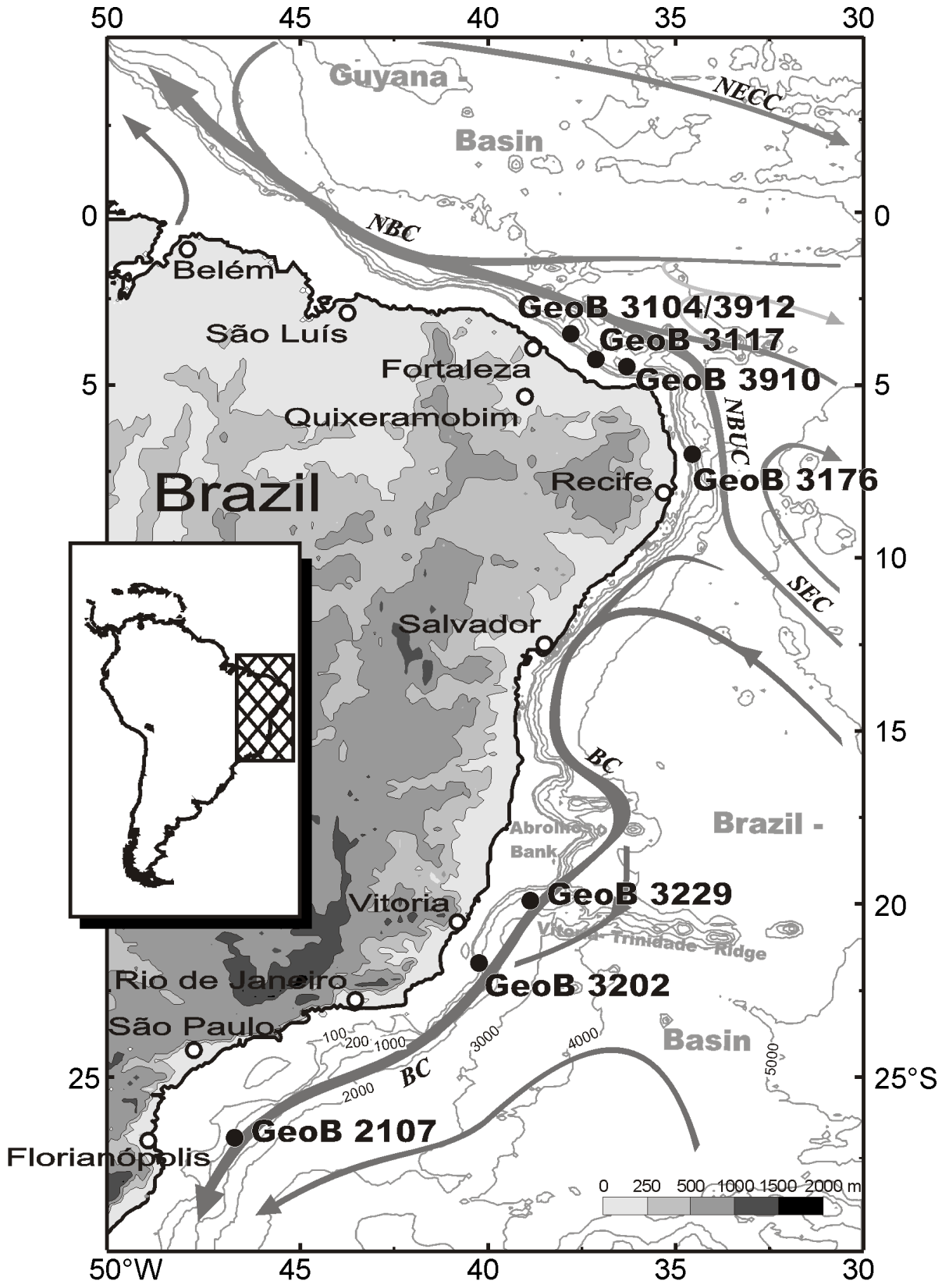

Figure 4: Oceanographic sitemap showing the main surface ocean currents in the western tropical to southern subtropical Atlantic and sediment archives off the East Brazilian coast used in this study. NBC represents the North Brazil Current, NBUC the North Brazil Undercurrent, BC the Brazil Current, SEC the South Equatorial Current and NECC the North Equatorial Counter Current.

average sea surface salinities (SSS) 36.0 ‰ with a seasonal amplitude of 0.3 ‰ (Levitus et al., 1994). Below the thermocline, the vertical structure of the tropical Atlantic is relatively stable, with South Atlantic Central Water (SACW) extending to about 500 m depth (Curry and Oppo, 2005), Antarctic Intermediate Water (AAIW) and the underlying Upper Circumpolar Deep Water (UCDW) flowing between 500 and 1200 m depth, North Atlantic Deep Water (NADW) extending from 1200 to 3900 m depth (Andrié, 1996; Rhein et al., 1996) and Antarctic Bottom Water (AABW) flowing between 3900 m depth and the ocean bottom (Fig. 5; Curry and Oppo, 2005).

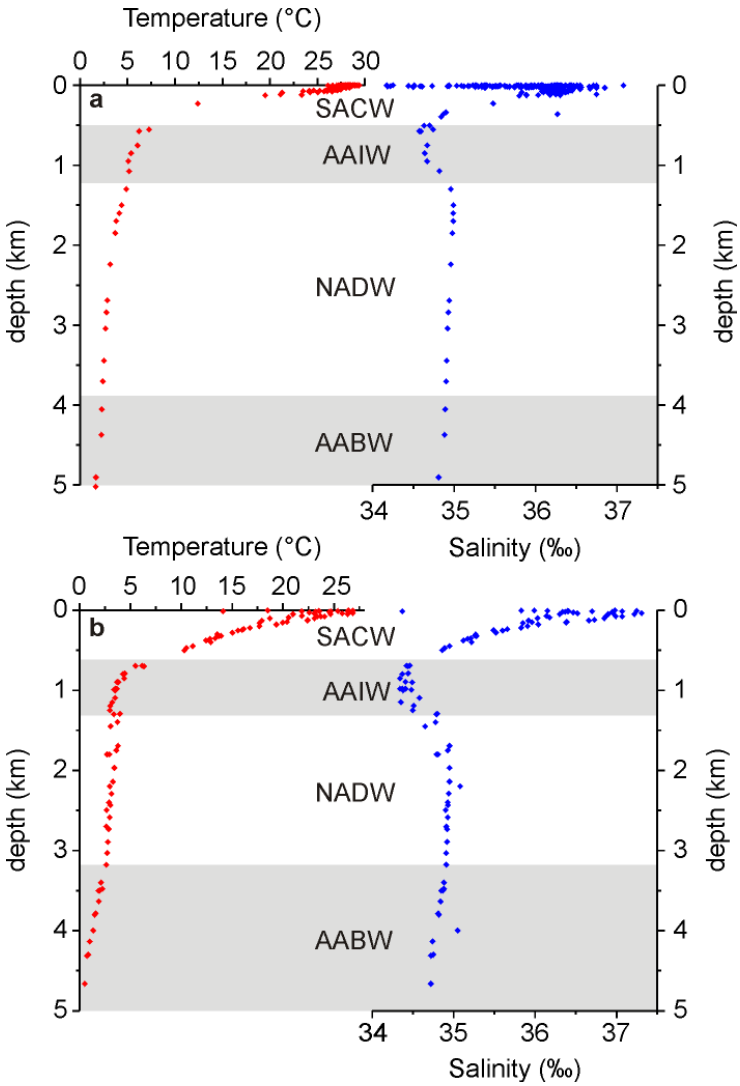

Figure 5: Temperature and Salinity water column profiles for **a)** the western tropical Atlantic and **b)** the western subtropical Atlantic (data from Schmidt et al., 1999)

SACW represents South Atlantic Central Water, AAIW Antarctic Intermediate Water, NADW North Atlantic Deep Water and AABW Antarctic Bottom Water

At its northwestern boundary, the NBC feeds the Guyana Current, which continues towards the Caribbean. Therefore, the NBC is an important factor for the heat distribution in the Atlantic as it transports warm, salty water from the South to the North Atlantic. Whereas the NBC water enters the Guyana Current almost completely in boreal spring, a part of the NBC is advected eastward into the North Equatorial Countercurrent (NECC) from June to January (Bourles et al., 1999; Schott et al., 1998). Therefore, the oceanic heat transport from the tropics to the North Atlantic is diminished from June to January. The retroflection of NBC water to the NECC is probably driven by the northward shift of the ITCZ and the associated trade wind system during boreal summer and autumn (Condie, 1991; Memery et al., 2000).

The BC is a relatively weak western boundary current (Peterson et al., 2000). While the NBC receives about 12 Sv (1 Sv = 10^6 m^3*s^{-1}) from the SEC, the BC receives only about 4 Sv (Stramma et al., 1990). This might be related to the THC, which enhances NBC transport and diminishes BC transport (Memery et al., 2000; Schott et al., 1998). The BC transport volume does not increase significantly between 10 and 20°S, but increases at a rate of about 5% per 100 km south of 24°S (Gordon and Greengrove, 1986). Therefore, the BC dominates the upper 600 m of the water column in the western subtropical Atlantic with transport volumes of about 14 Sv (Evans and Signorini, 1985; Garzoli, 1993; Stramma, 1989). Only the upper 50 m of the water column are affected by seasonally varying temperatures in the western subtropical Atlantic (Stramma, 1989). Annual mean SST are 22.5 °C and average SSS 36.2 ‰ (Conkright et al., 2002). Below this mixed layer, the thermocline-SACW-AAIW structure is rather uniform throughout the year, with the thermocline and the underlying SACW extending down to the bottom of the BC (Schmid et al., 1995). Below the BC, AAIW flows northward between water depths of 600 and 1300 m (Evans and Signorini, 1985; Stramma, 1989). NADW extends zfrom 1300 to about 3200 m depth and AABW fills the ocean bottom below 3200 m depth (Fig. 5; Curry and Oppo, 2005).

Between 28 and 33°S the BC recirculates partly and thereby increases its transport (Stramma, 1989). The BC continues to the Malvinas Confluence Zone (MCZ), which lies between 35 and 40°S (Gordon and Greengrove, 1986). North of this Zone, the BC begins to separate from the South American shelf and heads towards the east (Olson et al., 1988). The latitude where the BC separates from the coast varies between 33°S in austral winter and 38°S in austral summer (Garzoli, 1993; Garzoli and Garraffo, 1989; Olson et al., 1988). Therefore, neither the MCZ nor the southward lying Malvinas Current influences the sedimentation area of the western subtropical Atlantic directly.

Concerning their volume transports and flywheels, it is important to note that the NBC starts with three times more volume transport than the BC (12 Sv vs. 4 Sv; Stramma et al., 1990) and grows into a huge, finally 300 km wide current with a volume transport of 35 Sv (Bourles et al., 1999; da Silveira et al., 1994; Schott et al., 1998), whereas the BC is a relatively small western boundary current until reaching 20°S (Stramma et al., 1990). The bulk of the difference in volume transport is related to the THC; which strengthens the NBC and weakens the BC (Memery et al., 2000; Schott et al., 1998). Furthermore, surface transport in the NBC is also enhanced by southeastern trade winds (Johns et al., 1998).

2.2.3 Modern Climate

South American precipitation patterns are largely governed by the main atmospheric circulation systems and mountain systems of the continent (Fig. 6). Precipitation patterns in the tropics primarily depend on the ITCZ, which is the main centre of tropical atmospheric convectivity and therefore generally features high precipitation rates. The ITCZ shifts between the northern tropics in boreal summer and the southern tropics in austral summer and therefore gives rise to high precipitation rates in the northern tropics during boreal summer and in the southern tropics during austral summer (Hastenrath, 1990). During austral summer, when the ITCZ reaches its southernmost position throughout the year, a monsoon climate establishes over subtropical eastern South America and causes very high precipitation rates there (Zhou and Lau, 1998). The same region experiences relatively high precipitation rates during austral winter, when inflows of polar to mid-latitude cold air masses induce cyclonic wind systems over the subtropical western South Atlantic and thereby induce the inflow of moist air masses from the Atlantic onto the continent (Vera et al., 2002). Another region of high precipitation rates exists in temperate western South America, where westwinds

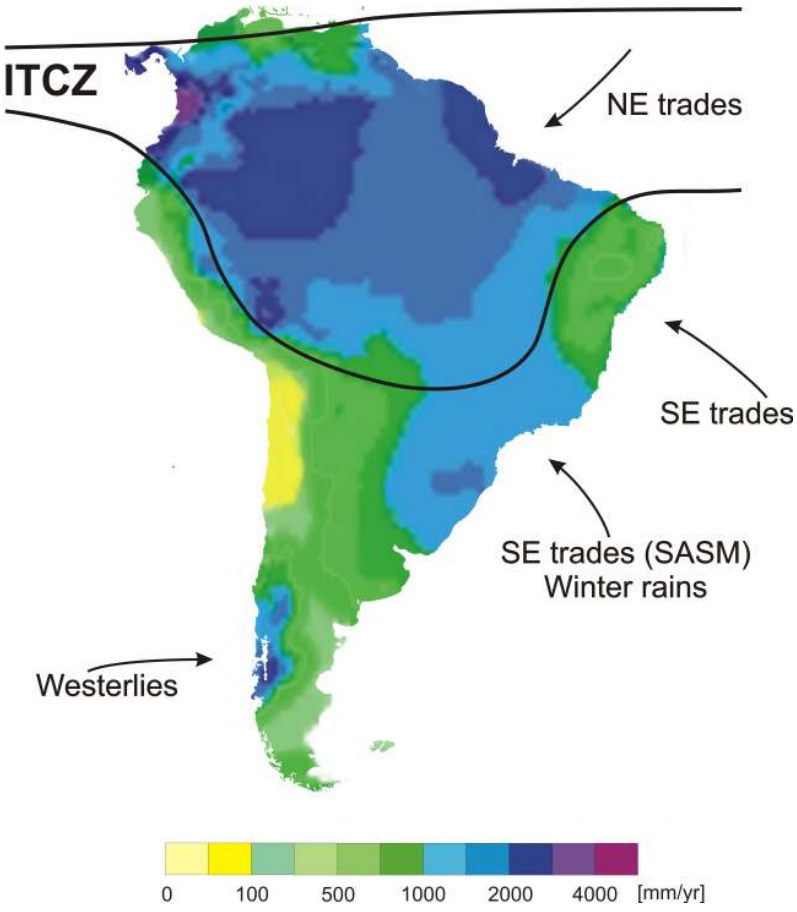

Figure 6: Average annual mean precipitation rates in South America from 1951 to 2000 and main tropical to subtropical South American atmospheric circulation systems (precipitation data from Beck et al., 2004)

Note the relatively dry conditions in Northeast Brazil and the relation of tropical precipitation patterns to the position of the ITCZ. Furthermore, note the markedly wet South Brazilian conditions (caused by the South American Summer Monsoon, SASM, and winter rains driven by the influx of mid- to high latitude cold air masses) compared to dry conditions in eastern subtropical South America.

(the Westerlies) transport moisture from the Pacific Ocean to the South American continent. This wind system is driven by the strong circum-Antarctic wind current, which is relatively constant throughout the year and therefore supports wet conditions in temperate western South America.

The main mountain systems further refine South American precipitation patterns. As precipitation in tropical South America mainly derives from easterly winds (the trade winds), precipitation rates are markedly higher east of the Andes than on the western side. This wind shadow effect of the Andes is especially pronounced in subtropical western South America, where the Atacama Desert exhibits very dry conditions. In temperate South America, the Andes act as rain shadow for the Westerlies and induce semiarid conditions in Patagonia (temperate eastern South America).

In Northeast Brazil, the Brazilian Highlands block the southeastern trades and induce high precipitation rates in the coastal area of Northeast Brazil as well as dry conditions in central Northeast Brazil. The northern focus investigation area, the catchment area of the Rio Piranhas, belongs to this semiarid part of Northeast Brazil known as the “Nordeste”. The climate of this region is characterized by a long dry season from August to December and a rainy season with high precipitation rates from March to April (Fig. 7a; Hastenrath, 1990). Average annual precipitation is 864 mm, the mean annual temperature is 26.6 °C and there is only minor seasonal variability in temperatures.

Three major factors promote precipitation in the rainy season: First, the ITCZ, being the zone of major tropical convective rainfall, reaches its southernmost position throughout the year (Hastenrath and Heller, 1977). Second, the equatorial South Atlantic waters are warmest in March and April, which enhances evaporation and, consequentially, the moisture content of the trade winds (Hastenrath, 1990). Third, the interhemispheric SST gradient in the tropical Atlantic (the temperature contrast between surface waters lying north and south of the equator) is weakest in this period of the year. Whereas a high interhemispheric SST gradient induces subsidence over the “Nordeste” which hampers precipitation, a low gradient reduces this effect (Hastenrath, 1990).

Rain anomalies in the “Nordeste” primarily result from enhancements or reductions of the average annual cycle. Drought years are characterized by an anomalously far northern position of the ITCZ, reduced northeast trades and an anomalously high interhemispheric SST gradient (resulting from positive SST anomalies in the tropical North Atlantic and negative ones in the tropical South Atlantic; Hastenrath, 1990). Correspondingly, a far southern ITCZ

position, increased northeast trades and a low interhemispheric SST gradient (resulting from negative SST anomalies in the tropical North Atlantic and positive ones in the tropical South Atlantic) should increase yearly precipitation.

In contrast to the Nordeste, the catchment area of the Rio Itajaí (the southern focus investigation area) is marked by a humid, warm (subtropical) climate without a distinct dry season (Fig. 7b; Nimer, 1989). Average annual precipitation is over 2000 mm, and the mean annual temperature is 14.5 °C. The high precipitation rates result in part from the topography of the Rio Itajaí's catchment area, as the mountain chains at its border form an orographic barrier for northerly, easterly and southerly winds.

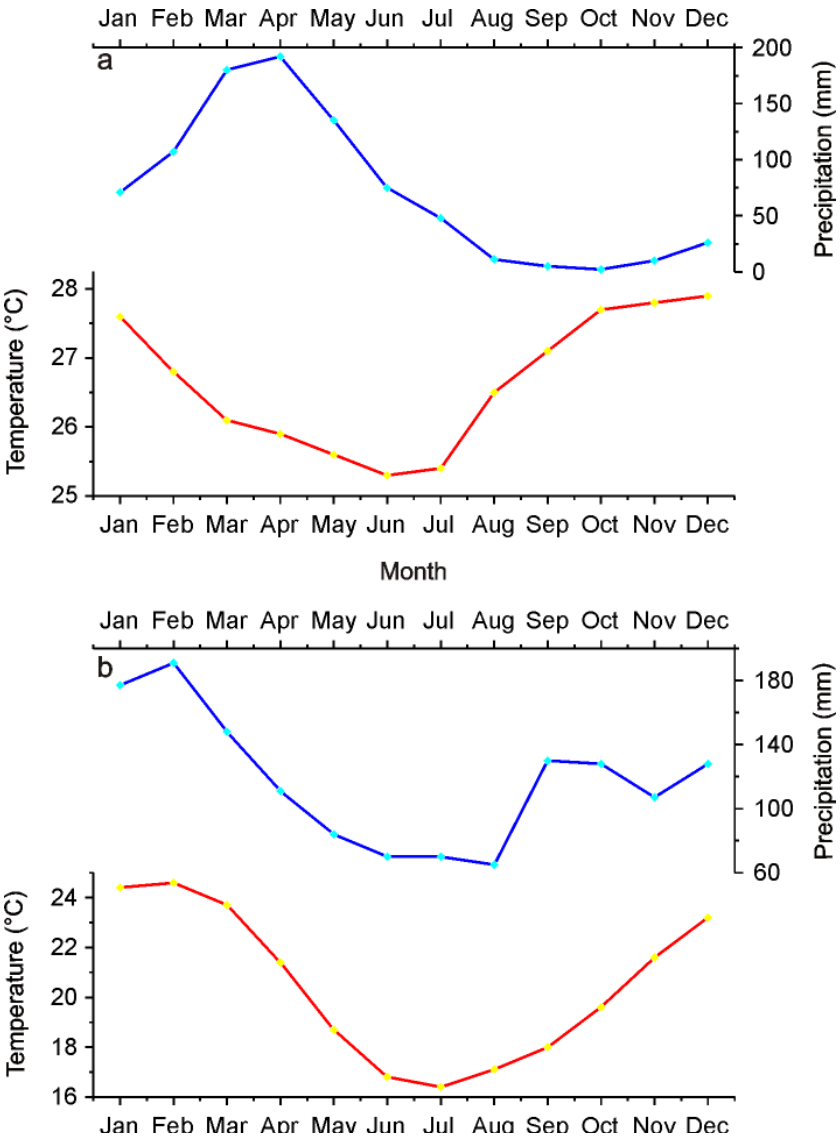

Figure 7: Climate diagrams of **a)** Quixeramobim (Northeast Brazil) and **b)** Florianopolis (South Brazil; the location of the climate stations is shown in Fig. 3 and 4)

Note the short rainy season from March to April and the long dry season from August to December in Quixeramobim **(a)** compared to the longer wet season from September to March in Florianopolis **(b)**

Although distinct wet and dry seasons are not observed, winter and summer precipitation is related to different atmospheric circulation systems (Carvalho et al., 2002; Xie and Arkin, 1997). During austral summer (January to February), the ITCZ reaches its southernmost position and strengthens the South American Summer Monsoon (SASM), which transports large amounts of moisture from the subtropical Atlantic onto the continent

and causes very high precipitation rates in southern Brazil (Rao et al., 1996; Zhou and Lau, 1998). In the Rio Itajaí's catchment area, a significant fraction of summer precipitation derives from this moisture flux (Fig. 7b). Therefore, although not directly beneath the centre of tropical convectivity, summer precipitation in the Rio Itajaí's catchment area is influenced by the position of the ITCZ.

During austral winter and early spring (June to August), the southern polar fronts reach their northernmost position and trigger equatorward incursions of mid- to high-latitude cold air. This results in cyclonic wind systems, which transport large amounts of moisture from the Atlantic Ocean onto the continent (Vera et al., 2002). Over southern Brazil, these cold air masses meet warm tropical ones, resulting in strong precipitation (Hastenrath, 1991; Nimer, 1989). Although South Brazilian winter precipitation rates are much lower than summer precipitation rates, a significant part of South Brazilian precipitation derives from the moisture flux during winter (Fig. 7b).

2.2.4 Paleoclimate

Millennial to multi-millennial variations in tropical South American paleoprecipitation are in part related to the same forcing mechanisms which govern modern precipitation patterns on seasonal to interannual timescales. Precipitation records from various locations of the South American tropics indicate variations in tropical precipitation patterns that were probably caused by shifts in the position of the ITCZ (Arz et al., 1998, 1999; Auler et al., 2004; Baker et al., 2001a, 2001b; Behling et al., 2000; Jennerjahn et al., 2004; Peterson et al., 2000; Thompson et al., 1995, 1998; Wang et al., 2004). The driving mechanism of these ITCZ shifts, however, remains unclear. Millennial-scale variations in tropical South American precipitation patterns generally coincide with pronounced temperature shifts in the high northern latitudes which occurred during Dansgaard/Oeschger cycles and Heinrich events (e.g. Arz et al., 1998; Peterson et al., 2000). A recent modelling study suggests high northern latitude temperature shifts may increase meridional temperature gradients in the northern hemisphere, which, in turn, may trigger hemisphere-wide reorganisations of the atmospheric circulation including the ITCZ (Fig. 8; Chiang and Bitz, 2005). However, this modelling study lacks a proxy record which directly relates North Atlantic meridional temperature gradients to tropical precipitation patterns. This study addresses this issue by providing a combined and stratigraphically well-defined proxy record of the temperature gradient between the tropical Atlantic and the mid-latitude North Atlantic as well as a precipitation record from tropical Northeast Brazil (Manuscript 1).

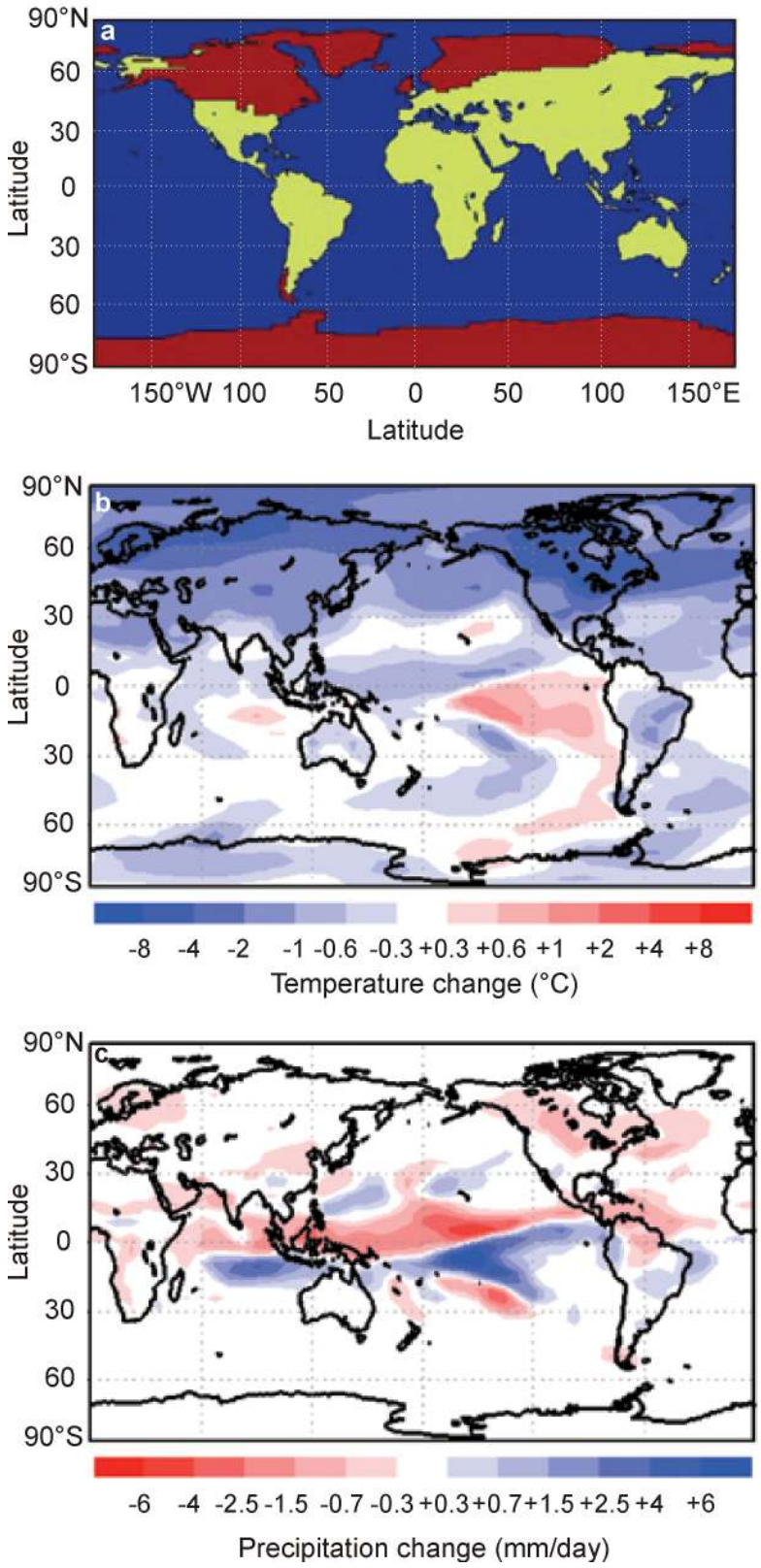

Figure 8: Effect of high northern latitude cooling on global temperatures and precipitation patterns (Chiang and Bitz, 2005). **a)** modern climate system with imposed ice cover representing Last Glacial Maximum ice extent (shown in red); **b)** resulting temperature change; **c)** resulting precipitation change

Note the increase in the temperature gradient between the high latitude North Atlantic and the tropical Atlantic **(b)** and the resulting southward shift of the Intertropical Convergence Zone represented by dryer conditions in the northern and wetter conditions in the southern tropics **(c)**

Due to the paucity of high-resolution precipitation records, the spatial extent of the ITCZ shifts is yet defined relatively imprecisely. Whereas Venezuelan precipitation patterns were altered during Dansgaard/Oeschger cycles and Heinrich events (Peterson et al., 2000), precipitation records from Northeast Brazil (e.g. Arz et al., 1998; Wang et al., 2004) and the Bolivian to Peruvian Andes (e.g. Thompson et al., 1995, 1998) suggest ITCZ shifts during Heinrich events only. However, the resolution of the Northeast Brazilian precipitation records is insufficient to investigate Dansgaard/Oeschger cycles. Due to the lack of precipitation records from interior subtropical South America, the southernmost extent of these ITCZ shifts is largely unknown. A recent study from Cruz et al. (2005) indicates millennial-scale changes in subtropical South Brazilian precipitation patterns related to, but not directly caused by ITCZ shifts. However, these millennial-scale precipitation pattern changes are clearly subordinate to longer-term precipitation pattern variations of orbital frequency. This study includes a review of tropical South American precipitation records (Manuscripts 1 and 2) and a study on the spatial extent of ITCZ shifts in eastern South America (Manuscript 3).

Whereas a basic understanding of the mechanistic coupling of tropical precipitation patterns to high northern latitude temperatures has been gained during the last years (e.g. Chiang and Bitz, 2005; Peterson et al., 2000; Wang et al., 2001), the relation between tropical Atlantic SST and millennial to multi-millennial changes in tropical South American precipitation patterns is rather unexamined. In the modern climate system, tropical Atlantic SST influence Northeast Brazilian precipitation patterns directly by governing the moisture content of the northeastern trades (see Chapter 2.2.3). Furthermore, at least in coastal Northeast Brazil the position of the ITCZ is related to tropical Atlantic SST (Hastenrath, 1990). Therefore, this study includes an analysis of the relation between millennial to multi-millennial variations in Northeast Brazilian precipitation patterns and changes in tropical Atlantic SST (Manuscript 1).

2.3 References Chapter 2

Alverson, K., and Oldfield, F. (2000). PAGES - Past global changes and their significance for the future: An introduction. *Quaternary Science Reviews* **19,** 3-7.

Andrié, C. (1996). Chlorofluoromethanes in the deep equatorial Atlantic revisited. *In "The South Atlantic: Present and past circulation"* (edited by G. Wefer, W. H. Berger, G. Siedler, and D. J. Webb), pp. 273-288. Springer-Verlag, Berlin.

Arz, H. W., Pätzold, J., and Wefer, G. (1998). Correlated millennial-scale changes in surface hydrography and terrigenous sediment yield inferred from last-glacial marine deposits off northeastern Brazil. *Quaternary Research* **50,** 157-166.

Arz, H. W., Pätzold, J., and Wefer, G. (1999). Climatic changes during the last deglaciation recorded in sediment cores from the northeastern Brazilian continental margin. *Geo-Marine Letters* **19,** 209-218.

Auler, A. S., Wang, X., Edwards, R. L., Cheng, H., Cristalli, P. S., Smart, P. L., and Richards, D. A. (2004). Quaternary ecological and geomorphic changes associated with rainfall events in presently semi-arid northeastern Brazil. *Journal of Quaternary Science* **19,** 693-701.

Baker, P. A., Rigsby, C. A., Seltzer, G. O., Fritz, S. C., Lowenstein, T. K., Bacher, N. P., and Veliz, C. (2001a). Tropical climate changes at millennial and orbital timescales on the Bolivian Altiplano. *Nature* **409,** 698-701.

Baker, P. A., Seltzer, G. O., Fritz, S. C., Dunbar, R. B., Grove, M. J., Tapia, P. M., Cross, S. L., Rowe, H. D., and Broda, J. P. (2001b). The history of South American tropical precipitation for the past 25,000 years. *Science* **291,** 640-643.

Bard, E., Rostek, F., Turon, J.-L., and Gendrau, S. (2000). Hydrological impact of Heinrich events in the subtropical northeast Atlantic. *Science* **289,** 1321-1324.

Beck, C., Grieser, J., and Rudolf, B. (2004). "A new monthly precipitation climatology for the global land areas for the period 1951 to 2000". DWD, *Klimastatusbericht 2004* (http://www.dwd.de/de/FundE/Klima/KLIS/prod/KSB/ksb04/28_precipitation.pdf).

Behling, H., Arz, H. W., Pätzold, J., and Wefer, G. (2000). Late Quaternary vegetational and climate dynamics in northeastern Brazil, inferences from marine core GeoB 3104-1. *Quaternary Science Reviews* **19,** 981-994.

Bender, M., Sowers, T., Dickson, M.-L., Orchardo, J., Grootes, P., Mayewski, P. A., and Meese, D. A. (1994). Climate correlations between Greenland and Antarctica during the past 100,000 years. *Nature* **372,** 663-666.

Bond, G., Showers, W., Cheseby, M., Lotti, R., Almasi, P., deMenocal, P., Priore, P., Cullen, H., Hajdas, I., and Bonani, G. (1997). A pervasive millennial-scale cycle in North Atlantic Holocene and glacial climates. *Science* **278,** 1257-1266.

Bond, G. C., Broecker, W. S., Johnsen, S., McManus, J., Labeyrie, L., Jouzel, J., and Bonani, G. (1993). Correlations between climate records from North Atlantic sediments and Greenland ice. *Nature* **365,** 143-147.

Bourles, B., Gouriou, Y., and Chuchla, R. (1999). On the circulation and upper layer of the western equatorial Atlantic. *Journal of Geophysical Research* **104,** 21151-21170.

Broecker, W. S. (2003). Does the trigger for abrupt climate change reside in the ocean or in the atmosphere? *Science* **300,** 1519 - 1522.

Broecker, W. S. (2005). Millennial climate change revisited. *Global and Planetary Change*.

Cane, M., and Clement, A. C. (1999). *In "Mechanisms of global climate change at millennial time scales*" (edited by P. U. Clark, R. S. Webb, and L. D. Keigwin), *Geophysical Monograph* **112**, pp. 373-383. American Geophysical Union, Washington, DC.

Carvalho, L., Jones, C., and Liebmann, B. (2002). Extreme precipitation events in southeastern South America and large-scale convective patterns in the South Atlantic convergence zone. *Journal of Climate* **15,** 2377–2394.

Chang, P., Ji, L., and Li, H. (1997). A decadal climate variation in the tropical Atlantic Ocean from thermodynamic air-sea interactions. *Nature* **385,** 516-518.

Chiang, J. C. H., and Bitz, C. M. (2005). Influence of high latitude ice cover on the marine Intertropical Convergence Zone. *Climate Dynamics* **25,** 477-496.

Condie, S. A. (1991). Separation and recirculation of the North Brazil Current. *Journal of Marine Research* **49,** 1-19.

Conkright, M. E., Antonov, J. I., Baranova, O., Boyer, T. P., Garcia, H. E., Gelfeld, R., Johnson, D., O'Brien, T. D., Smolyar, I., and Stephens, C. (2002). "World ocean database 2001, Volume 1: Introduction." U.S. Government Printing Office, Washington, D.C.

Cruz, F. W., Burns, S. J., Karmann, I., Sharp, W. D., Vuille, M., Cardoso, A. O., Ferrari, J. A., Silva Dias, P. L., and Viana, O. (2005). Insolation-driven changes in atmospheric circulation over the past 116,000 years in subtropical Brazil. *Nature* **434,** 63-66.

Curry, W. B., and Oppo, D. W. (2005). Glacial water mass geometry and the distribution of $\delta^{13}C$ of ΣCO^2 in the western Atlantic Ocean. *Paleoceanography* **20,** doi:10.1029/2004PA001021.

da Silveira, I. C. A., de Miranda, L. B., and Brown, W. S. (1994). On the origins of the North Brazil Current. *Journal of Geophysical Research* **99,** 501-512.

Evans, D. L., and Signorini, S. S. (1985). Vertical structure of the Brazil Current. *Nature* **315,** 48-50.

Garzoli, S. L. (1993). Geostrophic velocity and transport variability in the Brazil-Malvinas Confluence. *Deep-Sea Research* **40,** 1379-1403.

Garzoli, S. L., and Garraffo, Z. (1989). Transport, frontal motions and eddies at the Brazil-Malvinas Confluence. *Deep-Sea Research* **36,** 681-703.

Gordon, A. L., and Greengrove, C. L. (1986). Geostrophic circulation of the Brazil-Falkland Confluence. *Deep-Sea Research* **33,** 573-585.

Grootes, P. M., and Stuiver, M. (1997). Oxygen 18/16 variability in Greenland snow and ice with 103- to 105-year time resolution. *Journal of Geophysical Research* **102,** 26455-26470.

Grootes, P. M., Stuiver, M., Withe, J. W. C., Johnsen, S., and Jouzel, J. (1993). Comparison of oxygen isotope records from the GISP2 and GRIP Greenland ice cores. *Nature* **366,** 552-554.

Hastenrath, S. (1990). Prediction of Northeast Brazil rainfall anomalies. *Journal of Climate* **3,** 893-904.

Hastenrath, S. (1991). "Climate dynamics of the tropics." Kluwer, Dordrecht.

Hastenrath, S., and Heller, L. (1977). Dynamics of climatic hazards in Northeast Brazil. *Quarterly Journal of the Royal Meteorological Society* **103,** 77-92.

Hastenrath, S., and Merle, J. (1987). Annual cycle of subsurface thermal structure in the tropical Atlantic Ocean. *Journal of Physical Oceanography* **17,** 1518-1538.

IPCC (2001). "IPCC third assesment report: Climate change 2001: The scientific basis." Cambridge University Press, Cambridge.

Jennerjahn, T. C., Ittekkot, V., Arz, H. W., Behling, H., Pätzold, J., and Wefer, G. (2004). Asynchronous terrestrial and marine signals of climate change during Heinrich events. *Science* **306,** 2236-2239.

Johns, W. E., Lee, T. N., Beardsley, R. C., Candela, J., Limeburner, R., and Castro, B. (1998). Annual cycle and variability of the North Brazil Current. *Journal of Physical Oceanography* **28,** 103-128.

Kaiser, J., Lamy, F., and Hebbeln, D. (2005). A 70-kyr sea surface temperature record off southern Chile (Ocean Drilling Program Site 1233). *Paleoceanography* **20,** doi:10.1029/2005PA001146.

Kowsmann, R. O., and de Ataide Costa, M. P. (1979). Sedimentação quaternária da margem continental brasiliera e das áreas oceanicâs adjacentes. *In "Reconhecimento global da margem continental brasileira, Projecto REMAC"* (edited by L. A. M. de Mello), 55 pp. Petrobás, Rio de Janeiro.

Levitus, S., Burgett, R., and Boyer, T. P. (1994). "World ocean atlas 1994, Volume 3: Salinity." U.S. Department of Commerce, Washington D.C.

Martins, L. R., and Coutinho, P. N. (1981). The brazilian continental margin. *Earth-Science Reviews* **17,** 87-107.

Memery, L., Arhan, M., Alvarez-Salgado, X. A., Messias, M. J., Mercier, H., Castro, C. G., and Rios, A. F. (2000). The water masses along the western boundary of the south and equatorial Atlantic. *Progress in Oceanography* **47,** 69-98.

Nimer, E. (1989). "Climatologia do Brasil." IBGE, Rio de Janeiro.

Olson, D. B., Podesta, G. P., Evans, R. H., and Brown, O. B. (1988). Temporal variations in the separation of Brazil and Malvinas currents. *Deep-Sea Research* **35,** 1971-1990.

Peterson, L. C., Haug, G. H., Hughen, K. A., Röhl, Ursula. (2000). Rapid changes in the hydrologic cycle of the tropical Atlantic during the last glacial. *Science* **290,** 1947-1951.

Peterson, R. G., and Stramma, L. (1990). Upper-level circulation in the South Atlantic Ocean. *Progress in Oceanography* **26,** 1 - 73.

Ponte, F. C., and Asmus, H. E. (1978). Geological framework of the Brazilian continental margin. *Geologische Rundschau* **67,** 201-235.

Rachwal, M. F. G., and Curcio, G. R. (1994). Principais tipos de solos do Estado do Paraná, suas características e distribuição na paisagem. *In "A vegetação natural do estado do Paraná."* 20 pp. Instituto Paranense de Desenvolvimento Econômico e Social, Curitiba.

Rao, V. B., Cavalcanti, I. F. A., and Hada, K. (1996). Annual variation of rainfall over Brazil and water vapor characteristics over South America. . *Journal of Geophysical Research* **101,** 26539–26551.

Rhein, M., Schott, F., Fischer, J., Send, U., and Stramma, L. (1996). The deep water regime in the equatorial Atlantic. *In "The South Atlantic: Present and past circulation"* (edited by G. Wefer, W. H. Berger, G. Siedler, and D. J. Webb), pp. 261-271. Springer-Verlag, Berlin.

Richardson, P. L., and Walsh, D. (1986). Mapping climatological seasonal variations of surface currents in the tropical Atlantic using ship drifts. *Journal of Geophysical Research* **91,** 10,537-10,550.

Schmid, C., Schäfer, H., Podesta, G., and Zenk, W. (1995). The Vitória eddy and its relation to the Brazil Current. *Journal of Physical Oceanography* **25,** 2532-2546.

Schmidt, G. A., Bigg, G. R., and Rohling, E. J. (1999). Global seawater oxygen-18 database (http://data.giss.nasa.gov/o18data/).

Schobbenhaus, C., de Almeida Campos, D., Derze, G. R., and Asmus, H. E. (1995). Mapa geológico do Brasil. Serviço Geológico do Brasil, Rio de Janeiro.

Schott, F. A., Fischer, J., and Stramma, L. (1998). Transports and pathways of the upper-layer circulation in the western tropical Atlantic. *Journal of Physical Oceanography* **28,** 1904-1928.

Schott, F. A., Stramma, L., and Fischer, J. (1995). The warm water inflow into the western tropical Atlantic boundary regime, spring 1994. *Journal of Geophysical Research* **100,** 24745–24760.

Schulz, H., von Rad, U., and Erlenkeuser, H. (1998). Correlation between Arabian Sea and Greenland climate oscillations of the past 110,000 years. *Nature* **393,** 54-57.

Stramma, L. (1989). The Brazil Current transport south of 23° S. *Deep-Sea Research* **36,** 639-646.

Stramma, L., Fischer, J., and Reppin, J. (1995). The North Brazil Undercurrent. *Deep-Sea Research* **42,** 773–795.

Stramma, L., Ikeda, Y., and Peterson, R. G. (1990). Geostrophic transport in the Brazil Current region north of 20°S. *Deep-Sea Research* **37,** 1875-1886.

Summerhayes, C. P., Coutinho, P. N., França, A. M. C., and Ellis, J. P. (1975). Part III. Salvador to Fortaleza, northeastern Brazil. *In "Upper continental margin sedimentation off Brazil"* (edited by J. D. Milliman, and C. P. Summerhayes), pp. 45-77. E. Schweizerbart'sche Verlagsbuchhandlung, Stuttgart.

Thompson, L. G., et al. (1998). A 25,000-Year tropical climate history from Bolivian ice cores. *Science* **282,** 1858-1864.

Thompson, L. G., Mosley-Thompson, E., Davis, M. E., Lin, P.-N., Henderson, K. A., Cole-Dai, J., Bolzan, J. F., and Liu, K.-B. (1995). Late glacial stage and Holocene tropical ice core records from Huascarán, Peru. *Science* **269,** 46-50.

Vera, C. S., Vigliarolo, P. K., and Berbery, E. H. (2002). Cold season synoptic-scale waves over subtropical South America. *Monthly Weather Reviews* **130,** 684–699.

Vidal, L., Labeyrie, L., Cortijo, E., Arnold, M., Duplessy, J. C., Michel, E., Becque, S., and van Weering, T. C. E. (1997). Evidence for changes in the North Atlantic Deep Water linked to meltwater surges during the Heinrich events. *Earth and Planetary Science Letters* **146,** 13-27.

Wang, X., Auler, A. S., Edwards, R. L., Cheng, H., Cristalli, P. S., Smart, P. L., Richards, D. A., and Shen, C.-C. (2004). Wet periods in northeastern Brazil over the past 210 kyr linked to distant climate anomalies. *Nature* **432,** 740-743.

Wang, Y. J., Cheng, H., Edwards, R. L., An, Z. S., Wu, J. Y., Shen, C.-C., and Dorale, J. A. (2001). A high-resolution absolute-dated Late Pleistocene monsoon record from Hulu Cave, China. *Science* **294,** 2345-2348.

Wang, Y. J., et al. (2004). Hulu cave stalagmite oxygen isotope data, IGBP PAGES/World Data Center for Paleoclimatology, data contribution series #2004-023. NOAA/NGDC paleoclimatology progam, Boulder.

Xie, P., and Arkin, P. A. (1997). Global precipitation: A 17-year monthly analysis based on gauge observations, satellite estimates, and numerical model outputs. *Bulletin of the American Meteorological Society* **78,** 2539–2558.

Zhou, J., and Lau, K. M. (1998). Does a monsoon climate exist over South America? *Journal of Climate* **11,** 1020–1040.

3 Material and Methods

3.1 Material and Overview of Methods

This study is based on the analysis of sediment cores from the western tropical to subtropical Atlantic situated off the Northeast and South Brazilian coast (Table 1, Fig. 3). Cores GeoB 2107 and 3910, retrieved during Meteor cruises M 23-2 (Bleil et al., 1993) and M 34-4 (Fischer et al., 1996), were chosen as master cores and studied intensively. Supportive analysis and reanalysis was performed on the other sediment cores. Furthermore, this study includes a review of precipitation records from other sediment archives in the tropical to subtropical South American region (Table 1, Fig. 3).

Table 1: Archives and records generated (in red) or used (in black) in this study

Archive	Type of Archive	Location	Water depth / altitude	Type of record
GeoB 2107	Marine sediment core	27°10,6'S, 46°27,1'W (western subtrop. South Atlantic)	1048 m bsl	$\delta^{18}O_{benthic}$, Fe/Ca, Ti/Ca
GeoB 3910	Marine sediment core	4°14,7'S, 36°20,7'W (western trop. Atlantic)	2362 m bsl	$\delta^{18}O_{planktic}$, $\delta^{18}C_{benthic}$, SST, Fe/Ca, Ti/Ca
GeoB 3912	Marine sediment core	3°40,0'S, 37°43,0'W (western trop. Atlantic)	772 m bsl	Fe/Ca
GeoB 3117	Marine sediment core	4°11,1'S, 37°38,0'W (western trop. Atlantic)	930 m bsl	Fe/Ca
GeoB 3176	Marine sediment core	7°00,7'S, 34°26,5'W (western trop. Atlantic)	1385 m bsl	Fe/Ca
GeoB 3202	Marine sediment core	21°37,0'S, 39°58,7'W (western subtrop. South Atlantic)	1090 m bsl	Fe/Ca
GeoB 3229	Marine sediment core	19°38,5'S, 38°43,0'W (western subtrop. South Atlantic)	780 m bsl	Fe/Ca
ODP 1002 C	Marine sediment core	10°42,7'N, 65°10,2'W (South Caribbean Sea)	893 m bsl	Fe/Ca
Jacaré valley stalagmites and travertines	Stalagmites and travertines	10°10'S, 40°50'W (Jacaré valley)	500 m asl	U/Th datings
Stalagmite BT2	Stalagmite	27°13,4'S, 49°09,3'W (Botuverá cave)	230 m asl	$\delta^{18}O$
HS core 2	Ice core	9°07,0'S, 77°37,0'W (Huascaran Ice Cap)	6048 m asl	$\delta^{18}O$
Sajama core 1	Ice core	18°06,0'S, 68°53,0'W (Sajama Ice Cap)	6542 m asl	$\delta^{18}O$
MD 952042	Marine sediment core	37°46,0'N, 10°11,0'W (eastern temp. North Atlantic)	3146 m bsl	SST

GeoB 3910, raised from the upper continental slope off Northeast Brazil, consists of homogenous foraminifer and nanofossil bearing ooze to clay. While the upper 507 cm of the core are undisturbed, the lower part contains some turbidites. Therefore, only these upper 507 cm were analysed in this thesis. GeoB 2107, raised from the continental slope off the East coast of South Brazil, consists of homogeneous dark grey nannofossil-bearing silt with two small sandy silt layers. The core offers a 783 cm long sediment sequence of which the upper 6 m show minor signs of bioturbation. The two small sandy silt layers occur at 0.8 and 3.5 m depth and have been removed from the sedimentary record. Except for these layers, the core shows a continuous and undisturbed sediment sequence.

The sediment cores were dated with help of the radiocarbon method. We made use of foraminiferal stable isotopes ($\delta^{18}O$ and $\delta^{13}C$) and Mg/Ca ratios to examine oceanic conditions of the western South Atlantic. X-ray fluorescence analyses provide semiquantitative information about the light metal content of all cores, which was used to investigate changes in the catchment areas of the cores. Altogether, we report 6460 analyses on 4482 samples here. Table 2 gives an overview of the used methods.

Table 2: Methods used in this study

Kiel represents the Leibnitz-Laboratory for Radiometric Dating and Isotope Research of the University of Kiel, RCOM the DFG Research Center Ocean Margins at the University of Bremen and LDEO the Lamont-Doherty Earth Observatory of the Columbia University of New York

Method	Material	No. of analyses	Institute
AMS-^{14}C dating	GeoB 2107	6	Kiel
	GeoB 3910	6	Kiel
	GeoB 3912	9	Kiel
Stable isotopes ($\delta^{18}O$ and $\delta^{13}C$)	GeoB 2107	2052	RCOM
	GeoB 3910	1160	RCOM
Foraminiferal Mg/Ca	GeoB 2107	165	LDEO
	GeoB 3910	407	LDEO
XRF scanning	GeoB 2107	760	RCOM
	GeoB 3910	1354	RCOM
	GeoB 3912	541	RCOM

3.2 Radiocarbon dating

Radiocarbon dating is a method of obtaining age estimates on organic materials which is based on the decay of the radioactive carbon isotope ^{14}C. Isotopes are variants of an element with different masses due to different numbers of neutrons. There are three naturally occurring carbon isotopes in the earth system with relative abundances of 98.89 % (^{12}C), 1.11 % (^{13}C) and $1*10^{-10}$ % (^{14}C; Hoefs, 2003). Whereas ^{12}C and ^{13}C are stable carbon

isotopes, the radioactive isotope ^{14}C is produced in the upper atmosphere, where cosmic rays produce free neutrons (^{1}n). These, in turn, react with light nitrogen isotopes (^{14}N) to form radioactive carbon (^{14}C) and protons (^{1}p):

$$^{1}n + {}^{14}\mathrm{N} \rightarrow {}^{14}\mathrm{C} + {}^{1}p$$

^{14}C is rapidly oxidised to CO_2 which mixes evenly throughout the atmosphere within few days; therefore, CO_2 is evenly distributed in the atmosphere (Keeling et al., 1993). Atmospheric CO_2 constantly mixes with the CO_2 reservoirs of the upper ocean and the biosphere through gas exchange processes. Surface ocean organisms, in turn, are constantly exchanging ^{14}C with the surrounding surface seawater. Once they die, however, the gas exchange ceases while the ^{14}C included in the organisms continues to decay. Thereby, the radioactive ^{14}C emits beta (ß) particles and is transformed back into non-radioactive ^{14}N:

$$^{14}\mathrm{C} \rightarrow {}^{14}\mathrm{N} + {}^{0}\beta$$

^{14}C has a half-life of 5730±40 years (Cambridge half-life; Godwin, 1962). For dating purposes, however, a half-life of 5568±30 years (Libby half-life; Arnold and Libby, 1949) is used to avoid inconsistencies with records generated before 1962.

For paleoceanographic applications, planktic marine microorganisms are most widely used for dating purposes (e.g. Bard et al., 2004). When these organisms die, they settle down to the ocean floor relatively rapidly. Therefore, the time of death of these organisms represents the age of deposition of the sediments in which they occur. The time passed since the death of the organisms can be dated vith the radiocarbon method. Therefore, their initial ^{14}C concentration, their actual ^{14}C concentration and the half-life of ^{14}C need to be known. The amount of ^{14}C in a dating sample is measured with accelerator mass spectrometers as the ratio of ^{14}C versus ^{12}C in the sample as relative deviation from the $^{14}C/^{12}C$ ratio of a standard. This is generally expressed in the delta notation ($\delta^{14}C$) and calculated as follows:

$$\delta^{14}C(‰) = \left[\frac{\left(^{14}C/^{12}C\right)_{sample} - \left(^{14}C/^{12}C\right)_{s\,\mathrm{tan}\,dard}}{\left(^{14}C/^{12}C\right)_{s\,\mathrm{tan}\,dard}} \right] * 1000$$

Assuming the atmospheric ^{14}C concentration was constant in the past, past upper ocean $\delta^{14}C$ values should equal modern ones. Therefore, the initial $\delta^{14}C$ values of planktic marine microorganisms should also stay constant over time. With these assumptions, the actual $\delta^{14}C$ value of the sample can be used to calculate the time passed since the death of the analysed organisms:

$$t = -\frac{1}{\lambda} * \ln \frac{\delta^{14}C}{\delta^{14}C_0}$$

Thereby, t represents the sample age (which equals the time passed since the death of the analysed organisms), λ is a decay constant which is calculated from the ^{14}C half-life ($t_{1/2}$) via $\lambda = \frac{\ln 2}{t_{1/2}}$, $\delta^{14}C$ represents the measured $\delta^{14}C$ value and $\delta^{14}C_0$ the sample's initial $\delta^{14}C$ content.

The ages calculated with this method are referred to as ^{14}C-ages. For samples of marine organisms, ^{14}C-ages have to be corrected for the reservoir effect (Bard et al., 1988). In the upper ocean, surface waters mix with upwelled deep waters, which are depleted in ^{14}C. Therefore, upper ocean organisms will yield ^{14}C-ages which are too old. This artificial aging is referred to as the reservoir effect, which on average amounts to 400 years in the world's oceans (Bard, 1988). Reservoir-corrected ^{14}C-ages are usually reported in years before present (yr BP). However, they are dated relative to the year 1950 rather than relative to the present, as nuclear bomb testing significantly increased the ^{14}C amount in the atmosphere after 1950 (Stuiver and Polach, 1977).

In contrast to the assumption of constant past atmospheric ^{14}C concentration levels, these varied considerably during the last 50,000 years (the time period where radiocarbon datings are possible; Bard et al., 2004). Therefore, ^{14}C-ages have to be calibrated in order to calculate absolute (calendar) ages. The scientific community therefore puts much effort to get combined ^{14}C- and calendar age measurements from samples of the last 50,000 years (e.g. Fairbanks et al., 2005; Hughen et al., 2004). Calendar ages can be obtained directly by dendrochronology and varve chronology as well as by U/Th dating of corals and speleothems (e.g. Chiu et al., 2005; Wang et al., 2001). Fig. 9 gives the most recent compilation of paired ^{14}C- and calendar ages (Fairbanks et al., 2005).

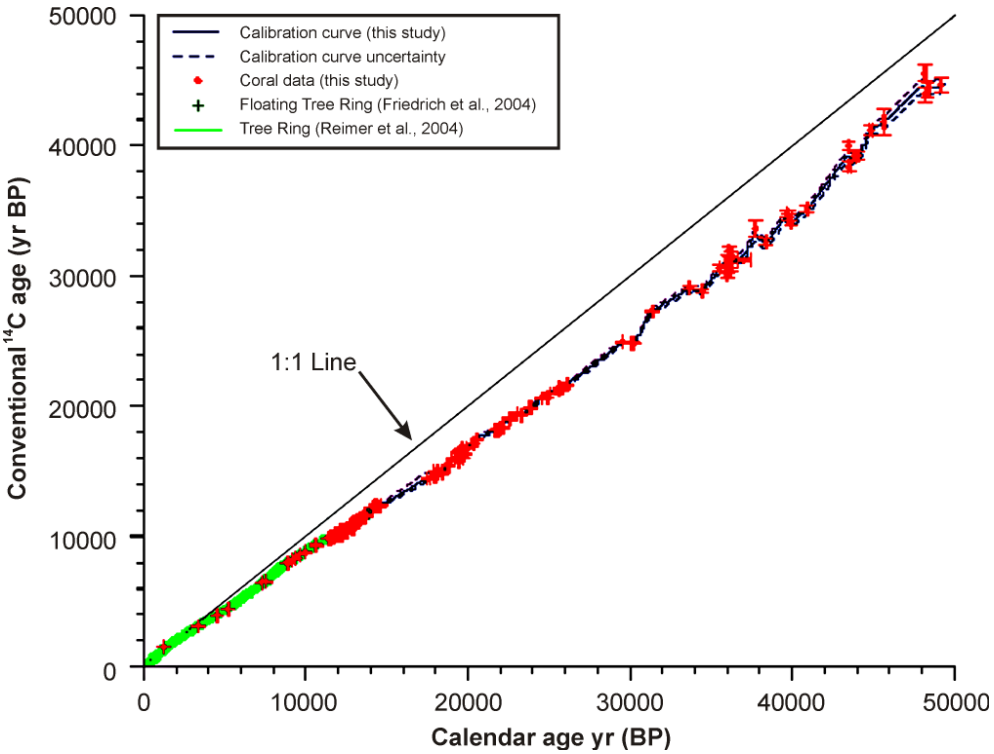

Figure 9: Calibration curve for the conversion of ^{14}C-ages to Calendar Ages (Fairbanks et al., 2005)

This study is based on radiocarbon datings of samples consisting of 600 to 800 foraminifers (representing about 10 µg carbonaceous material per sample). These foraminifers were disintegrated in an acidic solution and the carbon from the foraminiferal shells was oxidised to CO_2. Finally, $\delta^{14}C$ ratios of the CO_2 were measured with an accelerator mass-spectrometer at the Leibniz-Laboratory for Radiometric Dating and Isotope Research of the University of Kiel, Germany. After the calculation of radiocarbon ages from the measured $\delta^{14}C$ values, these were corrected by a uniform reservoir age of 400 years (Bard, 1988) and converted to calendar ages using the calibration curve GRIP_SFCP_2005 of the radiocarbon age calibration program CalPal online (Weninger et al., 2005), which is a statistical mean of various recent radiocarbon age calibration curves with the latest addition coming from Fairbanks et al. (2005; Fig. 9).

3.3 Stable Oxygen Isotopes

There are three stable oxygen isotopes, of which ^{16}O is the most abundant (99.76 %) in the earth system, whereas ^{17}O (0.04%) and ^{18}O (0.2%) contribute a minor portion to the total natural oxygen reservoir (Hoefs, 2003). Most studies concentrate on the ratio of the most abundant isotopes ^{18}O and ^{16}O (Mulitza et al., 2003b). The isotopic composition of a sample thereby is conventionally expressed as $\delta^{18}O$ (in per mil), which represents a relative deviation from a standard:

$$\delta^{18}O(‰) = \left[\frac{\left(^{18}O/^{16}O\right)_{sample} - \left(^{18}O/^{16}O\right)_{s\,\mathrm{tan}\,dard}}{\left(^{18}O/^{16}O\right)_{s\,\mathrm{tan}\,dard}} \right] * 1000$$

Generally, carbonate samples are measured relative to the Vienna Pee-Dee Belemnite (VPDB) standard and water samples relative to the Vienna Standard Mean Ocean Water (VSMOW) standard (Coplen, 1996).

Whenever water undergoes a phase transition, the different masses of ^{18}O and ^{16}O lead to temperature-dependent kinetic fractionation processes of the water parcels (Craig, 1961). Water evaporating from the sea surface is depleted in heavy isotopes relative to ocean water, while rain precipitating from a cloud is enriched relative to the cloud's moisture (Clark and Fritz, 1997). As tropical oceans are the primary source of atmospheric water vapour, poleward transport of meteoric water results in a gradual rainout of water enriched in ^{18}O and depletion of ^{18}O in the remaining moisture (Craig, 1961). Furthermore, decreasing temperatures enhance the gradual rainout of water enriched in ^{18}O during poleward transport of atmospheric moisture (Dansgaard, 1964). Hence, the isotopic composition of precipitation

shows a close relation to geographic factors like latitude, altitude and temperature (Craig, 1961; Dansgaard, 1964; Epstein and Mayeda, 1953).

The distribution of oxygen isotopes in seawater ($\delta^{18}O_w$) is primarily controlled by precipitation and evaporation (Mulitza et al., 2003b). Therefore, it is closely related to the kinetic fractionation processes in atmospheric moisture. The isotopic composition of seawater is also affected by the formation of sea ice, but the fractionation effect is negligible compared to the atmospheric fractionation processes. Variations in continental ice volume, however, have a prominent effect on global $\delta^{18}O_w$. Due to the depletion of $\delta^{18}O$ in atmospheric moisture during transport, continental ice generally has very low $\delta^{18}O_w$ values (Dansgaard, 1964). Therefore, waxing and waning of continental ice caps, which occurred regularly during the late quaternary (Hemming and Hajdas, 2003), changes the oceanic $\delta^{18}O_w$ reservoir. Waxing of ice caps results in trapping isotopically light $\delta^{18}O$ in the ice sheets, while leading to a relative enrichment of isotopically heavy $\delta^{18}O$ in the global ocean. Waning of ice caps, in contrast, results in releasing the trapped isotopically light $\delta^{18}O$ to ocean and leads to decreased global $\delta^{18}O_w$ values. This effect of continental ice volume on global $\delta^{18}O_w$ is called the "ice effect" (Fairbanks, 1989). Estimates for the mean change in global $\delta^{18}O_w$ from the Last Glacial Maximum (LGM) to the Holocene, e.g., range between -1.3 ‰ (Fairbanks, 1989) and -1.0 ‰ (Labeyrie et al., 1987; Schrag and dePaolo, 1993).

The $\delta^{18}O$ values recorded in planktic foraminifers primarily depend on the $\delta^{18}O_w$ values in which these foraminifers calcify. In addition, temperature- and species-dependent fractionation processes occur during the calcification (Mulitza et al., 2003a). Besides temperature and $\delta^{18}O_w$, the so-called carbonate ion or pH effect (Bijma et al., 1999; Spero et al., 1997) and the photosynthetic activity of symbiont algae (Spero and Lea, 1993) influence foraminiferal $\delta^{18}O$ values. The carbonate ion effect reflects the sensitivity of foraminiferal $\delta^{18}O$ values to pH values of surrounding seawater (Spero et al., 1997). Both increased pH values and increased photosynthetic activity result in decreased $\delta^{18}O$ values in foraminiferal shells. The carbonate ion effect may be species-dependent (Mulitza et al., 2003b), as the pH in the microenvironment of foraminiferal shells can deviate considerably from the pH of surrounding seawater (Jørgensen et al., 1985; Wolf-Gladrow et al., 1999). However, as the western tropical Atlantic is no high-productivity area and as pH values are typical of open ocean values, the species-dependent fractionation processes may be neglected in this study.

As temperature has the most prominent effect on foraminiferal $\delta^{18}O$ values besides $\delta^{18}O_w$ of ambient seawater, important issues in evaluating foraminiferal $\delta^{18}O$ values are whether these represent annual average or seasonally biased temperatures and in which depth these foraminifers calcify. This work includes analyses on the foraminiferal species *Globigerinoides ruber* (*G. ruber*), Cibicidoides wuellerstorfi (*C. wuell.*) and *Uvigerina peregrina* (*U. peregr.*). *G. ruber* calcifies in a narrow depth range, probably within the upper 30 to 50 m of the water column (Fairbanks and Wiebe, 1980; Ravelo et al., 1990), and therefore mainly represents sea surface conditions. As there is only little seasonal SST variability in the western tropical Atlantic (Conkright et al., 2002), $\delta^{18}O$ values of *G. ruber* approximately represent annual average sea surface conditions in this region. In the western subtropical Atlantic, however, $\delta^{18}O$ values of *G. ruber* may be a little biased towards summer temperatures. *U.peregr.* and *C. wuell.* are benthic species and reflect ocean bottom seawater conditions. As temperatures are relatively stable in the deep ocean, $\delta^{18}O$ values of these species primarily record the global ice effect and changes in deepwater circulation (e.g. Shackleton et al., 2004).

After deposition, the $\delta^{18}O$ values of foraminiferal shell assemblages may be altered by bioturbation and calcite dissolution. Bioturbation may cause shifts of maxima and minima within a $\delta^{18}O$ record and muting of variations in $\delta^{18}O$ (Mulitza et al., 2003b). Partial dissolution can alter the isotopic composition of foraminiferal shells, especially if $\delta^{18}O$ values are inhomogenously distributed in the shells (Barker et al., 2003). For our investigations, we can neglect these issues as the analysed sediment cores show little bioturbation and we primarily picked foraminifers with minor signs of dissolution.

3.4 Stable Carbon Isotopes

There are two stable carbon isotopes in the earth system, ^{12}C and ^{13}C, with natural abundances of 98.89 % (^{12}C) and 1.11 % (^{13}C; Hoefs, 2003). Paleoceanographic studies of stable carbon isotopes concentrate on the ratio of ^{13}C to ^{12}C, which is reported as relative deviation from a standard:

$$\delta^{13}C(‰) = \left[\frac{\left(^{13}C/^{12}C\right)_{sample} - \left(^{13}C/^{12}C\right)_{s\,\mathrm{tan}\,dard}}{\left(^{13}C/^{12}C\right)_{s\,\mathrm{tan}\,dard}} \right] * 1000$$

For the analysis of $\delta^{13}C$ in carbonates, the same standards are used as for $\delta^{18}O$ analyses (VPDB and VSMOW; Coplen, 1996).

There are three main carbon reservoirs with different average $\delta^{13}C$ values: marine organic matter, terrestrial organic matter and sedimentary carbonates. The production of organic matter (photosynthesis) is associated with fixation of CO_2 into organic biomass:

$$CO_2 + H_2O + energy(sunlight) \Rightarrow CH_2O + O_2$$

Photosynthesis is strongly discriminative in favour of ^{12}C and against ^{13}C (Park and Epstein, 1960; Swart, 1983). The strong preferential uptake of ^{12}C causes marine phytoplankton to form organic matter with $\delta^{13}C$ values which are -20 to -23 ‰ lower than ambient seawater (Garlick, 1974; Hoefs, 2003). Therefore, as photosynthesis only occurs within the euphotic surface layer, the dissolved carbon in surface seawater is strongly enriched in ^{13}C. Carbonaceous organisms living in the euphotic surface layer, in turn, record the resulting $\delta^{13}C$ increase. When organic matter, which is strongly depleted in ^{13}C, sinks from the surface ocean to the deep sea and remineralises there, this remineralisation will cause a lowering of $\delta^{13}C$ in deep waters. This also will be recorded in calcareous deep sea organisms. Hence, increases in export productivity will cause increasing gradients between $\delta^{13}C$ enrichment in surface waters and $\delta^{13}C$ depletion in deep waters.

As nutrient concentration governs the rate of photosynthetic activity in most parts of the ocean, $\delta^{13}C$ correlates to nutrient concentrations in surface waters (Ortiz et al., 1996). Furthermore, as remineralisation of organic matter at depth releases both $\delta^{13}C$ depleted CO_2 and nutrients into the deep water, $\delta^{13}C$ from fossil marine calcareous microorganisms may be used to assess past nutrient distribution in the surface and deep ocean (Boyle and Keigwin, 1985/86; Broecker, 1982; Broecker and Peng, 1982; Ortiz et al., 1996).

As $\delta^{13}C$ behaves as a conservative element in the ocean, changes in $\delta^{13}C$ of deep waters may only arise from mixing with water masses of another $\delta^{13}C$ composition and from remineralisation of organic matter in the deep ocean (Curry et al., 1988; Curry and Lohmann, 1982; Mix and Fairbanks, 1985). Hence, $\delta^{13}C$ of fossil calcareous organisms may be used to identify past deep water flow pathways and their source areas (Shackleton, 1977). Rapid changes of deep ocean $\delta^{13}C$ in areas of high surface productivity caused by remineralisation of organic matter in the deep sea may compromise the usability of $\delta^{13}C$ as deep ocean circulation tracer (Mackensen et al., 1993). However, as this effect is small (McCorkle and Holder, 2001) and limited in spatial extent (Curry and Oppo, 2005), it can be ignored for the assessment of large-scale circulation changes.

The use of $\delta^{13}C$ as deep ocean circulation tracer is mainly independent of terrestrial carbon sources (terrestrial organic and inorganic matter), as these may alter seawater $\delta^{13}C$ only in near-coastal environments. Considerable local $\delta^{13}C$ depletions may arise from the seepage of methane hydrates, which have very low $\delta^{13}C$ values of around -50 ‰ VPDB (Wefer et al., 1994). In the deep sea, which is absent from any methane hydrate deposits, this effect is neglectable as the mass of carbon generated by methane hydrates is not significant on a global scale.

The present-day deep high latitude North Atlantic, e. g., shows deep water $\delta^{13}C$ values around +1.0 ‰, relative to average surface water $\delta^{13}C$ of +1.6 ‰ (Kroopnick, 1985). This low gradient identifies the high latitude North Atlantic as a basin with active deep water formation. In the Weddell Sea of the Southern Ocean, the other major deep water formation area in the global ocean, low iron concentrations limit photosynthetic activity, which is much lower than in the high latitude North Atlantic (de Baar et al., 1995). Therefore, average $\delta^{13}C$ values amount +0.9 ‰ in the surface waters of the Southern Ocean and around +0.5 ‰ in the deep Southern Ocean (Kroopnick, 1985; Mackensen et al., 1993).

The water masses generated in the North Atlantic (North Atlantic Deep Water, NADW) and in the Southern Ocean (Antarctic Intermediate Water, AAIW, and Antarctic Bottom Water, AABW) spread out south- and northward in the deep ocean, respectively. Their flow path can clearly be identified on depth transects of $\delta^{13}C$ in the Atlantic (Fig. 10). NADW thereby can be identified to about 40°S, AAIW to about 40°N and AABW to about 30°N before mixing of these water masses reaches a grade that does not allow their clear identification anymore. As benthic calcareous microorganisms record the $\delta^{13}C$ values of the ambient water mass with some systematic offset (due to so-called vital effects, which result from equilibrium reactions occurring during the metabolism of these organisms), $\delta^{13}C$ values of benthic calcareous microfossils allow the evaluation of changes in the deep ocean circulation.

The Dansgaard/Oeschger cycles and Heinrich events of the last glacial were associated with large variations in the intensity of deep water formation in the North Atlantic (Keigwin and Jones, 1994; Oppo and Lehman, 1995; Vidal et al., 1997). This led to reorganizations of intermediate to deep water currents in the Atlantic, which include shallowing of North Atlantic Deep Water and increasing the $\delta^{13}C$ gradient between intermediate and deep waters (Fig. 10; Boyle and Keigwin, 1987; Broecker, 1991; Curry and Oppo, 2005). This study includes the analysis of benthic foraminiferal $\delta^{13}C$ ratios from the tropical Atlantic which allow investigating these reorganisations of the THC.

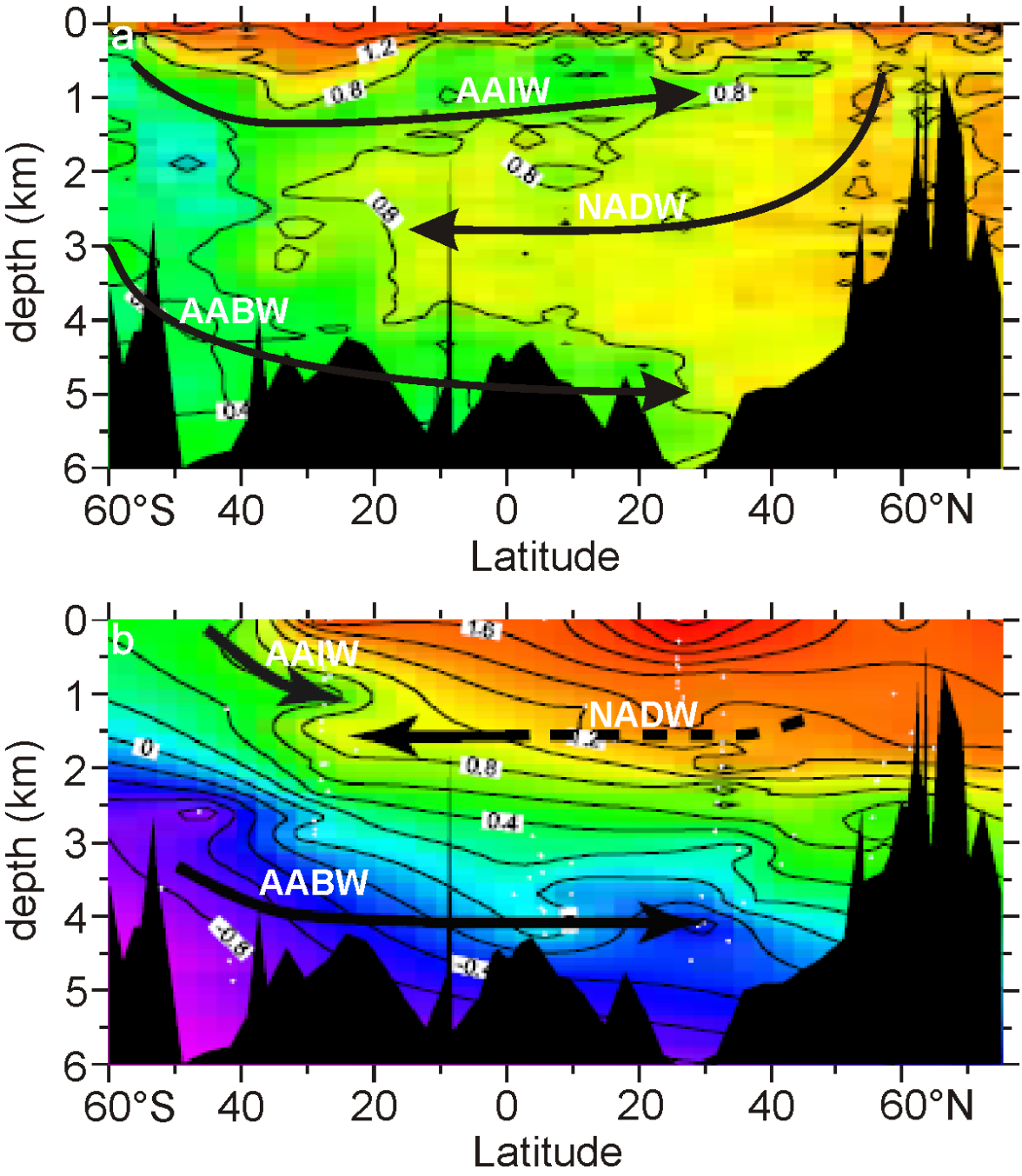

Figure 10: North-South depth profile of $\delta^{13}C$ in **a)** the modern Atlantic and **b)** the glacial Atlantic indicating the pathways of deep ocean currents (Curry and Oppo, 2005). NADW represents North Atlantic Deep Water, AAIW Antarctic Intermediate Water, AABW Antarctic Bottom Water. Note the shallowing of NADW and the strong vertical $\delta^{13}C$ gradient between NADW and AABW during glacial times **(b)**.

3.5 Mg/Ca Ratios

Mg is one of several divalent cations which may substitute for Ca during the formation of biogenic calcium carbonate. Its incorporation into foraminiferal calcite is dependent on the temperature of the surrounding seawater such that foraminiferal Mg/Ca ratios increase with increasing temperature. The temperature sensitivity of planktic foraminiferal Mg/Ca ratios was first reported by Chave (1954) and refined by Blackmon and Todd (1959), Kilbourne and Sen Gupta (1973), Duckworth (1977) and Cronblad and Malmgren (1981). The paleoceanographic application of Mg/Ca thermometry, however, is a relatively recent development which has become widely used in the last decade. Prominent developments in modern Mg/Ca thermometry include the works of Nürnberg et al. (1996), Lea et al. (1999), Elderfield and Ganssen (2000), Anand et al. (2003) and Barker et al. (2004).

Mg/Ca thermometry has distinct advantages over other temperature proxies. As the oceanic residence times for Ca and Mg are relatively long (10^6 and 10^7 years, respectively) the Mg/Ca ratio of seawater may be considered to be constant on glacial/interglacial timescales. Therefore, Mg/Ca ratios provide a temperature proxy independent of sea level changes. Since Mg/Ca and foraminiferal $\delta^{18}O$ are attained from a single medium (i.e. foraminiferal calcite), they can be combined in order to reconstruct $\delta^{18}O_w$ values (e.g. (Elderfield and Ganssen, 2000; Lea et al., 2002; Mashiotta et al., 1999)). This is a distinct advantage over the calculation of $\delta^{18}O_w$ values with other SST proxies such as alkenones or TEX^{86}, as these may record other environmental conditions than foraminifers.

This study includes analyses of foraminiferal Mg/Ca ratios of sediment core GeoB 3910. For each analysis, we used homogenized (crushed and mixed) samples of 30 specimens of *G. ruber* (sized between 350 and 400 µm). Samples were cleaned following the method of Boyle and Rosenthal (1996), which is a refinement of the cleaning method developed by Boyle (1981) and Boyle and Keigwin (1985/86) for the analysis of foraminiferal Cd/Ca and Ba/Ca ratios. The cleaning procedure includes rinsing of the samples in methanol (for the removal of silicates, which primarily constitute of clay minerals), bathing the samples in an oxidative (for the removal of organic matter) and a reductive (for the removal of Fe- and Mn-oxides) solution and leaching the samples in a weak acidic solution (for the removal of Mn-oxide coatings eventually covering the foraminifers). The removal of these contaminants, which may be incorporated into the foraminiferal shells, is necessary because they may contain small amounts of Mg, which would artificially increase foraminiferal Mg/Ca ratios

(Barker et al., 2003). This would result in higher calculated SST than indicated by the pure foraminiferal carbonate.

Fe/Ca ratios measured on the same material like Mg/Ca ratios indicate that possible contaminants have successfully been removed from most samples. About 2 % of all samples still show Fe/Ca ratios higher than 0.4 µg/g after cleaning and were removed from the datasets. For the remaining samples, Fe/Ca ratios do not correlate to temperatures derived from Mg/Ca ratios. Therefore, the bulk of the Fe still present within the foraminiferal shells of these samples is probably bound in minerals which do not contain Mg (e.g. pyrite).

The cleaned samples were measured on an Inductively Coupled Plasma Atomic Emission Spectrometer (ICP-AES, Jobin-Yvon Panorama 2000) at the Lamont-Doherty Earth Observatory of the Columbia University of New York, USA. Whereas the analytical precision of this ICP-AES is better than 0.3 %, the average reproducibility of the samples is better than 2 %. Combined, this accounts for a standard error (1σ) of 0.4°C. Mg/Ca ratios were converted to SST following the calibration of Anand et al. (2003; Fig. 11) for *G. ruber* in the size range of 350 to 500 µm:

$$Mg/Ca = 0.48 * \exp(0.085 * T)$$

$$\Leftrightarrow T = \ln[(Mg/Ca)/0.48]/0.085$$

Thereby, Mg/Ca is the foraminiferal Mg/Ca concentration in $^{mmol}/_{mol}$ and T the temperature in °C.

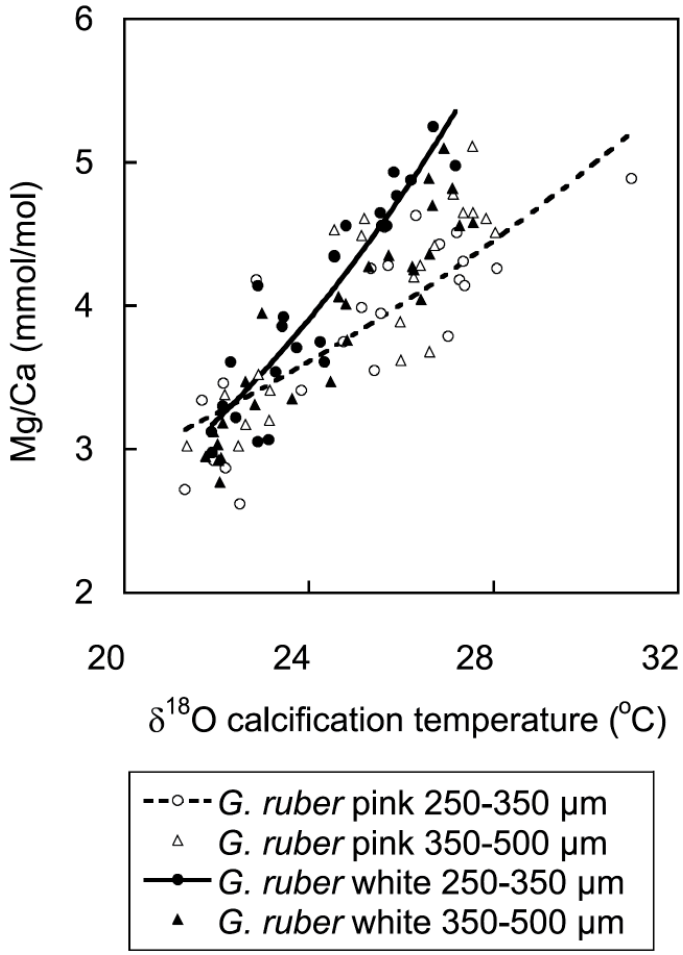

Figure 11: Species and size dependent calibration of foraminiferal Mg/Ca ratios versus calcification temperatures for the species *Globigerinoides ruber white* (used in this study) and *Globigerinoides ruber pink* (Anand et al., 2003)

A great advantage of the calibration of Anand et al. (2003) lies in its species and size dependency. As noted by Anand et al. (2003) and Barker et al. (2005), Mg/Ca temperatures derived from modern multispecies calibrations differ by up to 1°C from temperatures calculated with species dependent calibrations for *G. ruber*.

As the overall LGM – late Holocene SST difference amounts to only 2.0 to 3.5 °C in most tropical regions (Barker et al., 2005), it is important to use a species dependent calibration for calculating Mg/Ca temperatures. Foraminiferal shell size, however, has a minor effect on Mg/Ca temperatures (Anand et al., 2003). The species dependent calibration for G. ruber from Anand et al. (2003) is valid for temperatures between 21 and 28 °C, which covers the range of Mg/Ca temperatures in GeoB 3910.

The preservation of foraminifers is a critical issue for Mg/Ca thermometry. As many planktic foraminifers commonly migrate vertically throughout their life cycle, they record various environmental conditions in their shells. This results in heterogeneity of Mg/Ca ratios within the tests of individual foraminifers (Benway et al., 2003; Elderfield and Ganssen, 2000; Nürnberg, 1995). As the solubility of Mg-carbonates increases with Mg concentration, partial dissolution of foraminiferal shells results in a relative depletion of Mg versus Ca (Brown and Elderfield, 1996; Rosenthal et al., 2000). Therefore, partial dissolution may reduce Mg/Ca temperatures. However, this issue seems not to be critical for mixed layer species like *G. ruber*, as Mg/Ca ratios are probably relatively homogenously distributed in these (Anand et al., 2003; Lea et al., 2000). As we additionally exclusively used well-preserved foraminifers for Mg/Ca analysis, our Mg/Ca records are not subject to reflect partial dissolution conditions.

3.6 X-ray Fluorescence Spectroscopy

The concentrations of the elements with the atomic number 19 (K) to 38 (Sr) in split sediment cores can be analysed with the X-ray Fluorescence (XRF) core scanner of the University of Bremen (Kuhlmann et al., submitted; Röhl and Abrams, 2000). This scanner generates a X-ray beam, which is directed onto the surface of a split sediment core over a 1 cm^2 area. The incident X-rays increase the energy level in the atoms of the sediment core, which results in the emission of an electron from the inner shell of the atom. The emerging vacancy in the inner shell is instantly filled by an electron from an outer shell, which results in a release of energy as radiation. As the wavelength of this radiation is element specific (Potts, 1987), the measurement of the wavelength spectrum allows the calculation of so-called XRF element intensities. These element intensities allow the calculation of element concentrations by calibration of the XRF data with data derived from standard analytical methods on selected samples (Jansen et al., 1998; Kuhlmann et al., submitted). As some sediment properties of the analysed sediment cores influence XRF measurements but not wet chemistry analyses (e.g. pore space and water content; Kuhlmann et al., submitted), however, these calibrations have

to be done for every single core. Therefore, we directly interpret XRF element intensities in this study.

Major advantage of the XRF scanning method is the possibility of relatively rapid, non-destructive high-resolution analysis of split sediment cores. Disadvantages of this method arise from its dependency on pore space and water content of the analysed sediment cores. As the establishment of a calibration for the conversion of element intensities to element concentrations undermines the advantages of the XRF scanning method (the rapid and non-destructive analysis), it is reasonable to interpret element intensities rather than concentrations. Additionally, it is important to note that XRF scans only analyse the surface of split sediment cores, so that scans of material with a laterally heterogeneous composition may not reflect the real sediment composition. As all cores analysed in this thesis show a laterally homogenous sediment composition, the element intensity records presented here are representative for the respective sediment cores.

3.7 References Chapter 3

Anand, P., H. Elderfield & M. H. Conte. (2003). Calibration of Mg/Ca thermometry in planktonic foraminifera from a sediment trap time series. *Paleoceanography* **18,** 28-1 - 28-15.

Arnold, J. R., and Libby, W. F. (1949). Age determinations by radiocarbon content: checks with samples of known age. *Science* **110**.

Bard, E. (1988). Correction of accelerator mass spectrometry ^{14}C ages measured in planktonic foraminifera: Paleoceanographic implications. *Paleoceanography* **3**, 635-645.

Bard, E., Rostek, F., and Ménot-Combes, G. (2004). Radiocarbon calibration beyond 20,000 ^{14}C-yr B.P. by means of planktonic foraminifera of the Iberian Margin. *Quaternary Research* **61,** 204-214.

Barker, S., Cacho, I., Benway, H., and Tachikawa, K. (2005). Planktonic foraminiferal Mg/Ca as a proxy for past oceanic temperatures: a methodological overview and data compilation for the Last Glacial Maximum. *Quaternary Science Reviews* **24,** 821-834.

Barker, S., Greaves, M., and Harry, E. (2003). A study of cleaning procedures used for foraminiferal Mg/Ca paleothermometry. *Geochemistry Geophysics Geosystem* **4,** doi:10.1029/2003GC000559.

Barker, S., Kiefer, T., and Elderfield, H. (2004). Temporal changes in North Atlantic circulation constrained by planktonic foraminiferal shell weights. *Paleoceanography* **19,** doi:10.1029/2004PA001004.

Benway, H. M., Haley, B. A., Klinkhammer, G., and Mix, A. C. (2003). Adaptation of a flow-through leaching procedure for Mg/Ca paleothermometry. *Geochemistry Geophysics Geosystems* **4**.

Bijma, J., Spero, H. J., and Lea, D. W. (1999). Reassessing foraminiferal stable isotope geochemistry: Impact of the oceanic carbonate system (experimental results). *In "Use of proxies in paleoceanography"* (edited by G. Fischer and G. Wefer), pp. 489-512. Springer-Verlag, Berlin.

Blackmon, P. D., and Todd, R. (1959). Mineralogy of some foraminifera as related to their classification and ecology. *Journal of Paleontology* **33,** 1-15.

Bleil, U., et al. (1993). Report and preliminary results of Meteor Cruise 23/2. *Berichte, Fachbereich Geowissenschaften, Universität Bremen* **76**, 133 pp., Bremen.

Boyle, E. A. (1981). Cadmium, zinc, copper, and barium in foraminifera tests. *Earth and Planetary Science Letters* **53,** 11-35.

Boyle, E. A., and Keigwin, L. D. (1985/86). Comparison of Atlantic and Pacific paleochemical records for the last 215,000 years: changes in deep ocean circulation and chemical inventories. *Earth and Planetary Science Letters* **76,** 135-150.

Boyle, E. A., and Keigwin, L. D. (1987). North Atlantic thermohaline circulation during the past 20,000 years linked to high-latitude surface temperature. *Nature* **330,** 35-40.

Boyle, E. A., and Rosenthal, Y. (1996). Chemical hydrography of the South Atlantic during the Last Glacial Maximum: Cd vs. $\delta^{13}C$. *In "The South Atlantic: Present and past Circulation"* (edited by G. Wefer, W. H. Berger, G. Siedler, and D. J. Webb), pp. 423-443. Springer-Verlag, Berlin.

Broecker, W. S. (1982). Glacial to interglacial changes in ocean chemistry. *Progress in Oceanography* **11,** 151-197.

Broecker, W. S. (1991). The great ocean conveyor. *Oceanography* **4,** 79-89.

Broecker, W. S., and Peng, T. H. (1982). "Tracers in the sea." Eldigio Press, New York.

Brown, S. J., and Elderfield, H. (1996). Variations in Mg/Ca and Sr/Ca ratios of planktonic foraminifera caused by postdepositional dissolution: evidence of shallow Mg-dependent dissolution. *Paleoceanography* **11,** 543-551.

Chave, K. E. (1954). Aspects of the biogeochemistry of magnesium 1: Calcareous marine organisms. *Journal of Geology* **62,** 266-283.

Chiu, T.-C., Fairbanks, R. G., Mortlock, R. A., and Bloom, A. L. (2005). Extending the radiocarbon calibration beyond 26000 years before present using fossil corals. *Quaternary Science Reviews* **24,** 1797-1808.

Clark, I., and Fritz, P. (1997). "Environmental isotopes in hydrogeology." Lewis Publishers, CRC Press.

Conkright, M. E., Antonov, J. I., Baranova, O., Boyer, T. P., Garcia, H. E., Gelfeld, R., Johnson, D., O'Brien, T. D., Smolyar, I., and Stephens, C. (2002). "World ocean database 2001, Volume 1: Introduction." U.S. Government Printing Office, Washington, D.C.

Coplen, T. B. (1996). Editoral: More uncertainty than necessary. *Paleoceanography* **11,** 369-370.

Craig, H. (1961). Isotopic variations in meteoric waters. *Science* **133,** 1702.

Cronblad, H. G., and Malmgren, B. A. (1981). Climatically controlled variation of Sr and Mg in Quaternary planktonic foraminifera. *Nature* **291,** 61-64.

Curry, W. B., Duplessy, J. C., Labeyrie, L. D., and Shackleton, N. J. (1988). Changes in the distribution of $\delta^{13}C$ of deep water ΣCO_2 between the last glaciation and the Holocene. *Paleoceanography* **3,** 317-341.

Curry, W. B., and Lohmann, G. P. (1982). Carbon isotopic changes in benthic foraminifera from the western South Atlantic: Reconstruction of glacial abyssal circulation patterns. *Quaternary Research* **18,** 218-235.

Curry, W. B., and Oppo, D. W. (2005). Glacial water mass geometry and the distribution of $\delta^{13}C$ of ΣCO^2 in the western Atlantic Ocean. *Paleoceanography* **20,** doi:10.1029/2004PA001021.

Dansgaard, W. (1964). Stable isotopes in precipitation. *Tellus* **16,** 436-468.

de Baar, H. J. W., de Jong, J. T. M., Bakker, D. C. E., Löscher, B. M., Veth, C., Bathmann, U., and Smetacek, V. (1995). Importance of iron for plankton blooms and carbon dioxide drawdown in the Southern Ocean. *Nature* **373,** 412-415.

Duckworth, D. L. (1977). Magnesium concentration in the tests of the planktonic foraminifer Globorotalia truncatulinoides. *Journal of Foraminiferal Research* **7,** 304-312.

Elderfield, H., and Ganssen, G. (2000). Past temperature and $\delta^{18}O$ of surface ocean waters inferred from foraminiferal Mg/Ca ratios. *Nature* **405,** 442-445.

Epstein, S., and Mayeda, T. (1953). Variation of ^{18}O content of waters from natural sources. *Geochimica et Cosmochimica Acta* **4,** 213-224.

Fairbanks, R. G. (1989). A 17,000-year long glacio-eustatic sea level record: Influence of glacial melting rates on the Younger Dryas event and deep-ocean circulation. *Nature* **342,** 637-642.

Fairbanks, R. G., Mortlock, R. A., Chiu, T.-C., Cao, L., Kaplan, A., Guilderson, T. P., Fairbanks, T. W., Bloom, A. L., Grootes, P. M., and Nadeau, M.-J. (2005). Radiocarbon calibration curve spanning 10,000 to 50,000 years BP based on paired $^{230}Th/^{234}U/^{238}U$ and ^{14}C dates on pristine corals. *Quaternary Science Reviews* **25,** 1781-1796.

Fairbanks, R. G., and Wiebe, P. H. (1980). Foraminifera and chlorophyll maximum: Vertical distribution, seasonal succession and paleoceanographic significance. *Science* **209,** 1524-1526.

Fischer, G., et al. (1996). Report and preliminary results of Meteor cruise M 34-4 Recife–Bridgetown, 19.03. – 15.04.1996, *Berichte, Fachbereich Geowissenschaften, Universität Bremen* **80**, 105 pp., Universität Bremen, Bremen.

Garlick, G. D. (1974). The stable isotopes of oxygen, carbon, hydrogen in the marine environment. *In "The sea"* (edited by E. D. Goldberg), pp. 393-425. John Wiley & Sons, New York.

Godwin, H. (1962). Half-life of radiocarbon. *Nature* **195,** 984.

Hemming, S. R., and Hajdas, I. (2003). Ice-rafted detritus evidence from $^{40}Ar/^{39}Ar$ ages of individual hornblende grains for evolution of the eastern margin of the Laurentide ice sheet since 43 ^{14}C-kyr. *Quaternary International* **99-100,** 29-43.

Hoefs, J. (2003). "Stable Isotope Geochemistry." Springer, Berlin.

Hughen, K. A. et al. (2004). IntCal04 marine radiocarbon age calibration, 0-26 cal. kyr BP. *Radiocarbon* **46,** 1059-1086.

Jansen, J. H. F., Gaast, S. J. V., Koster, B., and Vaars, A. J. (1998). CORTEX, a shipboard XRF-scanner for element analyses in split sediment cores. *Marine Geology* **151,** 143-153.

Jørgensen, B. B., Erez, J., Revsbech, N. P., and Cohen, Y. (1985). Symbiotic photosynthesis in a planktonic foraminifera, Globigerinoides sacculifer (Brady), studied with microelectrodes. *Limnologic Oceanography* **30,** 1253-1267.

Keeling, R. F., Najjar, R. G., Bender, M. L., and Tans, P. P. (1993). What measurements of atmospheric oxygen can tell us about the global carbon cycle. *Global Biogeochemical Cycles* **7,** 37-67.

Keigwin, L. D., and Jones, G. A. (1994). Western North Atlantic evidence for millennial-scale changes in ocean circulation and climate. *Journal of Geophysical Research* **99,** 12397-12410.

Kilbourne, R. T., and Sen Gupta, B. K. (1973). Elemental composition of planktonic foraminiferal tests in relation to temperature-depth habitats and selective solution. Geological Society of America, *Abstracts with Programs* **5**, 408-409.

Kroopnick, P. (1985). The distribution of carbon-13 in the world oceans. *Deep-Sea Research* **32,** 57-84.

Kuhlmann, H., Meggers, H., Moreno, A., Freudenthal, T., Kasten, S., Hensen, C., and von Oppen, C. (submitted). Meridional shifts of the mediterranean and monsoonal climate system off Northwest Africa during the last 130 kyr: Implications from river discharge. *International Journal of Earth Sciences*.

Labeyrie, L. D., Duplessy, J. C., and Blanc, P. L. (1987). Variations in mode of formation and temperature of oceanic deep waters over the past 125,000 years. *Nature* **327,** 477-482.

Lea, D. W., Martin, P. A., Pak, D. K., and Spero, H. J. (2002). Reconstructing a 350 ky history of sea level using planktonic Mg/Ca and oxygen isotope records from a Cocos Ridge core. *Quaternary Science Review* **21,** 283-293.

Lea, D. W., Mashiotta, T. A., and Spero, H. J. (1999). Controls on magnesium and strontium uptake in planktonic foraminifera determined by live culturing. *Geochimica et Cosmochimica Acta* **63,** 2369-2379.

Lea, D. W., Pak, D. K., and Spero, H. J. (2000). Climate impact of Late Quaternary equatorial Pacific sea surface temperature variations. *Science* **289,** 1719-1724.

Mackensen, A., Hubberten, H. W., Bickert, T., Fischer, G., and Fütterer, D. K. (1993). The $\delta^{13}C$ in benthic foraminiferal tests on Fontbotia wuellerstorfi (Schwager) relative to the $\delta^{13}C$ of dissolved inorganic carbon in Southern Ocean deep water: Implications for glacial ocean circulation models. *Paleoceanography* **8,** 586-610.

Mashiotta, T. A., Lea, D. W., and Spero, H. J. (1999). Glacial-interglacial changes in subantarctic sea surface temperature and $\delta^{18}O_w$ using foraminiferal Mg. *Earth and Planetary Science Letters* **170,** 417-432.

McCorkle, D., and Holder, A. L. (2001). Calibration studies of benthic foraminiferal isotopic composition: Results from the Southeast Pacific. *EOS Trans. AGU **82**, Fall Meeting Supplement*.

Mix, A. C., and Fairbanks, R. G. (1985). North Atlantic surface ocean control of Pleistocene deep-ocean circulation. *Earth and Planetary Science Letters* **73,** 231-243.

Mulitza, S., Boltovskoy, D., Donner, B., Meggers, H., Paul, A., and Wefer, G. (2003a). Temperature:$\delta^{18}O$ relationships of planktonic foraminifera collected from surface waters. *Palaeogeography, Palaeoclimatology, Palaeoecology* **202,** 143-152.

Mulitza, S., Donner, B., Fischer, G., Paul, A., Pätzold, J., Rühlemann, C., and Segl, M. (2003b). The South Atlantic oxygen isotope record of planktic foraminifera. *In "The South Atlantic in the Late Quaternary: Reconstruction of material budgets and current systems"* (edited by G. Wefer, S. Mulitza, and V. Ratmeyer), pp. 121-142. Springer-Verlag, Berlin.

Nürnberg, D. (1995). Magnesium in tests of Neogloboquadrina pachyderma (sinistral) from high northern and southern latitudes. *Journal of Foraminiferal Research* **25,** 350-368.

Nürnberg, D., Bijma, J., and Hemleben, C. (1996). Assessing the reliability of magnesium in foraminiferal calcite as a proxy for water mass temperatures. *Geochimica et Cosmochimica Acta* **60,** 803-814.

Oppo, D. W., and Lehman, S. J. (1995). Suborbital timescale variability of North Atlantic Deep Water during the past 200,000 y. *Paleoceanography* **10,** 901-910.

Ortiz, J. D., Mix, A. C., Rugh, W., Watkins, J. M., and Collier, R. W. (1996). Deep-dwelling planktonic foraminifera of the northeastern Pacific Ocean reveal environmental control of oxygen and carbon isotopic disequilibria. *Geochimica et Cosmochimica Acta* **60,** 4509-4523.

Park, R., and Epstein, S. (1960). Carbon isotope fractionation during photosynthesis. *Geochimica et Cosmochimica Acta* **21,** 110-126.

Potts, P. J. (1987). "A handbook of silicate rock analysis." Blackie, Glasgow.

Ravelo, A. C., Fairbanks, R. G., and Philander, S. G. H. (1990). Reconstructing tropical Atlantic hydrography using planktonic foraminifera and an ocean model. *Paleoceanography* **5,** 409-431.

Röhl, U., and Abrams, L. J. (2000). High-resolution, downhole, and nondestructive core measurements from sites 999 and 1001 in the Caribbean Sea: Application to the Late Paleocene Thermal Maximum. *In "Proceedings of the Ocean Drilling Program, scientific results **165**"* (edited by R. M. Leckie, H. Sigurdsson, G. D. Acton, and G. Draper), pp. 191-203.

Rosenthal, Y., Lohmann, G. P., Lohmann, K. C., and Sherrell, R. M. (2000). Incorporation and preservation of Mg in Globigerinoides sacculifer: implications for reconstructing the temperature and O-18/O-16 of seawater. *Paleoceanography* **15,** 135-145.

Schrag, D. P., and dePaolo, D. J. (1993). Determination of $\delta^{18}O$ of seawater in the deep ocean during the Last Glacial Maximum. *Paleoceanography* **8,** 1-6.

Shackleton, N. J. (1977). ^{13}C in Uvigerina: Tropical rainforest history and the equatorial Pacific carbonate dissolution cycles. *In "Fate of fossil fuel CO_2 in the oceans"* (edited by N. Anderson and A. Malahof), pp. 401-427. Plenum, New York.

Shackleton, N. J., Fairbanks, R. G., Chiu, T.-C., and Parrenin, F. (2004). Absolute calibration of the Greenland time scale: Implications for Antarctic time scales and for $\delta^{14}C$. *Quaternary Science Reviews* **23,** 1513-1522.

Spero, H. J., Bijma, J., Lea, D. W., and Bemis, B. B. (1997). Effect of seawater carbonate concentration on foraminiferal carbon and oxygen isotopes. *Nature* **390,** 497-500.

Spero, H. J., and Lea, D. W. (1993). Intraspecific stable isotope variability in the planktic foraminifera Globigerinoides sacculifer: Results from laboratory experiments. *Marine Micropaleontology* **22,** 221-234.

Stuiver, M., and Polach, H. A. (1977). Discussion: Reporting of ^{14}C data. *Radiocarbon* **19,** 355-363.

Swart, P. K. (1983). Carbon and oxygen isotope fractionation in scleractinian corals: A review. *Earth-Science Reviews* **19,** 51-80.

Vidal, L., Labeyrie, L., Cortijo, E., Arnold, M., Duplessy, J. C., Michel, E., Becque, S., and van Weering, T. C. E. (1997). Evidence for changes in the North Atlantic Deep Water linked to meltwater surges during the Heinrich events. *Earth and Planetary Science Letters* **146,** 13-27.

Wang, Y. J., Cheng, H., Edwards, R. L., An, Z. S., Wu, J. Y., Shen, C.-C., and Dorale, J. A. (2001). A high-resolution absolute-dated Late Pleistocene monsoon record from Hulu Cave, China. *Science* **294,** 2345-2348.

Wefer, G., Heinze, P.-M., and Berger, W. H. (1994). Clues to ancient methane release. *Nature* **369,** 282.

Wolf-Gladrow, D. A., Bijma, J., and Zeebe, R. E. (1999). Model simulation of the carbonate chemistry in the microenvironment of symbiont bearing foraminifera. *Marine Chemistry* **64,** 181-198.

4 Manuscripts

4.1 Outline of Manuscripts

The main part of this thesis is divided into three manuscripts, which have been submitted or are to be submitted to peer-reviewed international journals.

The first manuscript "Forcing of tropical South American precipitation during the last 63,000 years" (*Gerrit M. N. Heil, Helge W. Arz, Peter B. deMenocal and Gerold Wefer*) analyses the temporal and regional patterns of millennial-scale precipitation changes in the tropics and the mechanisms causing these precipitation shifts. It shows tropical precipitation patterns vary coincidently with millennial-scale shifts in high northern latitude temperature and reorganisations of the oceanic THC. Furthermore, it provides evidence for a mechanistic coupling of tropical precipitation patterns to the temperature gradient between the tropics and the middle to high northern latitudes via the ITCZ. This is contrasting to the modern climate system, where tropical Atlantic SST define the position of the ITCZ.

The second manuscript "Last glacial millennial-scale changes in Atlantic Thermohaline Circulation and Northeast Brazilian precipitation" (*Gerrit M. N. Heil, Helge W. Arz and Gerold Wefer*) investigates the linkage between millennial-scale precipitation pattern changes in the tropics and reorganisations of the oceanic THC. It demonstrates both these parameters are closely coupled to high latitude North Atlantic SST and therefore vary coincidently. This provides an independent stratigraphic validation of the coupling of changes in tropical precipitation patterns to variations in the meridional temperature gradient in the North Atlantic. This paper furthermore analyses the regional pattern of millennial-scale precipitation changes in the South American tropics in more detail than the first one. It gives evidence for a close coupling of the spatial extent of ITCZ shifts to the amplitude of variations in the North Atlantic's meridional temperature gradient and thereby explains the difference between precipitation pattern changes in the equatorial and non-equatorial South American tropics.

The third manuscript "Extent of high northern latitude temperature forcing on millennial-scale precipitation changes in eastern South America" (*Gerrit M. N. Heil, Helge W. Arz, Hermann Behling and Gerold Wefer*) provides a focus study of the spatial extent of millennial-scale ITCZ shifts in eastern South America. It shows tropical precipitation patterns are dominated by millennial-scale changes, whereas variations of orbital frequency govern subtropical precipitation patterns. Subordinate millennial-scale variations in precipitation patterns related to ITCZ shifts, however, are still observable in the eastern South American subtropics.

4.2 Manuscript 1: Forcing of tropical South American precipitation during the last 63,000 years

Gerrit M. N. Heil[1], Helge W. Arz[2], Peter B. deMenocal[3] and Gerold Wefer[1]

1 DFG Research Center Ocean Margins, Universität Bremen, P.O. Box 330440, D-28334 Bremen, Germany (gerrit.heil@uni-bremen.de)

2 GeoForschungZentrum Potsdam, Telegrafenberg C322, D-14473 Potsdam, Germany

3 Lamont-Doherty Earth Observatory, Columbia University, Palisades, New York 10964 (NY)

submitted to *Nature*

Abstract

Modelled impacts of future climate change include significant drying of tropical and subtropical semiarid regions. To assess the impact of future climate shifts on natural freshwater supply, it is important to improve our mechanistic understanding of past low-latitude hydrologic changes. In this endeavour, millennial-scale climate changes of the last glacial hold great potential to investigate these mechanisms. Here, we present combined bulk sediment Ti/Ca and foraminiferal Mg/Ca records from the western tropical Atlantic, which give insight into the hydrologic regime of adjacent Northeast Brazil and sea surface temperatures of the western tropical Atlantic during the last 63 kyrs. The South American tropical hydrologic system shows significant millennial-scale changes coincident with Greenland Dansgaard/Oeschger cycles. We demonstrate these changes are primarily driven by shifts in the position of the Intertropical Convergence Zone, which, in turn, is governed by the temperature gradient between high and low latitude North Atlantic. Variations in tropical Atlantic sea surface temperatures, however, affect the South American tropical hydrologic system only secondarily on millennial timescales.

The global climate of the last glacial was extremely variable on millennial timescales. Climate variations occurred in quasi-regular cycles of approximately 1,470 yrs duration, called Dansgaard/Oeschger (D/O) cycles (Dansgaard et al., 1993). These were first observed in Greenland and North Atlantic sediments (e.g. Bond et al., 1993; Dansgaard et al., 1993; Grootes and Stuiver, 1997), but have since been recorded over large parts of the northern hemisphere (Cacho et al., 1999; Hendy and Kennet, 1999) and the tropics (Arz et al., 1998; Schulz et al., 1998; Wang et al., 2001) as well as in some parts of the southern hemisphere (Lowell, et al., 1995). Whereas D/O cycles are mainly expressed as temperature shifts in the high and mid-latitudes, they primarily manifest themselves in terms of variations in precipitation in the low latitudes (Broecker and Hemming, 2001). The established climatic links between these regions implicate global reorganizations of the atmospheric wind systems, which are amplified and supported by reorganizations of the oceanic thermohaline circulation (THC; Stocker, 2000).

Some D/O stadials are associated with so-called Heinrich (H) events, which are associated with larger disruptions of the oceanic THC than observed for D/O events, and therefore show stronger variations in temperature and precipitation in many records (e.g. Bard, 2002; Peterson et al., 2000; Schulz et al., 1998; Wang et al., 2001). In the semiarid region of Northeast (NE) Brazil, which is intensely prone to variations in freshwater supply (Hastenrath, 1990), corresponding precipitation shifts have been observed during H events (Arz et al., 1998; Behling et al., 2000; Jennerjahn et al., 2004; Wang et al., 2004). However, it remains unclear whether NE Brazilian precipitation also varied during D/O cycles. Therefore, we reconstructed NE Brazilian precipitation changes during the last glacial based on terrestrial sediment influx into sediment core GeoB 3910 from the upper continental slope off NE Brazil (Fig. 12; 4°14,7' S, 36°20,7' W, 2362 m water depth). Modern NE Brazilian precipitation rates primarily depend on the position of the Intertropical Convergence Zone (ITCZ) in austral summer (Hastenrath, 1990) and this, in turn, depends on sea surface temperatures (SST) in the tropical Atlantic (Hastenrath, 1990). Therefore, we also analyzed SST by means of foraminiferal Mg/Ca ratios based on the same material. This allows to directly compare changes in the NE Brazilian hydrologic system and western tropical Atlantic SST.

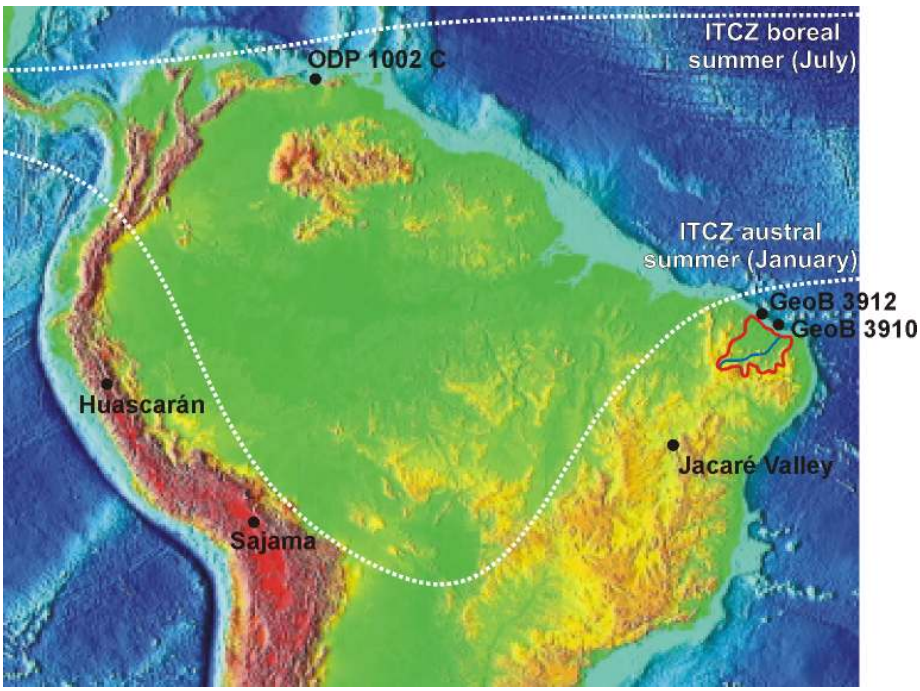

Figure 12: Map of northern South America showing the location of precipitation records mentioned in the text and the maximum northern and southern position of the ITCZ in the modern climate system

The records include the marine sediment core ODP 1002 C from the Southeast Caribbean Cariaco Basin (off North Venezuela; Peterson et al., 2000), the Peruvian Huascarán (Thompson et al., 1995) and Bolivian Sajama (Thompson et al., 1998) ice cores, the Jacaré valley stalagmite and travertine dating record (Wang et al., 2004), and the marine sediment cores GeoB 3910 (Arz et al., 1998; this study) and 3912 (Behling et al., 2000; Jennerjahn et al., 2004). The area marked in red represents the catchment area of the Rio Piranhas, which represents the source for terrestrial sediments of GeoB 3910 and 3912.

Sediment core GeoB 3910 provides an archive of NE Brazilian and western tropical Atlantic climate for the last 63 cal. kyrs BP. We analyzed Ti/Ca ratios for estimating the terrestrial influx into the study site. As Ti in GeoB 3910 represents the siliciclastic sediment fraction and mainly derives from the erosion of tropical soils, whereas Ca mainly derives from marine biogenic carbonates (Arz et al., 1998), the Ti/Ca ratio is indicative of the ratio of terrestrial influx versus marine carbonate production. Maximum Ti/Ca ratios and sedimentation rates occur during H event stadials, which have been identified before as wet periods in NE Brazil (Arz et al., 1998; Behling et al., 2000; Jennerjahn et al., 2004; Wang et al., 2004). As eolian input of African dust into the study site plays a minor role only (Zabel et al., 2001) and dust input from South America is negligible due to prevailing easterly trade winds, Ti/Ca ratios mainly represent riverine terrestrial influx from NE Brazil and serve as an indicator of the intensity of fluvial runoff and precipitation in NE Brazil.

Ti/Ca ratios are highly variable on millennial timescales and show changes coincident with Greenland D/O cycles (Fig. 13f). Whereas interstadial Ti/Ca ratios lie between 0.3 and 1, D/O stadials feature approximately doubled interstadial values (1.2 to 2.2), H event stadials about 20 times the interstadial values (10.0 to 30.0) and the YD four times the interstadial values (2.0 to 4.0). During the Holocene, Ti/Ca ratios are low and stable (< 0.2). The doubling of Ti/Ca ratios from interstadials to D/O stadials indicates NE Brazilian precipitation increased significantly during D/O cycles. However, as H event stadial Ti/Ca ratios are an order of magnitude higher than D/O stadial ones, the precipitation increase was much more pronounced during H event stadials. Although a quantitative estimation of NE Brazilian precipitation is not possible with GeoB 3910 Ti/Ca ratios, the implied relative precipitation rate changes are large.

In contrast to the Ti/Ca ratios, there is no uniform relation between western tropical Atlantic SST and Greenland D/O cycles. SST increased during some stadials, but exhibit minima during others (Fig. 13d). H events and D/O cycles are known to coincide with reorganizations of the THC (Bond et al., 1993), also affecting SST in the western tropical Atlantic (Stocker, 2000). We therefore assume the western tropical South Atlantic is located in a transitional zone of the Atlantic see-saw pattern (Stocker, 2000), thus being affected by North Atlantic cooling during some H events and by South Atlantic warming during others. Additionally, SST of the subtropical southeast Atlantic are suggested to be driven by southern hemisphere insolation (Sachs et al., 2001), and western tropical Atlantic SST probably show a complex signal influenced by THC reorganizations and southern hemisphere insolation variability.

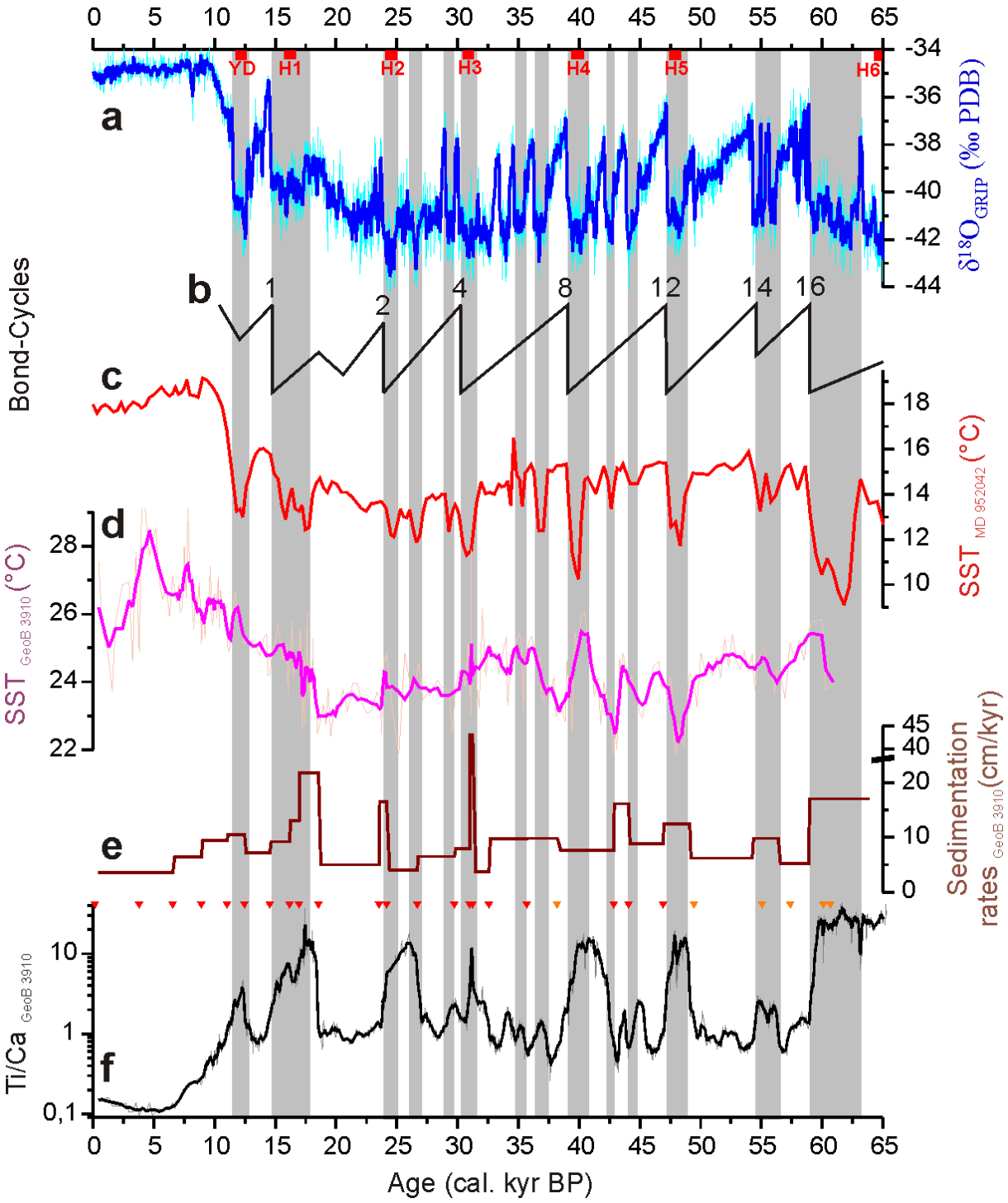

Figure 13: Western tropical Atlantic sea surface temperature and northeast Brazilian precipitation records compared to Greenland and North Atlantic temperatures.

a) GRIP $\delta^{18}O$ record from central Greenland (Shackleton et al., 2004); **b)** schematic Bond Cycles from the high latitude North Atlantic (Bond et al., 1993); **c)** Alkenone SST of sediment core MD 952042 from the eastern temperate North Atlantic (Bard, 2002); **d)** Mg/Ca SST of sediment core GeoB 3910; **e)** sedimentation rates of sediment core GeoB 3910; **f)** bulk sediment Ti/Ca record of sediment core GeoB 3910. Red triangles mark radiocarbon datings, orange triangles indicate where the Ti/Ca record has been tuned to GRIP $\delta^{18}O$, YD marks the Younger Dryas and H1 to H6 denote Heinrich events 1 to 6.

The observed variations in NE Brazilian precipitation probably arise from shifts in the position of the ITCZ. On the long-term average, the ITCZ lies north of the catchment area of the Rio Piranhas throughout the year in the modern climate system (Fig. 12), causing semiarid conditions in the catchment area (Hastenrath, 1990). Years of an anomalous southward displacement of the ITCZ during austral summer are marked by high precipitation in NE Brazil, whereas years of an anomalous northern ITCZ position are often associated with drought events (Hastenrath, 1990). Assuming a similar mechanism for NE Brazilian precipitation during the last glacial, the ITCZ was probably shifted southward during D/O stadials and reached the catchment area of the Rio Piranhas more often than in the modern climate system, causing a modest increase in precipitation. During H event stadials, the ITCZ was shifted further southward than during D/O stadials, reaching the catchment area of the Rio Piranhas quite regularly and leading to a significant increase in precipitation.

To constrain the spatial extent of ITCZ shifts during stadials, we compare our precipitation record to other records from northern South America (Fig. 14). A Ti/Ca record from Cariaco Basin sediment core ODP 1002 C indicates wet Venezuelan conditions during interstadials and dry conditions during stadials (Peterson et al., 2000). Lowest Venezuelan precipitation occurred during H event stadials. A speleothem and travertine growth record from the interior NE Brazilian Jacaré Valley suggests wet conditions were confined to H event stadials there (Wang et al., 2004). During other stadials, interstadials and the Holocene, the interior of NE Brazil was relatively dry, suppressing speleothem and travertine growth. In western South America, oxygen isotope records from the Huascarán (Peru; Thompson et al., 1995) and Sajama (Bolivia; Thompson et al., 1998) ice cores indicate wet conditions during the stadials associated with H1 and the YD. This is supported by a record of natural γ-radiation from the Bolivian Andean lake Salar de Uyuni, which serves as an indicator of clay mineral content and points to wet conditions during the YD and H events 1 to 5 (Baker et al., 2001).

Collectively, these various paleoclimate records support our conclusion based on GeoB 3910 Ti/Ca ratios that the ITCZ shifted southward during cool North Atlantic intervals. A southward displacement of the ITCZ would account for dryer conditions in Venezuela (Peterson et al., 2000) and wetter conditions in NE Brazil (Arz et al., 1998; Behling et al., 2000; Jennerjahn et al., 2004; Wang et al., 2004; this study), NE Peru (Thompson et al., 1995) and NE Bolivia (Baker et al., 2001; Thompson et al., 1998). In contrast to the modern climate system, however, these ITCZ shifts were not driven by changes in tropical Atlantic SST. This follows from the comparison of Ti/Ca ratios and Mg/Ca SST from GeoB 3910, which show no consistent relation to each other as Ti/Ca ratios are high during all stadials, whereas Mg/Ca

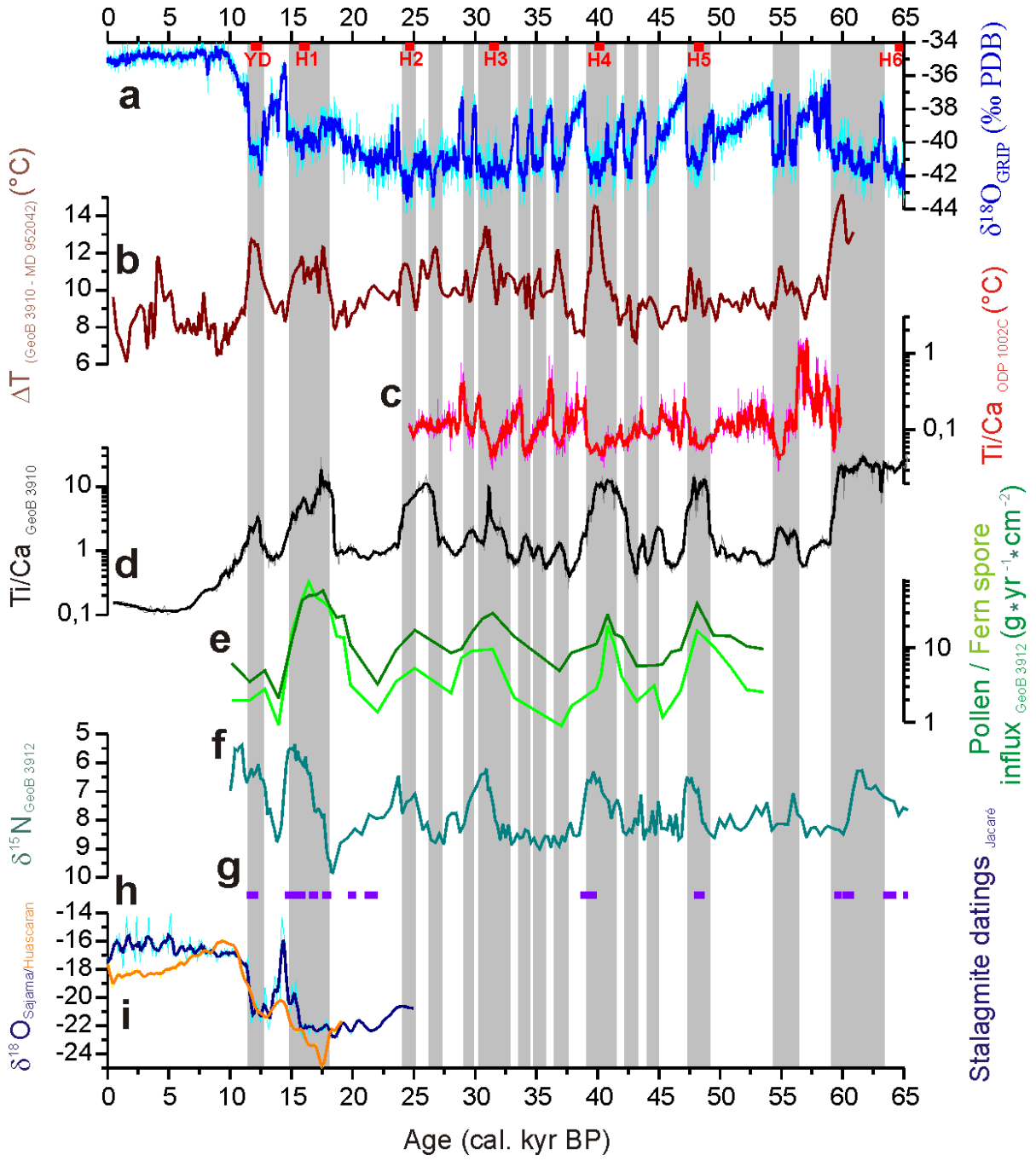

Figure 14: Compilation of South American precipitation records suggest episodic shifts of the ITCZ.

a) GRIP $\delta^{18}O$ from central Greenland (Shackleton et al., 2004); **b)** SST difference between the western tropical Atlantic (Fig. 13d) and the eastern temperate North Atlantic (Fig. 13c); **c)** Ti/Ca of sediment core ODP 1002 C from the Cariaco Basin (Peterson et al., 2000); **d)** Ti/Ca of sediment core GeoB 3910; **e)** pollen and fern spore influx from sediment core GeoB 3912, western tropical Atlantic (Behling et al., 2000); **f)** $\delta^{15}N$ of organic material from sediment core GeoB 3912 (Jennerjahn et al., 2004); **g)** stalagmite and travertine datings from the central NE Brazilian Jacaré Valley (Wang et al., 2004); **h)** $\delta^{18}O$ of the Sajama ice core, Peru (Thompson et al., 1998); **i)** $\delta^{18}O$ of the Huascarán ice core, Bolivia (Thompson et al., 1995). YD marks the Younger Dryas and H1 to H6 denote Heinrich events 1 to 6.

SST feature minima during some stadials but maxima during others (Fig 13). Maxima in GeoB 3910 Ti/Ca ratios rather coincide with cold periods in the North Atlantic as shown e.g. by SST off the Iberian Margin (Bard, 2002; Fig. 13).

A modelling study of Chiang et al. (2005) addresses the relation between tropical rainfall patterns and high northern latitude temperatures. In their simulations, pronounced high northern latitude cooling increases the temperature gradient between high and low latitudes in the northern hemisphere during stadials. This induces an intensification of the northern hemisphere atmospheric circulation, which subsequently cools the northern mid- and low latitudes. Due to cooler northern tropics, the ITCZ shifts southward and changes the tropical atmospheric circulation, leading to drying of the northern tropics and wetter conditions in the southern tropics. This agrees with the reconstructed variations in tropical South American precipitation (Arz et al., 1998; Baker et al., 2001; Behling et al., 2000; Jennerjahn et al., 2004; Peterson et al., 2000; Thompson et al., 1995, 1998; Wang et al., 2004; this study). To test the hypothesis of the dependency of the ITCZ position on the meridional temperature gradient in the northern hemisphere (Chiang et al., 2005), we calculated a SST gradient between the eastern temperate North Atlantic and the western tropical Atlantic and compared it to the reconstructed NE Brazilian precipitation changes (Fig. 14). As changes in this meridional SST gradient covary closely with NE Brazilian precipitation shifts, our data generally confirm the modeling results of Chiang et al. (2005).

We presented evidence that Greenland D/O cycles are accompanied by changes in the tropical hydrologic system caused by shifts in the position of the ITCZ. The rate of ITCZ shift is dynamically linked to the magnitude of change in the North Atlantic's meridional SST gradient. For future climate change, this possibly implies modest high northern latitude temperature shifts could alter the tropical climate system significantly, changing precipitation and water supply in ecologically vulnerable tropical regions. For societies already or nearly facing water scarcity, this might present severe impacts.

Methods

Material

Sediment core GeoB 3910 consists of homogenous foraminifer and nanofossil bearing ooze to clay. We analysed the upper 507 cm of the core, which represent an undisturbed, continuous sediment sequence.

Stratigraphy

The stratigraphy of GeoB 3910 is based on 22 calibrated and linearly interpolated radiocarbon ages spanning the last 47 cal. kyrs (Table 3). Radiocarbon dating was performed on mainly monospecific (*Globigerinoides sacculifer*) carbonate samples at the Leibniz Laboratory in Kiel, Germany. Radiocarbon ages were uniformly corrected for a reservoir age of 400 years (Bard, 1988) and calibrated with CalPal using the CalPal_SFCP_2005 calibration curve (Weninger et al., 2005). As maxima in the bulk sediment Ti/Ca ratio of GeoB 3910 coincide with GRIP $\delta^{18}O$ minima in the radiocarbon dated part, the Ti/Ca signal was used to adjust the older part (47 cal. kyr and older) of GeoB 3910 to the GRIP record. GeoB 3910 spans the last 63 cal. kyr BP with highly variable sedimentation rates between 3.5 and 43 cm/kyr. Average sedimentation rates are 8 cm/kyr.

Table 3: Datings for age model of sediment core GeoB 3910 (supplementary information)

Accelerator mass spectrometry (AMS) radiocarbon (^{14}C) ages were obtained from monospecific (*Globigerines sacculifer*) samples. ^{14}C ages were corrected for a reservoir age of 400 years (Bard, 1988) and calibrated with CalPal using the CalPal_SFCP_2005 calibration curve (Weninger et al., 2005). Correlations to GRIP were obtained from correlation of GeoB 3910 Ti/Ca ratios to GRIP $\delta^{18}O$ (Shackleton et al., 2004).

Core depth (cm)	^{14}C-age (yr)	+error (yr)	-error (yr)	Cal. age (yr)	±error (yr)	Type of dating	Lab ID
0	565	30	30	170	90	AMS ^{14}C dating	KIA 6800
13	3930	35	35	3800	60	AMS ^{14}C dating	KIA 6799
23	6160	40	40	6560	60	AMS ^{14}C dating	KIA 6798
38	8430	40	40	8900	100	AMS ^{14}C dating	KIA 7225
58	10090	60	60	11020	140	AMS ^{14}C dating	KIA 6815
73	10940	70	70	12460	200	AMS ^{14}C dating	KIA 6814
88	12840	110	100	14550	370	AMS ^{14}C dating	KIA 6813
103	13550	70	70	16170	500	AMS ^{14}C dating	KIA 25825
113	14000	70	70	16940	230	AMS ^{14}C dating	KIA 25824
148	15780	110	110	18550	250	AMS ^{14}C dating	KIA 6812
173	20000	170	160	23540	280	AMS ^{14}C dating	KIA 6811
183	20580	150	150	24150	310	AMS ^{14}C dating	KIA 25822
193	22480	220	210	26670	440	AMS ^{14}C dating	KIA 6808
213	25130	260	250	29730	320	AMS ^{14}C dating	KIA 25821
223	26830	360	350	30990	270	AMS ^{14}C dating	KIA 6807
233	27160	310	300	31220	220	AMS ^{14}C dating	KIA 25820
238	28280	430	410	32580	780	AMS ^{14}C dating	KIA 6806
268	30860	430	410	35680	400	AMS ^{14}C dating	KIA 22411
293				38940		Correlation to GRIP	
328	38600	1610	1340	42830	790	AMS ^{14}C dating	KIA 6804
348	41000	860	780	44070	770	AMS ^{14}C dating	KIA 21829
373	44480	1340	1150	46920	1690	AMS ^{14}C dating	KIA 21830
400				49100		Correlation to GRIP	
432				54240		Correlation to GRIP	
453				56390		Correlation to GRIP	
538				65990		Correlation to GRIP	

Bulk sediment Ti/Ca ratios

At intervals of 1 cm (last 9 kyrs, average time resolution of 225 yrs) to 0.4 cm (9 – 63 kyrs, average time resolution of 45 yrs), GeoB 3910 was analyzed for bulk sediment chemistry on the XRF core scanner of the University of Bremen (Röhl and Abrams, 2000).

Mg/Ca paleothermometry

We measured Mg/Ca ratios of the foraminifer *Globigerinoides ruber* for the calculation of SST. Homogenized samples of 30 specimens (350 – 400 μm) were analyzed in a resolution of 2 cm (average time resolution of 250 yrs), in parts (e.g. YD, H1, Holocene) of 1 cm. Every fourth sample was analyzed in duplicate. Cleaned samples (Boyle and Rosenthal, 1996) were measured on an Inductively Coupled Plasma Atomic Emission Spectrometer (Jobin-Yvon Panorama 2000) at the Lamont-Doherty Earth Observatory of the Columbia University of New York, USA. Analytical precision (1σ) is better than 0.2 – 0.3 %, average reproducibility of the standards 2.6 % and average reproducibility of the samples 1.6 % (0.3 – 0.4 °C). The Mg/Ca data were converted to SST following the calibration of Anand et al. (2003) for *G. ruber* (white) in the size range of 350 – 500 μm:

$$Mg/Ca = 0.48 * \exp(0.085 * T)$$

$$\Leftrightarrow T = \ln[(Mg/Ca)/0.48]/0.085$$

Mg/Ca is the foraminiferal Mg/Ca concentration in $^{mmol}/_{mol}$ and T is the temperature in °C.

References

Anand, P., H. Elderfield, and M. H. Conte. (2003). Calibration of Mg/Ca thermometry in planktonic foraminifera from a sediment trap time series. *Paleoceanography* **18,** 28-1 - 28-15.

Arz, H. W., Pätzold, J., and Wefer, G. (1998). Correlated millennial-scale changes in surface hydrography and terrigenous sediment yield inferred from last-glacial marine deposits off northeastern Brazil. *Quaternary Research* **50,** 157-166.

Baker, P. A., Rigsby, C. A., Seltzer, G. O., Fritz, S. C., Lowenstein, T. K., Bacher, N. P., and Veliz, C. (2001a). Tropical climate changes at millennial and orbital timescales on the Bolivian Altiplano. *Nature* **409,** 698-701.

Bard, E. (1988). Correction of accelerator mass spectrometry ^{14}C ages measured in planktonic foraminifera: Paleoceanographic implications. *Paleoceanography* **3**, 635-645.

Bard, E. (2002). Abrupt climate changes over millennial time scales: Climate shock. *Physics Today* **55**, 32-38.

Behling, H., Arz, H. W., Pätzold, J., and Wefer, G. (2000). Late Quaternary vegetational and climate dynamics in northeastern Brazil, inferences from marine core GeoB 3104-1. *Quaternary Science Reviews* **19,** 981-994.

Bond, G. C., Broecker, W. S., Johnsen, S., McManus, J., Labeyrie, L., Jouzel, J., and Bonani, G. (1993). Correlations between climate records from North Atlantic sediments and Greenland ice. *Nature* **365,** 143-147.

Boyle, E. A., and Rosenthal, Y. (1996). Chemical hydrography of the South Atlantic during the Last Glacial Maximum: Cd vs. $\delta^{13}C$. *In "The South Atlantic: Present and past Circulation"* (edited by G. Wefer, W. H. Berger, G. Siedler, and D. J. Webb), pp. 423-443. Springer-Verlag, Berlin.

Broecker, W. S., and Hemming, S (2001). Climate swings come into focus. *Science* **294**, 2308-2309.

Cacho, I., Grimalt, J. O., Pelejero, C., Canals, M., Sierro, F. J., Flores, J. A., and Shackleton, N. (1999). Dansgaard-Oeschger and Heinrich event imprints in the Alboran Sea paleotemperatures. *Paleoceanography* **14**, 698-705 (1999).

Chiang, J. C. H., and Bitz, C. M. (2005). Influence of high latitude ice cover on the marine Intertropical Convergence Zone. *Climate Dynamics* **25,** 477-496.

Dansgaard, W. et al. (1993). Evidence for general instability of past climate from a 250-kyr ice-core record. *Nature* **364**, 218-220.

Grootes, P. M., and Stuiver, M. (1997). Oxygen 18/16 variability in Greenland snow and ice with 103- to 105-year time resolution. *Journal of Geophysical Research* **102,** 26455-26470.

Hastenrath, S. (1990). Prediction of Northeast Brazil rainfall anomalies. *Journal of Climate* **3,** 893-904.

Hendy, I. L., and Kennett, J. P. Latest Quaternary North Pacific surface-water responses imply atmosphere-driven climate instability. *Geology* **27**, 291-294 (1999).

Jennerjahn, T. C., Ittekkot, V., Arz, H. W., Behling, H., Pätzold, J., and Wefer, G. (2004). Asynchronous terrestrial and marine signals of climate change during Heinrich events. *Science* **306,** 2236-2239.

Lowell, T. V., Heusser, C. J., Andersen, B. G., Moreno, P. I., Hauser, A., Heusser, L. E., Schluchter, C., Marchant, D. R., and Denton, G. H. (1995). Interhemispheric correlation of Late Pleistocene glacial events. *Science* **269**, 1541-1549.

Peterson, L. C., Haug, G. H., Hughen, K. A., Röhl, Ursula. (2000). Rapid changes in the hydrologic cycle of the tropical Atlantic during the last glacial. *Science* **290,** 1947-1951.

Röhl, U., and Abrams, L. J. (2000). High-resolution, downhole, and nondestructive core measurements from sites 999 and 1001 in the Caribbean Sea: Application to the Late Paleocene Thermal Maximum. *In "Proceedings of the Ocean Drilling Program, scientific results **165**"* (edited by R. M. Leckie, H. Sigurdsson, G. D. Acton, and G. Draper), pp. 191-203.

Sachs, J. P., Anderson, R. F., and Lehman, S. J. (2001). Glacial surface temperatures of the Southeast Atlantic Ocean. *Science* **294**, 2077-2079.

Schulz, H., von Rad, U., and Erlenkeuser, H. (1998). Correlation between Arabian Sea and Greenland climate oscillations of the past 110,000 years. *Nature* **393**, 54-57.

Shackleton, N. J., Fairbanks, R. G., Chiu, T.-C., and Parrenin, F. (2004). Absolute calibration of the Greenland time scale: Implications for Antarctic time scales and for $\delta^{14}C$. *Quaternary Science Reviews* **23,** 1513-1522.

Stocker, T. F. (2000). Past and future reorganizations in the climate system. *Quaternary Science Reviews* **19**, 301-319.

Thompson, L. G., et al. (1998). A 25,000-Year tropical climate history from Bolivian ice cores. *Science* **282,** 1858-1864.

Thompson, L. G., Mosley-Thompson, E., Davis, M. E., Lin, P.-N., Henderson, K. A., Cole-Dai, J., Bolzan, J. F., and Liu, K.-B. (1995). Late glacial stage and Holocene tropical ice core records from Huascarán, Peru. *Science* **269,** 46-50.

Wang, X., Auler, A. S., Edwards, R. L., Cheng, H., Cristalli, P. S., Smart, P. L., Richards, D. A., and Shen, C.-C. (2004). Wet periods in northeastern Brazil over the past 210 kyr linked to distant climate anomalies. *Nature* **432,** 740-743.

Wang, Y. J., Cheng, H., Edwards, R. L., An, Z. S., Wu, J. Y., Shen, C.-C., and Dorale, J. A. (2001). A high-resolution absolute-dated Late Pleistocene monsoon record from Hulu Cave, China. *Science* **294,** 2345-2348.

Weninger, B., Danzeglocke, U., and Jöris, O. (2005). "Comparison of dating results achieved using different radiocarbon-age calibration curves and data."

Zabel, M., Schneider, R. R., Wagner, T., Adegbie, A. T., deVries, U., Kolonic, S. (2001). Late Quaternary climate changes in central Africa as inferred from terrigenous input to the Niger Fan. *Quaternary Research* **56**, 207-217.

Supplementary information accompanies the paper on **www.nature.com/nature**

Acknowledgements We thank F. Lamy, C. Rühlemann, S. Mulitza and S. Barker for discussions, R. daRocha, V. Stratmann and D. Hitschel for helping with preparing samples for the Mg/Ca analyses and M. Bryan for providing insight into the cleaning of foraminifers for Mg/Ca analysis. This work was generously supported by the Gary Comer Foundation.

Competing interest statement The authors declare that they have no competing financial interest.

Correspondence and request for materials should be addressed to G.M.N.H. (gerrit.heil@uni-bremen.de).

4.3 Manuscript 2: Last Glacial millennial-scale changes in Atlantic Thermohaline Circulation and Northeast Brazilian precipitation

Gerrit M. N. Heil[1*], Helge W. Arz[2] and Gerold Wefer[1]

1 DFG Research Center Ocean Margins, Universität Bremen, P.O. Box 330440, D-28334 Bremen, Germany (gerrit.heil@uni-bremen.de)

2 GeoForschungZentrum Potsdam, Telegrafenberg C322, D-14473 Potsdam, Germany

* Corresponding author. Tel.: +49-421-21865680; Fax: +49-421-21865505
E-Mail: gerrit.heil@uni-bremen.de

submitted to *Paleoceanography*

Abstract

Stable carbon isotope measurements of the foraminifer *Cibicidoides wuellerstorfi* and X-Ray fluorescence derived measurements of titanium, iron and calcium content of bulk sediment imply parallel, millennial-scale oscillations in western tropical Atlantic deep water circulation and Northeast Brazilian precipitation occurred during Marine Isotope Stages 2 and 3. Low values of *C. wuellerstorfi* stable carbon isotopes coincide with high titanium/calcium and iron/calcium ratios, showing periods of reduced North Atlantic Deep Water production are in phase with high Northeast Brazilian precipitation rates.

Tropical deep water circulation and Northeast Brazilian precipitation are not directly linked, but are both coupled to North Atlantic Sea Surface Temperatures. Changes in North Atlantic Sea Surface Temperatures coincide with shifts in North Atlantic Deep Water production intensity and also influence tropical rainfall patterns by altering atmospheric circulation systems over the North and Tropical Atlantic. This includes shifts in the position of the Intertropical Convergence Zone, which largely governs Northeast Brazilian precipitation rates. Cool temperatures in the high northern latitudes result in a more southern position of the Intertropical Convergence Zone, warm temperatures in a more northern one.

Additionally to previously identified Northeast Brazilian climate variations coinciding with the North Atlantic Heinrich events, our records show precipitation variability from coastal Northeast Brazil correlating to Greenland Dansgaard/Oeschger cycles. This implies the tropical atmospheric system is also very sensitive to smaller high northern latitude climate fluctuations. Precipitation records from regions further away from the Intertropical Convergence Zone range still show millennial-scale changes related to high northern latitude climate variations, but are dominated by insolation-driven multi-millennial cycles.

4.3.1 Introduction

The last glacial period is characterized by millennial-scale climate variability, as observed in Greenland and Antarctic ice cores (Blunier et al., 1998; Dansgaard et al., 1993; Grootes and Stuiver, 1997; Jouzel et al., 1993) and North Atlantic sediments (Bond et al., 1993; Elliot et al., 2002). Quasi-periodic temperature cycles of approx. 1,500 years duration, called

Dansgaard/Oeschger (D/O) cycles (Grootes and Stuiver, 1997), formed longer-term cooling trends, which culminated in massive iceberg discharge into the North Atlantic during Heinrich (H) events (Bond and Lotti, 1995; Broecker, 1994; Heinrich, 1988). H events were generally followed by abrupt warming in Greenland and the North Atlantic (Bond et al., 1993; Dansgaard et al., 1993; Elliot et al., 2002; Grootes and Stuiver, 1997), initiating a new long-term cooling trend. This sequence of abrupt warming and long-term cooling repeated several times during the last glacial, making up a cyclic sequence of so-called Bond cycles (Bond et al., 1993; Bond and Lotti, 1995).

Last glacial Greenland and North Atlantic D/O temperature shifts were accompanied by reorganizations of the global thermohaline circulation (THC; e.g. McManus et al., 2004; Rahmstorf, 2002; Stocker, 1998; Vidal et al., 1997), North Atlantic atmospheric circulation patterns (Cruz et al., 2005; Lohmann, 2003; Peterson et al., 2000), and significant changes in global atmospheric methane and carbon dioxide concentration (Blunier and Brook, 2001). For global millennial-scale climate variations, THC reorganizations play an important role to lock the global climate system in an alternate state for centuries (Broecker, 2003). Furthermore, THC reorganizations have been shown to alter climate conditions globally during stadials associated with H events (Broecker, 2003; Broecker and Hemming, 2001; Voelker et al., 2002). The effect of D/O cycle related THC reorganizations on the tropics, however, still is poorly constrained. Only few well-dated high-resolution records showing regional climate variability correlating to Greenland D/O cycles exist, including a temperature record from the Eastern Pacific Santa Barbara Basin (Hendy and Kennett, 2000), an East Asian monsoon intensity record from the Chinese Hulu Cave (Wang et al., 2001), and an Arabian Monsoon intensity record from the Arabian Sea (Schulz et al., 1998). Therefore, we especially need a better understanding of millennial-scale changes in the tropical climate system to better understand the forcing mechanisms of D/O cycles (Broecker, 2003).

Last glacial climate records from the western tropical Atlantic and the adjacent South American continent generally only show coincidence between THC reorganizations and climate shifts during stadials associated with H events. Based on a planktic foraminiferal $\delta^{18}O$ record, Curry and Oppo (1997) showed tropical Atlantic Sea Surface Temperatures (SST) were lower during H event stadials. Arz et al. (1998, 1999), Auler et al. (2004), Behling et al. (2000), Jennerjahn et al. (2004) and Wang et al. (2004) documented changes in the precipitation regime of Northeast Brazil associated with shifts in the position of the Intertropical Convergence Zone (ITCZ) during these stadials. Hüls and Zahn (2000), Rühlemann et al. (1999) and Schmidt et al. (2004) demonstrated Caribbean SST variability is

linked to THC reorganizations during H1 and the Younger Dryas (YD). Based on a sediment core from the Venezuelan Cariaco Basin, Peterson et al. (2000) suggested variations in Venezuelan precipitation rates relate to shifts in the position of the ITCZ, which are coincident with Greenland temperature change. As the Cariaco Basin data provides the yet only climate record from the tropical Atlantic showing climate variability related to Greenland D/O cycles, Broecker and Hemming (2001) assumed the spatial pattern of the impacts of D/O cycles may be quite different from that of H events. Therefore, we investigated the spatial pattern of precipitation changes in the South American tropics during H events and D/O cycles. This study furthermore allows analyzing whether the primary difference between the impacts of D/O cycles and H events on South American climate lies in the spatial pattern or the magnitude of these changes.

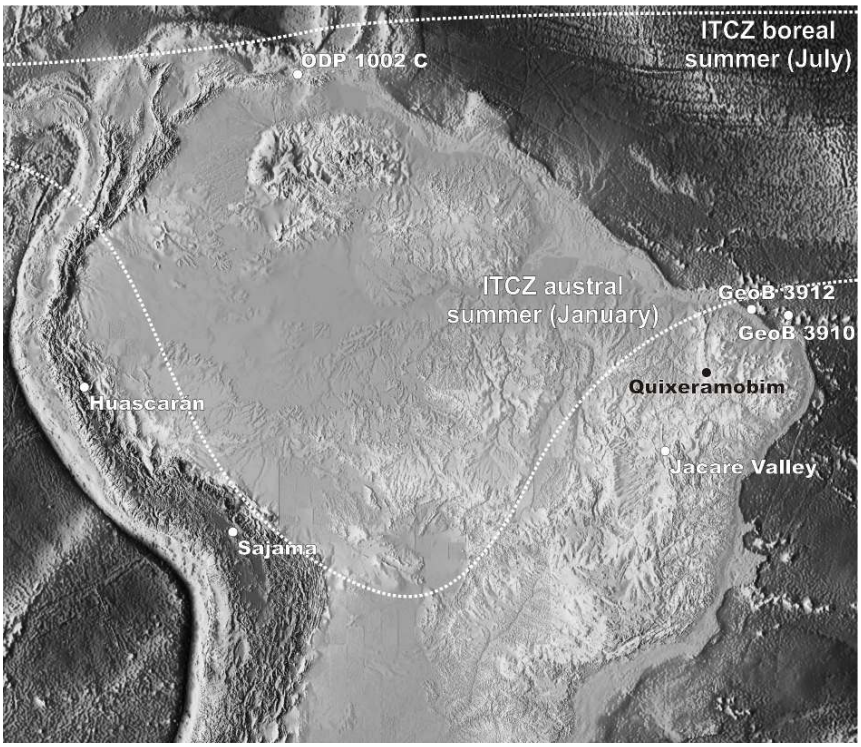

Figure 15: Map of northern South America showing the location of precipitation records mentioned in the text and the maximum northern and southern position of the Intertropical Convergence Zone in the modern climate system.

The records include the marine sediment core ODP 1002 from the Southeast Caribbean Cariaco Basin (off North Venezuela; Peterson et al., 2000), the Peruvian Huascarán (Thompson et al., 1995) and Bolivian Sajama (Thompson et al., 1998) ice cores, the Jacaré valley stalagmite and travertine dating record (Wang et al., 2004), and the marine sediment cores GeoB 3910 (Arz et al., 1998; this study) and 3912 (Behling et al., 2000; Jennerjahn et al., 2004). Note the location of the climate station Quixeramobim (climate diagram shown in Fig. 16).

We investigated changes in the amount of Northeast Brazilian precipitation during the last glacial based on centennial resolution analysis of sediment input into the western tropical Atlantic recorded in sediment cores GeoB 3910 and GeoB 3912 (see Fig. 15 for locations). We show Northeast Brazilian precipitation rates strongly depend on temperatures in the North Atlantic, which are coupled to the intensity of North Atlantic Deep Water (NADW) production. We furthermore examined

deep ocean conditions of the western tropical Atlantic based on benthic foraminiferal stable carbon isotopes ($\delta^{13}C$) in GeoB 3910. As this proxy provides a record of deep water production in the North Atlantic, we are able to directly relate Northeast Brazilian precipitation shifts to THC reorganizations without stratigraphic uncertainties, which often are a major obstacle in correlating paleoclimate records (Shackleton et al., 2004).

4.3.2 Study Area

4.3.2.1 Hydrography

Modern surface hydrology in the western tropical Atlantic is dominated by the North Brazil Current (NBC), which is strongly influenced by seasonally varying southeast trade wind intensity. This, in turn, is linked to the annual movement of the ITCZ. Both trade wind intensity and ITCZ position depend on the seasonally varying strength and position of the northern and southern subtropical high pressure systems (Hastenrath and Merle, 1987). The NBC is the only major surface ocean current crossing the equator northward in the Atlantic, therefore being responsible for most of the northward crossequatorial heat and salt transport. Warm salty water is delivered to the NBC by the South Equatorial Current (SEC), which crosses the Atlantic from the Namibian to the Brazilian coast. Main source of the SEC is the Benguela current, which, in turn, is mainly fed by the Agulhas Current (AC), which carries warm salty Indian Ocean water to the Atlantic (Garzoli et al., 1997). Partly retroflection of the northern branch of the Antarctic Circumpolar Current (ACC) is a minor contributor to the SEC.

The AC, SEC and NBC deliver warm salty ocean water from the Indic and South Atlantic to the North Atlantic (e.g. Peterson and Stramma, 1990; Schott et al., 1998). As deep water production in the North Atlantic is promoted by enhanced salinity, these three currents play a crucial role in the global THC (e.g. Johns et al., 1998). Furthermore, as the NBC is responsible for the northward crossequatorial heat transport, it cools the South Atlantic and warms the North Atlantic, thereby promoting relatively warm temperatures in the high northern latitudes (Arnault et al., 1999; Johns et al., 1998). NBC intensity therefore is a crucial factor for high northern latitude temperatures.

Below the mixed layer, South Atlantic Central Water (SACW) extends to about 500 (Curry and Oppo, 2005) or 700 (Gerhardt et al., 2000) m depth in the western tropical Atlantic. At depths of 500 – 700 to 1200 m, oxygen-enriched and low-salinity Antarctic Intermediate Water (AAIW) and the underlying oxygen-depleted Upper Circumpolar Deep

Water (UCDW) flow northward (Andrié, 1996; Rhein et al., 1996). Despite its low temperature and salinity, AAIW is the second largest ocean current transporting heat and salt northward across the equator. Thereby it supports the surface currents in maintaining the northward heat and salt flow necessary to allow deep water production in the high northern Atlantic (Johns et al., 1998). Between depths of 1200 and 3900 m, North Atlantic Deep Water (NADW) flows southward as Deep Western Boundary Current (Rhein et al., 1996). Below 3900 m, Lower Circumpolar Deep Water and Antarctic Bottom Water (AABW) flow northward (Andrié, 1996; Rhein et al., 1996). The water depth (2362 m) of the investigated sediment core is currently well within NADW.

4.3.2.2 Climate

The interior of northeastern Brazil (the Brazilian "Nordeste") is a semiarid region with a long dry season from August to December and a short rainy season with high precipitation rates during March and April (Fig. 16; Hastenrath, 1990). Three major factors promote precipitation in the rainy season: First, the ITCZ, being the zone of major tropical convective rainfall, reaches its southernmost position throughout the year (Hastenrath and Heller, 1977). Second, the equatorial South Atlantic waters are warmest in March and April, which enhances evaporation and, consequentially, the moisture content of the trade winds (Hastenrath, 1990). Third, the interhemispheric SST gradient in the tropical Atlantic (the temperature contrast between surface waters lying north and south of the equator) is weakest in this period of the year. Whereas a high interhemispheric SST gradient induces subsidence over the "Nordeste" which hampers precipitation, a low gradient reduces this effect (Hastenrath, 1990).

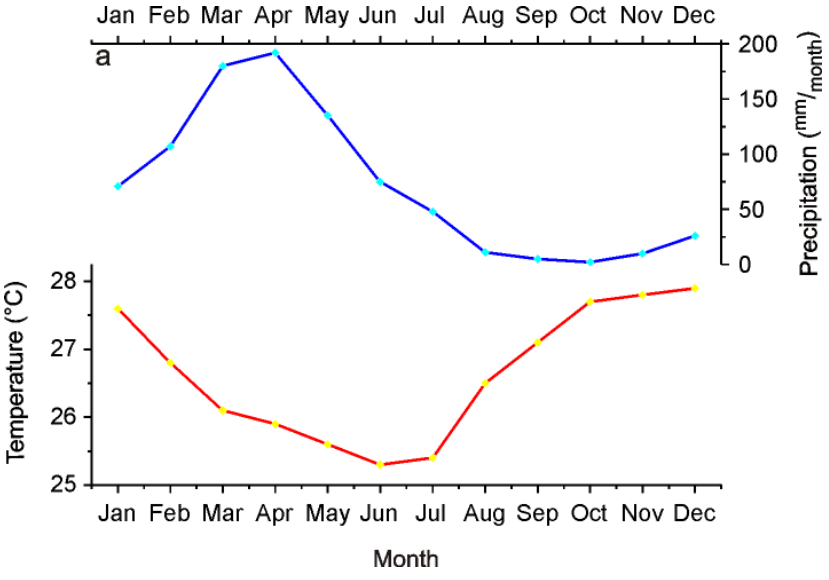

Figure 16: Climate diagram of Quixeramobim, Northeast Brazil (data from www.klimainfos.de)

See Fig. 15 for the location of Quixeramobim. Note the huge differences in the amount of precipitation between the rainy season (March to April) and the dry interval from August to December.

Rain Anomalies in the "Nordeste" primarily result from enhancements or reductions of the average annual cycle. Drought years are characterized by an anomalously far northern position of the ITCZ, reduced northeast trades and an anomalously high interhemispheric SST gradient (resulting from positive SST anomalies in the tropical North Atlantic and negative ones in the tropical South Atlantic; Hastenrath, 1990). Correspondingly, a far southern ITCZ position, increased northeast trades and a low interhemispheric SST gradient (resulting from negative SST anomalies in the tropical north Atlantic and positive ones in the tropical South Atlantic) should increase yearly precipitation.

4.3.3 Material and Methods

4.3.3.1 Material

We analyzed sediment core GeoB 3910 (4°14,7' S, 36°20,7' W, 2362 m water depth) and GeoB 3912 (3°40,0'S, 37°43,0'W, 767 m water depth), both raised from the continental slope off Northeast Brazil with RV Meteor (Fischer et al., 1996). At present, the site of GeoB 3910 lies well within NADW, whereas that of GeoB 3912 is situated in AAIW. GeoB 3910 consists of homogenous foraminifer and nanofossil bearing ooze to clay. While the upper 507 cm of the core are undisturbed, the lower part contains some turbidites. Therefore, we just analyzed the upper 507 cm of the core. Analogous to GeoB 3910, GeoB 3912 is made up of homogenous foraminifer and nannofossil bearing ooze to clay. Furthermore, GeoB 3912 does not show any sign of disturbances.

4.3.3.2 Methods

4.3.3.3 Bulk sediment composition

At intervals of 0.4 cm (average time resolution of 45 yrs), we analyzed GeoB 3910 for bulk sediment chemistry by X-Ray Fluorescence (XRF) on the XRF core scanner of the University of Bremen. This method allows the non-destructive analysis of split sediment cores regarding the concentrations of the chemical elements from atomic number 19 (potassium) to 38 (strontium; Röhl and Abrams, 2000). We also investigated GeoB 3912 by XRF at intervals of 0.4 cm for the uppermost 283 cm (average time resolution of 50 yrs) and of 2.5 cm for the rest of the core (average time resolution of 120 yrs). Here, we report ratios of titanium (Ti) and iron (Fe) versus calcium (Ca) of both cores.

4.3.3.4 Benthic stable carbon isotopes

Stable carbon isotope ratios of benthic foraminifers were determined for every cm of the glacial part of core GeoB 3910 (average time resolution of 115 yrs). Samples of the benthic foraminifer *Cibicidoides wuellerstorfi (C. wuell.)* (up to 5 specimens) were processed with an

automatic carbonate preparation system (Carbo type Bremen) and analyzed on a Finnigan MAT 252 mass spectrometer (values reported in ‰ $\delta^{13}C$ versus VPDB). Every tenth sample was analyzed in duplicate. Analytical internal longtime precision was better than ± 0.07 ‰ and average reproducibility ± 0.04 ‰.

4.3.4 Stratigraphy

The stratigraphy of GeoB 3910 is based on 22 calibrated and linearly interpolated radiocarbon ages spanning the last 47 cal. kyrs (table 4). Radiocarbon dating was performed on mainly monospecific (*Globigerinoides sacculifer*) carbonate samples at the Leibniz Laboratory in Kiel. Radiocarbon ages were uniformly corrected for a reservoir age of 400 years (Bard, 1988) and calibrated with CalPal (Weninger et al., 2005) using the GRIP_SFCP_2005 calibration curve, which is based on the radiocarbon calibration presented by Fairbanks et al. (2005).

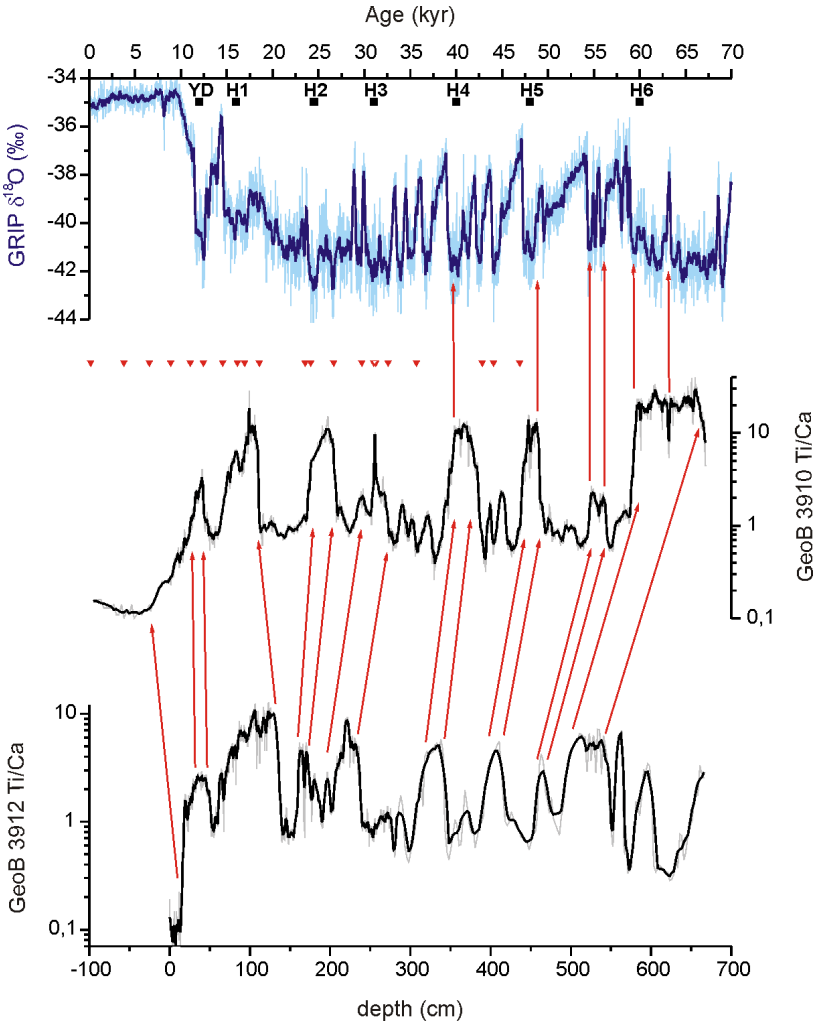

Figure 17: Stratigraphy of sediment cores GeoB 3910 (plotted versus age) and GeoB 3912 (plotted versus depth)

Red triangles mark radiocarbon datings of GeoB 3910, red arrows mark correlations of GeoB 3910 Ti/Ca to GRIP $\delta^{18}O$ and GeoB 3912 Ti/Ca to GeoB 3910 Ti/Ca, respectively. YD and H1 to H6 mark the Younger Dryas and Heinrich events 1 to 6, respectively, which provide the main checkpoints for correlating these three archives to each other.

As maxima in the bulk sediment Ti/Ca ratio of GeoB 3910 coincide with GRIP $\delta^{18}O$ minima in the radiocarbon dated part, they were used to adjust the older part (47 cal. kyr and older) of the core to the GRIP record (Fig. 17). The reported part of GeoB 3910 spans the period from 11 to 63 cal. kyr BP with highly variable sedimentation rates between 3.5 and 43 cm/kyr. Average sedimentation rates for this period are 8.5 cm/kyr.

The benthic $\delta^{13}C$ record of GeoB 3910 provides an independent validation of the stratigraphy of GeoB 3910. As we measured Ti/Ca ratios and benthic foraminiferal $\delta^{13}C$ from the same core, we can compare these records to each other without major stratigraphic uncertainties. Millennial-scale shifts in Ti/Ca ratios coincide with changes in $\delta^{13}C$ values (Fig. 18), and $\delta^{13}C$ values record variations in NADW production intensity (see section 5.3). These, in turn, are well-known to coincide with Greenland D/O cycles observed e.g. in GRIP $\delta^{18}O$ (Bond et al., 1999; Vidal et al., 1997). As variations in both GeoB 3910 Ti/Ca and $\delta^{13}C$ coincide with D/O cycles (Fig. 18), the $\delta^{13}C$ record validates the stratigraphy of GeoB 3910 with respect to GRIP $\delta^{18}O$.

Table 4: Age model of sediment core GeoB 3910

Accelerator mass spectrometry (AMS) radiocarbon (^{14}C) ages were obtained from monospecific (Globigerines sacculifer) samples. ^{14}C ages were corrected for a reservoir age of 400 years (Bard, 1988) and calibrated with CalPal Online using the GRIP_SFCP_2005 calibration curve (Weninger et al., 2005). Correlations to GRIP were obtained from correlating GeoB 3910 Ti/Ca ratios to GRIP $\delta^{18}O$.

Core depth (cm)	^{14}C-age (yr BP)	+error (yr)	-error (yr)	Cal. age (yr BP)	±error (yr)	Type of dating	Lab ID
0	565	30	30	170	90	AMS ^{14}C dating	KIA 6800
13	3930	35	35	3800	60	AMS ^{14}C dating	KIA 6799
23	6160	40	40	6560	60	AMS ^{14}C dating	KIA 6798
38	8430	40	40	8900	100	AMS ^{14}C dating	KIA 7225
58	10090	60	60	11020	140	AMS ^{14}C dating	KIA 6815
73	10940	70	70	12460	200	AMS ^{14}C dating	KIA 6814
88	12840	110	100	14550	370	AMS ^{14}C dating	KIA 6813
103	13550	70	70	16170	500	AMS ^{14}C dating	KIA 25825
113	14000	70	70	16940	230	AMS ^{14}C dating	KIA 25824
148	15780	110	110	18550	250	AMS ^{14}C dating	KIA 6812
173	20000	170	160	23540	280	AMS ^{14}C dating	KIA 6811
183	20580	150	150	24150	310	AMS ^{14}C dating	KIA 25822
193	22480	220	210	26670	440	AMS ^{14}C dating	KIA 6808
213	25130	260	250	29730	320	AMS ^{14}C dating	KIA 25821
223	26830	360	350	30990	270	AMS ^{14}C dating	KIA 6807
233	27160	310	300	31220	220	AMS ^{14}C dating	KIA 25820
238	28280	430	410	32580	780	AMS ^{14}C dating	KIA 6806
268	30860	430	410	35680	400	AMS ^{14}C dating	KIA 22411
293				38940		Correlation to GRIP	
328	38600	1610	1340	42830	790	AMS ^{14}C dating	KIA 6804
348	41000	860	780	44070	770	AMS ^{14}C dating	KIA 21829
373	44480	1340	1150	46920	1690	AMS ^{14}C dating	KIA 21830
400				49100		Correlation to GRIP	
432				54240		Correlation to GRIP	
453				56390		Correlation to GRIP	
538				65990		Correlation to GRIP	

The initial stratigraphy of GeoB 3912 is based on 6 radiocarbon ages from its twin core GeoB 3104 (Arz et al., 1998) and 6 new additional radiocarbon dates that were produced to individually validate the stratigraphy. The final age model used in the present study, however, derives from tuning GeoB 3912 Ti/Ca to the Ti/Ca record of the nearby sediment core GeoB 3910, which has a much better validated stratigraphy (Fig. 17). The calibrated radiocarbon ages agree within error with ages derived from tuning and therefore support the stratigraphy of GeoB 3912 (Table 5).

Table 5: Age model of sediment core GeoB 3912: Comparison of ages derived from correlating GeoB 3912 Ti/Ca to GeoB 3910 Ti/Ca with calibrated radiocarbon ages

Core depth (cm)	Age from Ti/Ca correlation (yr BP)	Cal. Age (yr BP)	±error (yr)	Lab ID
238	31510	31450	190	KIA 21831
278	35420	35630	300	KIA 21833
298	37950	38260	910	KIA 22412
303	38290	39200	1240	KIA 22413
343	42010	41850	250	KIA 21834
388	47320	47850	1530	KIA 21835

4.3.5 Results

4.3.5.1 Sediment composition

GeoB 3910 Ti/Ca and Fe/Ca ratios are highly variable on millennial timescales and show changes coincident with Greenland D/O cycles. Changes in Ti/Ca ratios are nearly identical to those in Fe/Ca ratios; they only show different amplitudes, as the Fe content of GeoB 3910 is much higher than the Ti content. We identified four predominant Ti/Ca and Fe/Ca ratio ranges, which are typical of interstadials, D/O stadials, stadials associated with H events and the YD (Fig. 18; Heil et al., submitted).

Whereas interstadial Ti/Ca ratios lie between 0.3 and 1, Fe/Ca ratios range from 0.5 to 1.5. D/O stadials are characterized by Ti/Ca ratios between 1.2 and 2.2 and Fe/Ca ratios between 2.0 and 5.0, indicating at least doubled interstadial values. With maximum Ti/Ca ratios from 10 to 30 and Fe/Ca ratios of 20 to 40, Ti/Ca and Fe/Ca ratios of stadials associated with H events are about 20 times higher than interstadial ones and 10 times higher than D/O stadial ones. Maximum YD Ti/Ca ratios of 4.0 and Fe/Ca ratios of 5.3 are about 5 times higher than interstadial and 2 times higher than D/O stadial Ti/Ca ratios, but only half as high as minimum H event Ti/Ca ratios.

4.3.5.2 Deep ocean stable carbon isotopes

The $\delta^{13}C$ record of GeoB 3910 indicates three periods of generally different deep water circulation conditions, which correspond to the Marine Isotope Stages (MIS) 4, 3 and 2 (Fig. 18). At the oldest part of the record, MIS 4 shows low $\delta^{13}C$ values of around -0.1 ‰. $\delta^{13}C$ increases by 1.0 ‰ from 60.4 to 58.6 kyr BP (representing the transition from MIS 4 to 3) and varies between 0.4 and 1.2 ‰ during MIS 3. There is no abrupt shift in $\delta^{13}C$ at the transition of MIS 3 to 2, but throughout MIS 2, $\delta^{13}C$ varies between -0.1 and +0.8 ‰.

During MIS 3 and 2, $\delta^{13}C$ is grouped in 6 cycles of 7 to 10 kyr duration. The first five cycles begin with an abrupt, large $\delta^{13}C$ increase (amplitudes between 0.4 and 0.8 ‰). This is followed by a $\delta^{13}C$ decrease trend superposed by smaller millennial cycles with amplitudes typically around 0.3 ‰ (overall, amplitudes of these cycles vary between 0.1 and 0.5 ‰). The gradual $\delta^{13}C$ decrease culminates in an abrupt decrease of 0.3 to 0.5 ‰. $\delta^{13}C$ stays on this low level for 1 to 2 kyr (except for the end of the fourth cycle, when low $\delta^{13}C$ values are kept for 200 yr only), before an abrupt $\delta^{13}C$ increase induces the next cycle. Except for the first cycle, $\delta^{13}C$ levels are nearly the same at the beginning and end of these multi-millennial cycles, respectively (around 1.2 ‰ at the beginning and between 0.3 and 0.4 ‰ at the end of these cycles).

The last multi-millennial $\delta^{13}C$ cycle, which begins at 23.9 kyr BP and encompasses the Last Glacial Maximum (LGM) and the beginning of the deglaciation, shows lower and fairly stable $\delta^{13}C$ levels in comparison to the previous five cycles. Maximum $\delta^{13}C$ values of 0.8 ‰ at 23.8 kyr BP are much lower than the 1.2 ‰ typical of the other $\delta^{13}C$ cycles. From 23.5 to 22.7 kyr BP, $\delta^{13}C$ values drop again to 0.6 ‰ and stay between 0.6 and 0.7 ‰ until 18.5 kyr BP. LGM $\delta^{13}C$ levels are lower than during most MIS 3 interstadials, but higher than during stadials associated with H events. Furthermore, $\delta^{13}C$ is on the same level like in the Bølling/Allerød (B/A).

The stadial associated with H1 presents extremely low $\delta^{13}C$ values. These decrease rapidly to 0.1 ‰ from 18.5 to 17.6 kyr BP and stay between -0.1 and +0.2 ‰ until 14.8 kyr BP. These $\delta^{13}C$ values are even lower than during stadials associated with H events 2 to 5, and are more comparable to MIS 4 $\delta^{13}C$ values.

From 14.8 to 13.9 kyr BP (the transition to the B/A), $\delta^{13}C$ increases from 0.0 to 0.7 ‰. Although these $\delta^{13}C$ values are distinctly higher than during the stadial associated with H1 and the YD, they are much lower than during most MIS 3 interstadials and comparable to LGM $\delta^{13}C$ rates.

From 13.9 to 12.9 kyr BP, $\delta^{13}C$ decreases by 0.3 ‰ and stays around 0.4 ‰ during the YD until at least 11.7 kyr BP. YD $\delta^{13}C$ values are on the same level like during stadials associated with H events 2 to 5, but higher than during the stadial associated with H1.

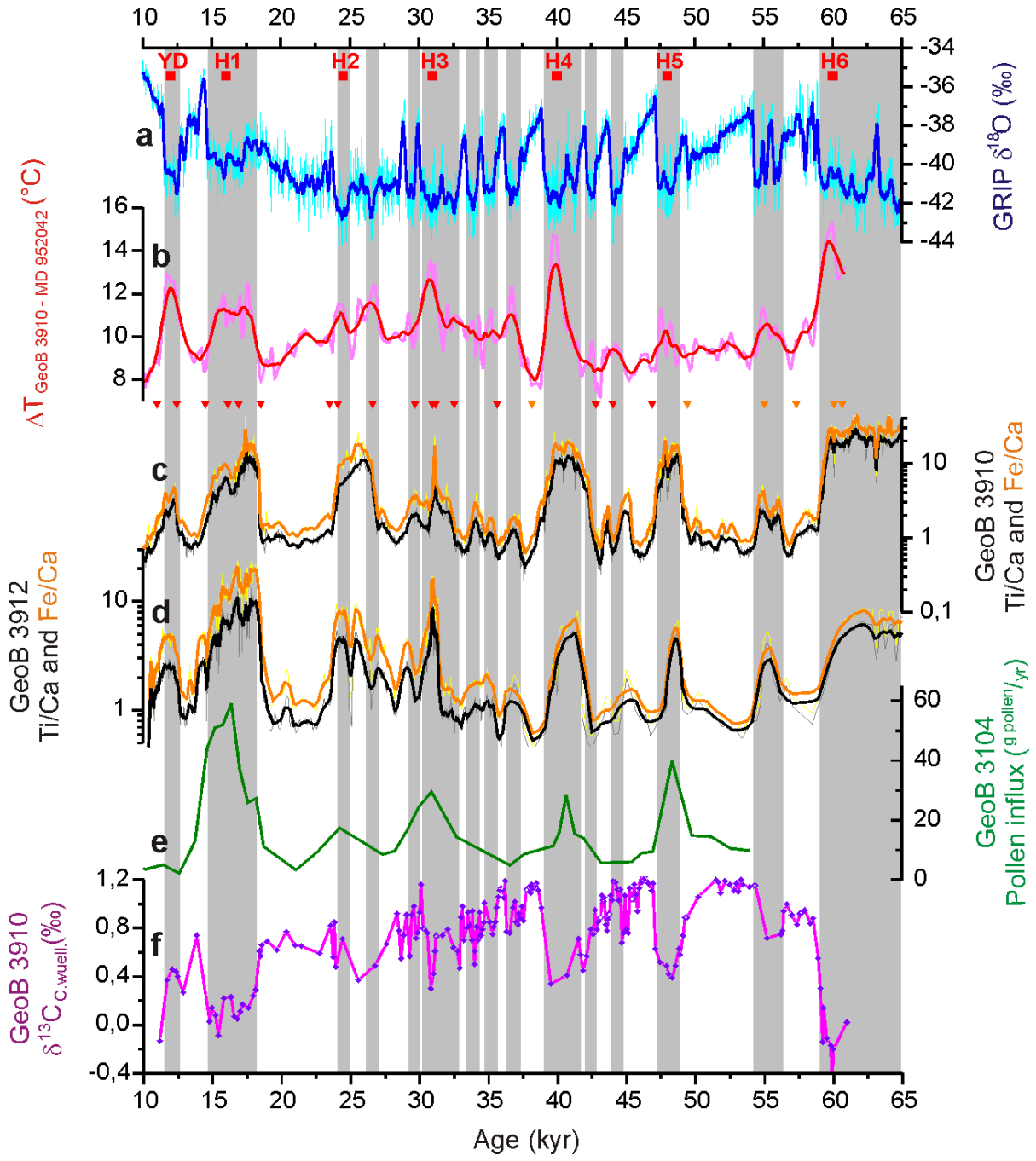

Figure 18: Relations between Northeast Brazilian precipitation, western tropical Atlantic deep water conditions and Greenland temperature

a) GRIP $\delta^{18}O$ record from central Greenland (Shackleton et al., 2004); **b)** Sea Surface Temperature difference between the western tropical Atlantic (GeoB 3910) and the eastern temperate North Atlantic (MD 952042; Heil et al., submitted); **c)** bulk sediment Ti/Ca (black) and Fe/Ca (orange) of sediment core GeoB 3910 (this study), red triangles mark radiocarbon datings, orange triangles indicate where the Ti/Ca record has been tuned to GRIP $\delta^{18}O$; **d)** bulk sediment Ti/Ca (black) and Fe/Ca (orange) of sediment core GeoB 3912 (this study); **e)** pollen influx into sediment core GeoB 3104 (Behling et al., 2000); **f)** GeoB 3910 benthic $\delta^{13}C$ (this study); gray boxes represent Greenland stadials; YD marks the Younger Dryas (Alley, 2000), H1 to H6 denote Heinrich events 1 to 6 (Broecker and Hemming, 2001).

4.3.6 Discussion

4.3.6.1 Coupling of Northeast Brazilian precipitation and the North Atlantic meridional temperature gradient

The Ti/Ca and Fe/Ca ratios of GeoB 3910 and 3912 mainly are a function of Northeast Brazilian precipitation (Arz et al., 1998, 1999). Ti and Fe derive from the fluviatile erosion of tropical soils, whereas Ca is mainly found in shells of marine microorganisms. Furthermore, the Ti and Fe XRF intensity curves of both cores mirror to the respective Ca XRF intensity curve (data not shown) and foraminifers do not show major signs of dissolution throughout GeoB 3910 and 3912. Therefore, shifts in Ti/Ca and Fe/Ca ratios mainly represent changes in Ti and Fe input into the western tropical Atlantic, which, in turn, are related to shifts in Northeast Brazilian precipitation (Arz et al., 1998, 1999).

Pollen counts of sediment core GeoB 3104 (Behling et al., 2000), a twin core of GeoB 3912, generally support the interpretation of GeoB 3910 and 3912 Ti/Ca and Fe/Ca ratios as precipitation proxies (Fig. 18). Due to limitations in e.g. its resolution, however, the humid intervals are confined to the H events and the YD in the pollen count record.

High Ti/Ca and Fe/Ca ratios indicate precipitation was largely increased during stadials associated with H events (Fig. 18; Arz et al., 1998, 1999). Higher precipitation was probably caused by a southward displacement of the ITCZ during these stadials (Peterson et al., 2000; Wang et al., 2004). Increased Ti/Ca and Fe/Ca ratios during most of the D/O stadials, however, suggest precipitation was also slightly increased during these periods. Ti/Ca and Fe/Ca ratios of the YD, lying in between D/O stadial and H event stadial ratios, suggest a moderate increase in precipitation. However, the deglacial sea level rise probably caused riverine sediments to become largely trapped on the flooded shelf during the YD, damping the Ti/Ca signal on the continental slope (Arz et al., 1999). Therefore, YD precipitation might have been higher than indicated by GeoB 3910 Ti/Ca and Fe/Ca ratios.

Ti/Ca and Fe/Ca ratios of GeoB 3912 are in good agreement with the XRF data of GeoB 3910. Both cores record the same number of D/O cycles in their Ti/Ca and Fe/Ca ratios. Furthermore, GeoB 3912 also allows the differentiation of interstadials (low Ti/Ca and Fe/Ca ratios), D/O stadials (moderately increased Ti/Ca and Fe/Ca ratios) and H event stadials (high Ti/Ca and Fe/Ca ratios). In contrast to GeoB 3910, however, GeoB 3912 Ti/Ca and Fe/Ca ratios of the YD and Greenland stadial 15 are only slightly lower than those of H event stadials, which may be related to differences in terrestrial influx due to the more proximal

position of GeoB 3912 to the coast. This also indicates that Ti/Ca and Fe/Ca ratios cannot be used to estimate absolute precipitation rates in the catchment area but rather to assess relative changes in the hydroclimatic regime.

Modern precipitation of Northeast Brazil is largely dependent on the extent of southward migration of the ITCZ during austral spring to summer (Hastenrath, 1990). Relatively cool North Atlantic SST increase the surface pressure over the North Atlantic then, resulting in a southward shift of the air masses over the North to Equatorial Atlantic, including the ITCZ (Hastenrath and Greischar, 1993). A similar effect can also be observed on millennial timescales. Modelling cool events during the last glacial, (Chiang et al., 2003; Chiang and Bitz, 2005) demonstrated an increased ice volume and decreased temperatures in the high northern latitudes result in a southward displacement of the ITCZ. In order to compensate for the loss of energy caused by increased ice volume at high northern latitudes, the Hadley circulation probably increased its northward heat transport (Cruz et al., 2005), resulting also in intensified trade winds and increased ITCZ rainfall intensity.

The observed variations in Northeast Brazilian precipitation can be interpreted as a direct consequence of these processes. Increased trade winds and a southward shift of the ITCZ account for generally increased Northeast Brazilian precipitation rates during the last glacial compared to the Holocene (Heil et al., submitted). The exceptionally strong precipitation increase during H event stadials, however, can only be explained by a significant southward shift of the ITCZ. North Atlantic meridional temperature gradients were highest during these stadials (Fig. 18) and likely produced the largest ITCZ southward displacements during the last glacial. A moderate precipitation increase as observed for the other D/O stadials indicates smaller ITCZ displacements related to less pronounced North Atlantic temperature gradients. The precipitation records of GeoB 3910 and 3912 therefore suggest the tropical atmospheric system is sensible also to smaller temperature change in the high northern latitudes. The magnitude of the temperature gradient between the high latitude and the tropical North Atlantic thereby defines the rate of the ITCZ southward shift, which changes tropical precipitation patterns accordingly (Fig. 20; Heil et al., submitted).

4.3.6.2 Spatial patterns of millennial-scale South American precipitation changes

A southward movement of the ITCZ, like deduced from the data of GeoB 3910 and 3912, also should alter precipitation in adjacent South American regions. Therefore, we compare our results to a marine sediment core record from the Venezuelan Cariaco Basin (Peterson et al., 2000), to Speleothem and Travertine records from the central Northeast Brazilian Jacaré Valley (Wang et al., 2004), to a speleothem record from southern Brazil (Cruz et al., 2005) and to ice core and lake sediment core records from the Peruvian and Bolivian Andes (Baker et al., 2001; Thompson et al., 1995, 1998).

ITCZ shifts analogous to those deduced from GeoB 3910 and 3912 have been reported from the northern margin of the ITCZ. Based on Ti, Fe and Ca XRF counts of Cariaco Basin sediment core ODP 1002 C, (Peterson et al., 2000) showed changes in Venezuelan precipitation rates coincide with Greenland temperature shifts during most of the Greenland D/O cycles (Fig. 19). Nowadays the ITCZ just reaches the catchment area of the Cariaco Basin in boreal summer causing high summer precipitation rates during the rainy season (Fig. 15). Assuming a similar northern position of the ITCZ during interstadial boreal summers, even minor southward shifts of the ITCZ during minor stadials would shorten the rainy season. A strong cooling in the North Atlantic region, like observed during major stadials (e.g. Bard et al., 2000; Bond et al., 1993; Cortijo et al., 1997) would cause a larger southward shift of the ITCZ (Heil et al., submitted), shortening the rainy season even more or preventing it.

Further evidence for ITCZ shifts during the last glacial comes from a speleothem and travertine record from the central Northeast Brazilian Jacaré Valley (Wang et al., 2004). As low rainfall and high evapotranspiration during dry intervals preclude speleothem and travertine formation in Northeast Brazil, speleothem and travertine growth phases indicate wet conditions in the past (Wang et al., 2004). Growth phases are only observed during stadials associated with H events, indicating wet conditions probably caused by southward shifts of the ITCZ (Fig. 19; Wang et al., 2004). Contrasting to our records, the Jacaré Valley precipitation record does not show precipitation to increase during other stadials. Whereas the catchment area of GeoB 3910 lies close to the present margin of the ITCZ, the Jacaré Valley is situated several hundred kilometers south of this margin. Therefore, a larger southward shift of the ITCZ would have been required for a significant increase in precipitation.. As relatively little rainfall increase is sufficient to trigger Jacaré Valley travertine growth (Wang et al., 2004), the observed distinct growth phases support the idea that ITCZ shifts affected the Jacaré Valley region during major stadials only.

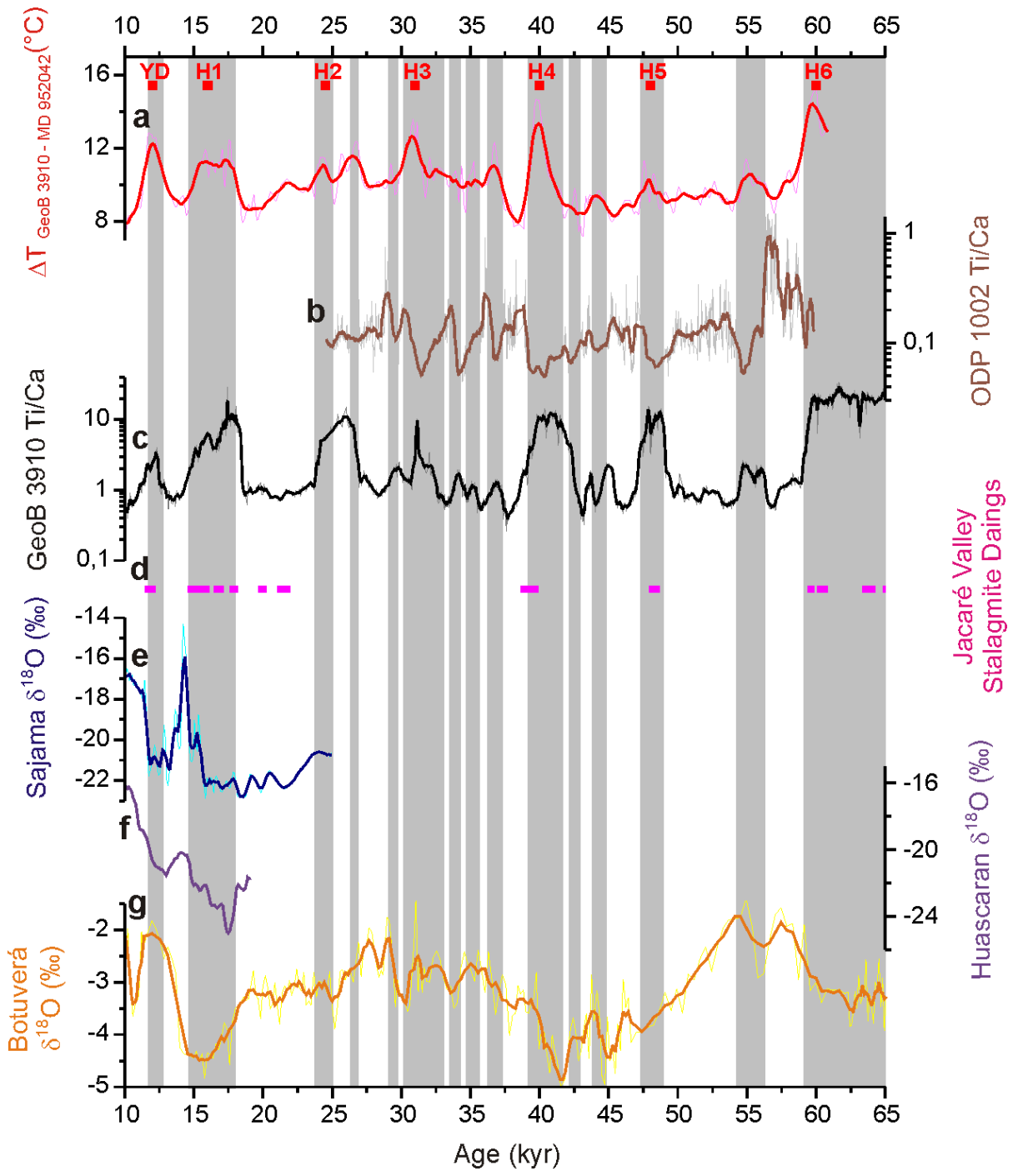

Figure 19: Compilation of South American precipitation records used to reconstruct shifts in the position of the Intertropical Convergence Zone (Fig. 20)

a) Sea Surface Temperature difference between the western tropical Atlantic (GeoB 3910) and the eastern temperate North Atlantic (MD 952042; Heil et al., submitted); **b)** Ti/Ca of sediment core ODP 1002 C from the Cariaco Basin (Peterson et al., 2000); **c)** Ti/Ca of sediment core GeoB 3910 from the western tropical Atlantic (this study); **d)** stalagmite and travertine datings from the central Northeast Brazilian Jacaré Valley (Wang et al., 2004); **e)** $\delta^{18}O$ of the Sajama ice core, Peru (Thompson et al., 1998); **f)** $\delta^{18}O$ of the Huascarán ice core, Bolivia (Thompson et al., 1995); **g)** $\delta^{18}O$ of stalagmite BT2 from Botuverá Cave, South Brazil (Cruz et al., 2005); gray boxes represent Greenland stadials; YD marks the Younger Dryas (Alley, 2000), H1 to H6 denote Heinrich events 1 to 6 (Broecker and Hemming, 2001).

Precipitation records from the Andes also indicate shifts in the position of the ITCZ during the last glacial. Thompson et al. (1995, 1998) presented ice core $\delta^{18}O$ records from the Peruvian Huascarán and the Bolivian Sajama ice cap that show shifts to more negative values which are interpreted to represent wet conditions during the stadials associated with H1 and the YD (Fig. 19). As both the Huascarán and the Sajama ice cap lie close to the modern southern margin of the ITCZ, a southward shift of the ITCZ in combination with increased trade winds would have caused higher precipitation at these sites (Thompson et al., 1995, 1998).

Baker et al. (2001) presented a record of natural γ-radiation from the Bolivian lake Salar de Uyuni, which supports the implications from Thompson et al. (1995, 1998). Variations in γ-radiation in the Salar de Uyuni core mainly reflect changes between siliciclastic and evaporitic sediments. As siliciclastic mud sediments preferably form during periods of a high lake level and salt deposits during times when lake evaporation exceeds lake precipitation, variations in natural γ-radiation reflect changes in local precipitation versus evaporation rates. γ-radiation varies mainly with January insolation at 15°S, indicating insolation mainly controls local precipitation rates (Baker et al., 2001). Superposed on these precessional cycles, however, some abrupt high γ-radiation excursions can be observed. These coincide with stadials associated with H events and the YD, indicating particularly wet conditions during these stadials. These observations are also in accordance with a southward shift of the ITCZ during these stadials.

Further indirect evidence for shifts in the position of the ITCZ during the last glacial comes from as far south as the tropical/subtropical border. Cruz et al. (2005) presented a stalagmite $\delta^{18}O$ record from the southeast Brazilian Botuverá Cave (27°S). They argue that changes in Botuverá $\delta^{18}O$ primarily reflect variations in local summer rainfall. These are related to shifts in the position of the South American Summer Monsoon (SASM) and the South American Convergence Zone (SACZ), which are primarily controlled by February insolation at 30°S (Cruz et al., 2005). Superposed on these precessional cycles, prominent excursions to more negative $\delta^{18}O$ values can be observed during the YD and H event stadials (Fig. 19). Cruz et al. (2005) interpret these negative $\delta^{18}O$ excursions to also reflect southward displacements of the SASM and SACZ. Conclusively, the whole tropical/subtropical South American atmospheric circulation system, including the ITCZ, the SASM and the SACZ, was shifted southward during the YD and H event stadials.

This collection of millennial-scale precipitation records from South America allows assessing forcing mechanisms of changes in tropical/subtropical South American precipitation patterns

during the last glacial. Venezuelan and coastal Northeast Brazilian precipitation, for example, vary during most Greenland D/O cycles due to shifts in the position of the ITCZ in response to changes in the North Atlantic meridional temperature gradient. On millennial timescales, the magnitude of this temperature gradient is mainly defined by high latitude temperatures, as the amplitude of millennial-scale temperature variations is significantly larger there than in the tropics (Heil et al., submitted). The high northern latitude cooling observed during D/O stadials results in an increased gradient, which, in turn, induces a southward shift of the ITCZ (Fig. 20). Precipitation rates in regions presently well outside the ITCZ range, like central Northeast Brazil and the Bolivian to Peruvian Andes increase during H event stadials only, indicating the displacement of the ITCZ was exceptionally large during these periods. High to mid-latitude North Atlantic temperatures decreased dramatically during these stadials (Bard, 2002; Bond et al., 1999), causing a strong increase in the North Atlantic meridional temperature gradient, which, in turn, induced a large southward shift of the ITCZ (Fig. 20). However, as millennial-scale precipitation variations only occurred during H events in central Northeast Brazil and the Bolivian to Peruvian Andes, the dominant mechanism for major precipitation rate changes in these areas is the southern insolation (Baker et al., 2001; Cruz et al., 2005; Thompson et al., 1995, 1998) rather than ITCZ shifts.

4.3.6.3 Changes in the Atlantic THC derived from western tropical Atlantic deep water properties

The coupling of tropical South American precipitation to high northern latitude temperatures suggests a link between variations in the oceanic THC and tropical precipitation (e.g. Lohmann, 2003). Whereas D/O cycles are associated with variations in the intensity of deep water formation in the North Atlantic, H events are coupled to a complete shutdown or strong reduction of North Atlantic Deep Water (NADW) production (Keigwin and Jones, 1994; Oppo and Lehman, 1995; Vidal et al., 1997). These variations in NADW production can be tracked in Atlantic deep ocean records (Broecker, 1991). During the last glacial, reduced deep water production in the North Atlantic induced shallowing of NADW to Glacial North Atlantic Intermediate water (GNAIW; Boyle and Keigwin, 1987). During the LGM, e.g., GNAIW extended from about 1200 to 2000 m in the western tropical Atlantic (Curry and Oppo, 2005). Between 2000 and 3000 m, a mixing zone between GNAIW and the underlying AABW established (Curry and Oppo, 2005). GeoB 3910 (retrieved from a water depth of 2362 m) recorded conditions of NADW in the modern ocean and of this mixing zone during the last glacial.

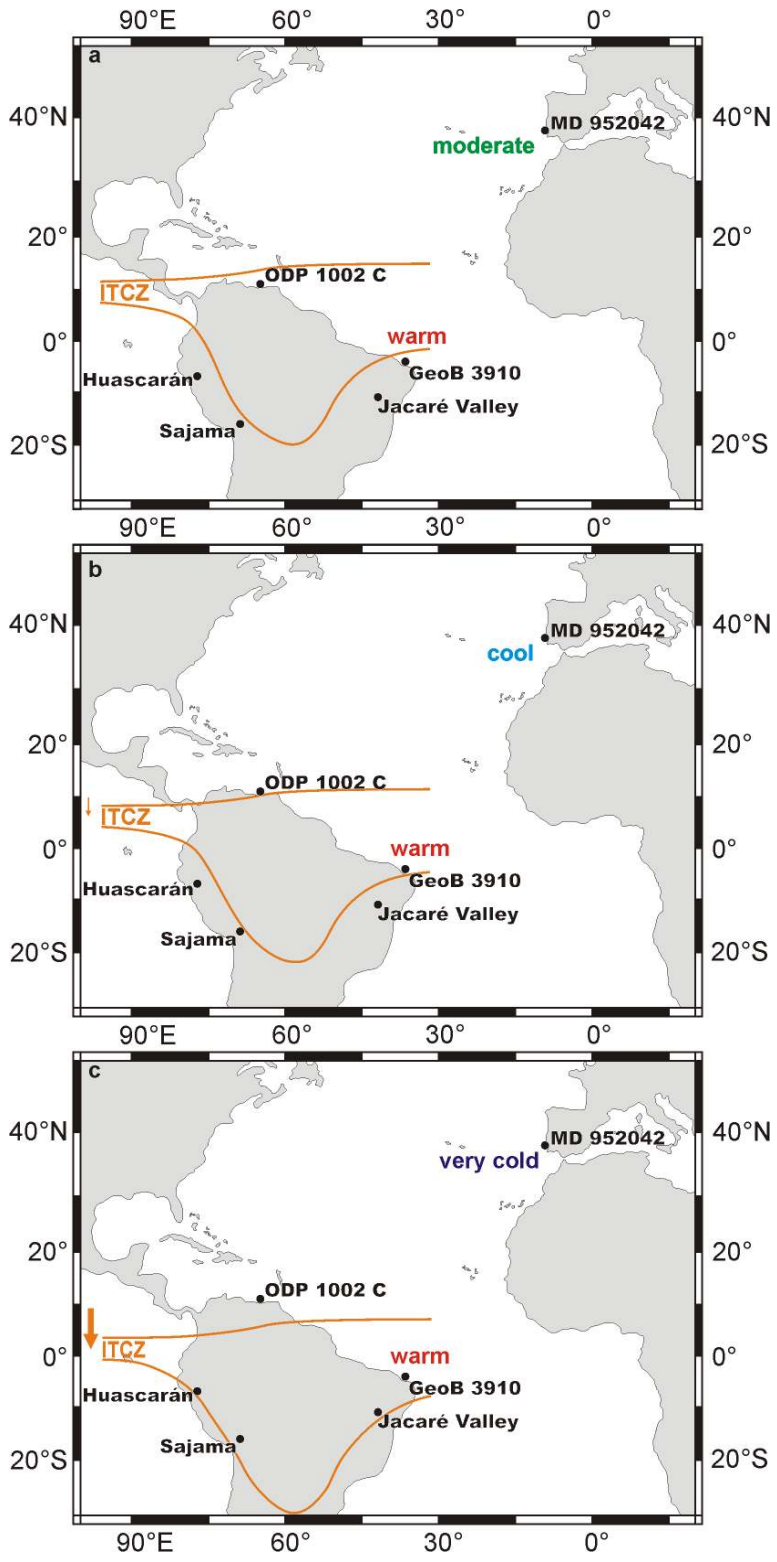

Figure 20: General variations in Sea Surface Temperatures in the mid-latitude eastern North Atlantic (sediment core MD 952042) and the western tropical Atlantic (sediment core GeoB 3910) and corresponding shifts of the Intertropical Convergence Zone due to the resulting changes in the meridional North Atlantic temperature gradient during interstadials **(a)**, Dansgaard/Oeschger stadials **(b)** and Heinrich event stadials **(c)**

The South American sediment archives shown in this Figure denote the precipitation records described in Fig. 19. Note that the meridional temperature gradient primarily varies due to temperature changes in the northern mid-latitudes.

Throughout the last glacial, GNAIW possessed high $\delta^{13}C$ values of around 1.5 ‰ (Oppo and Lehman, 1995), whereas AABW had much lower $\delta^{13}C$ values of down to -0.9 ‰ (Ninnemann and Charles, 2002). Therefore, the GNAIW/AABW mixing zone was characterized by a strong bathymetric $\delta^{13}C$ gradient at that time (Curry and Oppo, 2005). Depending on the strength of deep water production in the North Atlantic, shallowing or deepening of GNAIW influenced the depth level of this mixing zone (Curry and Oppo, 2005). Due to the large differences in $\delta^{13}C$ between GNAIW and AABW, changes in the depth level of this mixing zone had a strong impact on $\delta^{13}C$ of benthic foraminifera in the deep western tropical Atlantic. Therefore, the benthic $\delta^{13}C$ of GeoB 3910 can be used as a semiquantitative proxy for western tropical Atlantic deep water circulation and GNAIW production during the last glacial, with higher (lower) $\delta^{13}C$ values suggesting increased (reduced) GNAIW production.

Very low MIS 4 benthic $\delta^{13}C$ values indicate a strong presence of southern source waters in the deep western tropical Atlantic (Fig. 18). This reflects low GNAIW production rates during MIS 4 (e.g. Piotrowski et al., 2005). Significantly higher MIS 3 $\delta^{13}C$ values indicate a generally more vigorous GNAIW production during MIS 3. Additionally, pronounced millennial-scale variations in benthic $\delta^{13}C$ indicate cycles of upward/downward progression of the GNAIW/AABW mixing zone. While interstadials can be associated with a deep GNAIW/AABW mixing zone and strong GNAIW production, stadials suggest the presence of a shallow GNAIW/AABW mixing zone and reduced GNAIW production. The longer-term $\delta^{13}C$ cycles observed in GeoB 3910 generally parallel the Bond cycles observed in the GRIP ice core (Fig.18; Bond et al., 1993). Each of these $\delta^{13}C$ cycles begins with a large increase, which is coincident with one of the abrupt warming events over Greenland following H events. These $\delta^{13}C$ increases indicate recurrent strong deepenings of the GNAIW/AABW mixing zone, which reflect pronounced increases in GNAIW production. The large $\delta^{13}C$ increases are followed by gradual oscillating $\delta^{13}C$ decreases corresponding to the successive Greenland cooling cycles (D/O cycles). This gradual upward progression of the GNAIW/AABW mixing zone culminates during H events, reflecting largely reduced GNAIW production during H event stadials (Bard, 2002; Vidal et al., 1997).

All MIS 3 $\delta^{13}C$ Bond cycles show nearly identical $\delta^{13}C$ values at the beginning (high $\delta^{13}C$ values) as well as at the end (low $\delta^{13}C$ values) of each cycle. This suggests the GNAIW/AABW mixing zone was situated in a similar depth at the beginning (deep mixing zone) as well as at the end (shallow mixing zone) of each cycle (e.g. Vidal et al., 1997). Furthermore, similar amplitudes of D/O $\delta^{13}C$ cycles throughout MIS 3 point to similar

millennial-scale variations in mixing zone depth. These observations suggest GNAIW production rates of different MIS 3 Bond cycles were similar to each other and the amplitude of variations in GNAIW production during D/O cycles was quite constant during MIS 3. The MIS 2 $\delta^{13}C$ Bond cycle begins with lower $\delta^{13}C$ values than the MIS 3 Bond cycles, indicating a shallower GNAIW/AABW mixing zone and minor GNAIW production during MIS 2 (e.g. Piotrowski et al., 2005). Furthermore, stable $\delta^{13}C$ values during the LGM (from 22.7 to 18.5 kyr BP) suggest no major variations in the GNAIW/AABW mixing zone depth and GNAIW production occurred during this period (Elliot et al., 2002). Based on GeoB 3910 $\delta^{13}C$, LGM GNAIW production rates were lower than during most MIS 3 interstadials, but higher than during H event stadials. Furthermore, they are on the same level like in the B/A. This indicates reduced but quite active GNAIW production during the LGM (e.g. Curry and Oppo, 2005).

Following the LGM, very low $\delta^{13}C$ values indicate a strong shallowing of the GNAIW/AABW mixing zone and a strong reduction of GNAIW production during the stadial associated with H1 (McManus et al., 2004). Based on GeoB 3910 $\delta^{13}C$, GNAIW production was significantly lower during this stadial than during MIS 3 H event stadials (e.g. Vidal et al., 1997). YD $\delta^{13}C$ values are on the same level like during MIS 3 H event stadials, indicating similar shallowing of the GNAIW/AABW mixing zone and similarly reduced GNAIW production. This underlines the exceptionally shallow position of the mixing zone during the stadial associated with H1 (McManus et al., 2004).

Following the stadial associated with H1, the rapid increase to high $\delta^{13}C$ values during the B/A indicates a fast deepening of the GNAIW/AABW mixing zone and a strong increase in GNAIW production. This agrees with model studies from (Knorr and Lohmann, 2003), which suggest the THC may have switched abruptly from a glacial mode with minor and shallow GNAIW production to a Holocene mode with vigorous and deep NADW production at the onset of the B/A. However, our data indicates GNAIW production was not more intense during the B/A than during the LGM (McManus et al., 2004) and less intense than during MIS 3 interstadials. This suggests GNAIW production was increased during the B/A, but may not have switched to NADW production at its onset. Furthermore, this underlines GNAIW production was quite vigorous in MIS 3 interstadials (Curry and Oppo, 2005).

4.3.6.4 Relation between changes in South American precipitation patterns and variations in the oceanic THC

The variations in GeoB 3910 benthic foraminiferal $\delta^{13}C$ coincide with shifts in GeoB 3910 Ti/Ca (Fig. 18). H events as well as D/O cycles can be tracked in both records. However, there is no direct link between tropical South American precipitation and the oceanic THC. Both parameters are coupled to North Atlantic temperatures rather. Variations in tropical South American precipitation are caused by shifts in the position of the ITCZ, which, in turn, are coupled to changes in high northern latitude temperatures via the North Atlantic meridional temperature gradient. Variations in high northern latitude temperatures, in turn, are directly coupled to changes in the intensity of deep water production in the North Atlantic (Bond et al., 1999). Therefore, reorganizations of the oceanic THC may trigger or amplify millennial-scale variations in the North Atlantic meridional temperature gradient, which, in turn, lead to shifts in tropical precipitation patterns.

To validate the implied linkage of shifts in tropical precipitation patterns to reorganizations of the oceanic THC, it is crucial to verify the coupling between deep western tropical Atlantic properties and GNAIW production. Therefore, we compare the benthic $\delta^{13}C$ record of GeoB 3910 to deep ocean circulation records from the North Atlantic (Fig. 21; McManus et al., 2004; Vidal et al., 1997). Vidal et al. (1997) provide a benthic foraminiferal $\delta^{13}C$ record of the last 56 kyr from the central mid-latitude North Atlantic (sediment core NA 87-22) showing millennial-scale oscillations that coincide with Greenland D/O cycles. $\delta^{13}C$ values are high during Greenland interstadials and low during stadials. Minimum $\delta^{13}C$ values are confined to H event stadials. The strongest negative excursion thereby occurs during the stadial associated with H1. These observations suggest millennial-scale reorganizations of the Atlantic THC identical with those indicated by GeoB 3910. In addition, GeoB 3910 resolves more D/O cycles than NA 87-22, which is probably due to a higher resolution of GeoB 3910 during MIS 3.

McManus et al. (2004) provide a $^{231}Pa/^{230}Th$ ratio record of the last 20 kyr from the western subtropical North Atlantic (sediment core OCE 326-GGC5). $^{231}Pa/^{230}Th$ ratios record changes in deep ocean circulation, with low $^{231}Pa/^{230}Th$ ratios indicating strong NADW/GNAIW production and high ratios indicating weak NADW/GNAIW production in the Atlantic (McManus et al., 2004). The $^{231}Pa/^{230}Th$ record indicates vigorous GNAIW production of similar intensity during the LGM and the B/A. The stadial associated with H1 shows strongly increased $^{231}Pa/^{230}Th$ ratios, indicating GNAIW production nearly ceased during this stadial (McManus et al., 2004). During the YD, $^{231}Pa/^{230}Th$ ratios are moderately reduced, indicating

decreased but active GNAIW production. These observations agree with our findings deduced from GeoB 3910. Especially, they support our observations of a quite vigorous meridional overturning circulation during the LGM and of nearly ceasing GNAIW production during the stadial associated with H1.

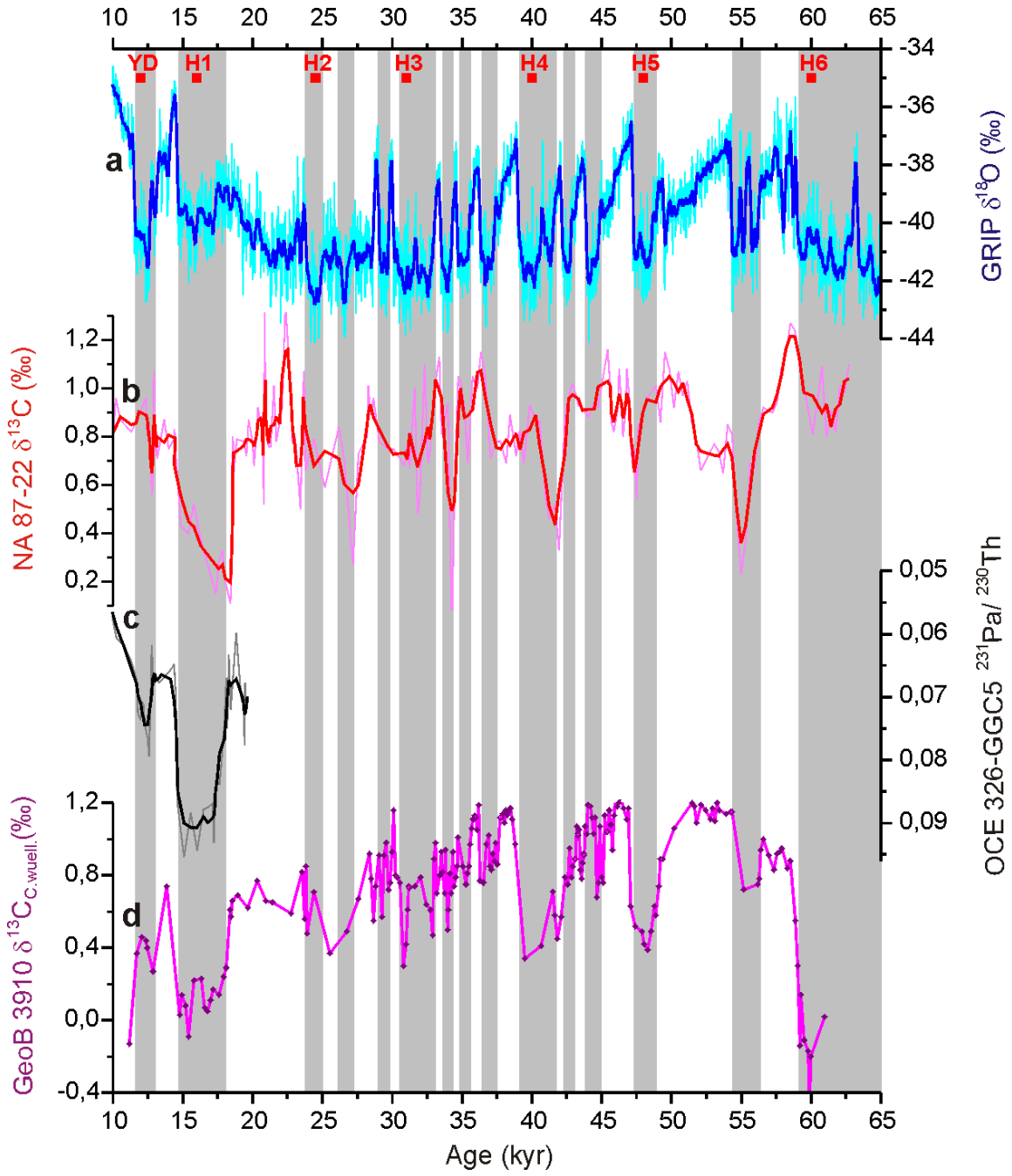

Figure 21: Coincidence of variations in Greenland temperature **(a)** and Glacial North Atlantic Intermediate Water production **(b, c, d)**

a) GRIP $\delta^{18}O$ from central Greenland (Shackleton et al., 2004); **b)** benthic foraminiferal $\delta^{13}C$ of sediment core NA 87-22 from the central subpolar North Atlantic (Vidal et al., 1997); **c)** $^{231}Pa/^{230}Th$ ratio of sediment core OCE 326-GGC5 from the western subtropical North Atlantic; **d)** benthic foraminiferal $\delta^{13}C$ of sediment core GeoB 3910 from the western tropical Atlantic (this study); gray boxes represent Greenland stadials; YD marks the Younger Dryas (Alley, 2000), H1 to H6 denote Heinrich events 1 to 6 (Broecker and Hemming, 2001).

4.3.7 Conclusions

We established centennial-scale records of changes in tropical South American precipitation patterns and deep western tropical Atlantic conditions. Millennial-scale changes in precipitation patterns are closely coupled to shifts in the position of the ITCZ. Therefore, precipitation records from regions close to the interstadial ITCZ range (which is similar to the modern one) are dominated by millennial-scale variations, whereas insolation-driven multi-millennial cycles dominate the precipitation records of regions further away from the equator.

Deep western tropical Atlantic conditions indicate millennial-scale shifts in the depth of the GNAIW/AABW mixing zone. These, in turn, are driven by changes in GNAIW production intensity, which are associated with high latitude North Atlantic temperature variations. Compared to earlier studies on the GNAIW/AABW mixing zone, our results provide a better resolution during MIS 3 and therefore allow the detection of D/O cyclicity in deep western tropical Atlantic conditions.

Synchronous changes in deep western tropical Atlantic conditions and tropical South American precipitation patterns indicate a linkage between THC reorganizations and shifts in tropical precipitation patterns via changes in North Atlantic SST, variations in the meridional North Atlantic temperature gradient and resulting shifts of the ITCZ. This linkage is present during D/O cycles and H events, but due to different amplitudes of temperature variations in the high latitude North Atlantic, the amplitude of variations in the meridional North Atlantic temperature gradient and the rate of ITCZ shifts are lower during D/O cycles than during H events. This leads to different spatial patterns of the impacts of THC reorganizations on tropical precipitation rates during D/O cycles and H events. The main difference of tropical South American D/O cycle and H event precipitation changes, however, is the amplitude of these changes.

Acknowledgements

We thank C. Rühlemann, F. Lamy, S. Mulitza and P. B. deMenocal for discussions and M. Segl and her team for helping with the isotope analyses. This work was generously supported by the Gary Comer Foundation.

4.3.8 References

Alley, R. B. (2000). The Younger Dryas cold interval as viewed from central Greenland. *Quaternary Science Reviews* **19**, 213-226.

Andrié, C. (1996). Chlorofluoromethanes in the deep equatorial Atlantic revisited. *In "The South Atlantic: Present and past circulation"* (edited by G. Wefer, W. H. Berger, G. Siedler and D. J. Webb), pp. 273-288. Springer-Verlag, Berlin.

Arnault, S., Bourles, B., Gouriou, Y., and Chuchla, R. (1999). Intercomparison of upper layer circulation of the western equatorial Atlantic Ocean: In situ and satellite data. *Journal of Geophysical Research* **104(C9)**, 21,171-21,194.

Arz, H. W., Pätzold, J., and Wefer, G. (1998). Correlated millennial-scale changes in surface hydrography and terrigenous sediment yield inferred from last-glacial marine deposits off northeastern Brazil. *Quaternary Research* **50,** 157-166.

Arz, H. W., Pätzold, J., and Wefer, G. (1999). Climatic changes during the last deglaciation recorded in sediment cores from the northeastern Brazilian continental margin, *Geo-Marine Letters* **19**, 209-218.

Auler, A. S., Wang, X., Edwards, R. L., Cheng, H., Cristalli, P. S., Smart, P. L., and Richards, D. A. (2004). Quaternary ecological and geomorphic changes associated with rainfall events in presently semi-arid northeastern Brazil. *Journal of Quaternary Science* **19**, 693-701.

Baker, P. A., Rigsby, C. A., Seltzer, G. O., Fritz, S. C., Lowenstein, T. K., Bacher, N. P., and Veliz, C. (2001). Tropical climate changes at millennial and orbital timescales on the Bolivian Altiplano. *Nature* **409,** 698-701.

Bard, E. (1988). Correction of accelerator mass spectrometry ^{14}C ages measured in planktonic foraminifera: Paleoceanographic implications. *Paleoceanography* **3**, 635-645.

Bard, E. (2002). Abrupt climate changes over millennial time scales: Climate shock. *Physics Today* **55**, 32-38.

Bard, E., Rostek, F., Turon, J.-L., and Gendrau, S. (2000). Hydrological impact of Heinrich events in the subtropical northeast Atlantic, *Science* **289**, 1321-1324.

Behling, H., Arz, H. W., Pätzold, J., and Wefer, G. (2000). Late Quaternary vegetational and climate dynamics in northeastern Brazil, inferences from marine core GeoB 3104-1. *Quaternary Science Reviews* **19,** 981-994.

Blunier, T., and Brook, E. J. (2001). Timing of millennial-scale climate change in Antarctica and Greenland during the last glacial period, *Science* **291**, 109-112.

Blunier, T., et al. (1998). Asynchrony of Antarctic and Greenland climate change during the last glacial period, *Nature* **394**, 739-743.

Bond, G. C., Broecker, W. S., Johnsen, S., McManus, J., Labeyrie, L., Jouzel, J., and Bonani, G. (1993). Correlations between climate records from North Atlantic sediments and Greenland ice. *Nature* **365,** 143-147.

Bond, G. C., and Lotti, R. (1995). Iceberg discharges into the North Atlantic on millenial timescales during the last glaciation. *Science* **267**, 1005-1010.

Bond, G. C., Showers, W., Elliot, M., Evans, M., Lotti, R., Hajdas, I., Bonani, G., and Johnson, S. (1999). The North Atlantic's 1-2 kyr climate rhythm: Relation to Heinrich events, Dansgaard/Oeschger cycles and the Little Ice Age. *Geophysical Monograph* **112**, 35-58.

Boyle, E. A., and Keigwin, L. D. (1987). North Atlantic thermohaline circulation during the past 20,000 years linked to high-latitude surface temperature. *Nature* **330**, 35-40.

Broecker, W. S. (1991). The great ocean conveyor. *Oceanography* **4**, 79-89.

Broecker, W. S. (1994). Massive iceberg discharges as triggers for global climate change. *Nature* **372**, 421-424.

Broecker, W. S. (2003). Does the trigger for abrupt climate change reside in the ocean or in the atmosphere? *Science* **300**, 1519-1522.

Broecker, W. S., and Hemming, S (2001). Climate swings come into focus. *Science* **294**, 2308-2309.

Chiang, J. C. H., Biasutti, M., and Battisti, D. S. (2003). Sensitivity of the Atlantic Intertropical Convergence Zone to Last Glacial Maximum boundary conditions. *Paleoceanography* **18**, doi:10.1029/2003PA000916.

Chiang, J. C. H., and Bitz, C. M. (2005). Influence of high latitude ice cover on the marine Intertropical Convergence Zone. *Climate Dynamics* **25,** 477-496.

Cortijo, E., Labeyrie, L., Vidal, L., Vautravers, M., Chapman, M., Duplessy, J.-C., Elliot, M., Arnold, M., Turon, J.-L., and Auffret, G. (1997). Changes in sea surface hydrology associated with Heinrich event 4 in the North Atlantic Ocean between 40° and 60°N. *Earth and Planetary Science Letters* **146**, 29-45.

Cruz, F. W., Burns, S. J., Karmann, I., Sharp, W. D., Vuille, M., Cardoso, A. O., Ferrari, J. A., Silva Dias, P. L., and Viana, O. (2005). Insolation-driven changes in atmospheric circulation over the past 116,000 years in subtropical Brazil. *Nature* **434**, 63-66.

Curry, W. B., and Oppo, D. W. (1997). Synchronous, high-frequency oscillations in tropical sea surface temperatures and North Atlantic Deep Water production during the last glacial cycle. *Paleoceanography* **12**, 1-14.

Curry, W. B., and Oppo, D. W. (2005). Glacial water mass geometry and the distribution of $\delta^{13}C$ of ΣCO_2 in the western Atlantic Ocean. *Paleoceanography* **20**, doi:10.1029/2004PA001021.

Dansgaard, W. et al. (1993). Evidence for general instability of past climate from a 250-kyr ice-core record. *Nature* **364**, 218-220.

Elliot, M., Labeyrie, L., and Duplessy, J.-C. (2002). Changes in North Atlantic deep-water formation associated with the Dansgaard-Oeschger temperature oscillations (60-10 ka). *Quaternary Science Reviews* **21**, 1153-1165.

Fairbanks, R. G., Mortlock, R. A., Chiu, T.-C., Cao, L., Kaplan, A., Guilderson, T. P., Fairbanks, T. W., Bloom, A. L., Grootes, P. M., and Nadeau, M.-J. (2005). Radiocarbon calibration curve spanning 10,000 to 50,000 years BP based on paired $^{230}Th/^{234}U/^{238}U$ and ^{14}C dates on pristine corals. *Quaternary Science Reviews* **25**, 1781-1796.

Fischer, G., et al. (1996). Report and preliminary results of Meteor cruise M 34-4 Recife–Bridgetown, 19.03. – 15.04.1996, *Berichte, Fachbereich Geowissenschaften, Universität Bremen* **80**, 105 pp., Universität Bremen, Bremen.

Garzoli, S. L., Goni, G. J., Mariano, A. J., and Olson, D. B. (1997). Monitoring the upper southeastern Atlantic transports using altimeter data. *Journal of Marine Research* **55**, 453-481.

Gerhardt, S., Groth, H., Rühlemann, C., and Henrich, R. (2000). Aragonite preservation in Late Quaternary sediment cores on the Brazilian continental slope: Implications for intermediate water circulation. *International Journal of Earth Sciences* **88**, 607-618.

Grootes, P. M., and Stuiver, M. (1997). Oxygen 18/16 variability in Greenland snow and ice with 103- to 105-year time resolution. *Journal of Geophysical Research* **102,** 26455-26470.

Hastenrath, S. (1990). Prediction of Northeast Brazil rainfall anomalies. *Journal of Climate* **3,** 893-904.

Hastenrath, S., and Greischar, L. (1993). Circulation mechanisms related to Northeast Brazil rainfall anomalies. *Journal of Geophysical Research* **98 (D3)**, 5093-5102.

Hastenrath, S., and Heller, L. (1977). Dynamics of climatic hazards in Northeast Brazil. *Quarterly Journal of the Royal Meteorological Society* **103**, 77-92.

Hastenrath, S., and Merle, J. (1987). Annual cycle of subsurface thermal structure in the tropical Atlantic Ocean. *Journal of Physical Oceanography* **17**, 1518-1538.

Heil, G. M. N., Arz, H.W., deMenocal, P. B., and Wefer, G. (submitted). Forcing of tropical South American precipitation during the last 63,000 years, *Nature*.

Heinrich, H. (1988). Origin and consequences of cyclic ice rafting in the northeast Atlantic Ocean during the past 130,000 years. *Quaternary Research* **29**, 142-152.

Hendy, I. L., and Kennett, J. P. (2000). North Pacific intermediate water temperature instability during Late Quaternary rapid climate change. Planktonic foraminiferal response to rapid climate change in Santa Barbara Basin, ODP 893 Hole A. *Paleoceanography* **15**, 30-42.

Hüls, M., and Zahn, R. (2000). Millennial-scale SST variability in the western tropical North Atlantic from planktonic foraminiferal census counts. *Paleoceanography* **15**, 731-737.

Jennerjahn, T. C., Ittekkot, V., Arz, H. W., Behling, H., Pätzold, J., and Wefer, G. (2004). Asynchronous terrestrial and marine signals of climate change during Heinrich events. *Science* **306,** 2236-2239.

Johns, W. E., Lee, T. N., Beardsley, R. C., Candela, J., Limeburner, R., and Castro, B. (1998). Annual cycle and variability of the North Brazil Current. *Journal of Physical Oceanography* **28**, 103-128.

Jouzel, J., et al. (1993). Extending the Vostok ice-core record of palaeoclimate to the penultimate glacial period. *Nature* **364**, 407-412.

Keigwin, L. D., and Jones, G. A. (1994). Western North Atlantic evidence for millennial-scale changes in ocean circulation and climate. *Journal of Geophysical Research* **99**, 12,397-12,410.

Knorr, G., and Lohmann, G. (2003). Southern Ocean origin for the resumption of Atlantic thermohaline circulation during deglaciation. *Nature* **424**, 532-536.

Lohmann, G. (2003). Atmospheric and oceanic freshwater transport during weak Atlantic overturning circulation. *Tellus* **A 55**, 438-449.

McManus, J. F., Francois, R., Gherardi, J.-M., Keigwin, L. D., and Brown-Leger, S. (2004). Collapse and rapid resumption of Atlantic meridional circulation linked to deglacial climate changes. *Nature* **428**, 834-837.

Ninnemann, U. S., and Charles, C. D. (2002). Changes in the mode of Southern Ocean circulation over the last glacial cycle revealed by foraminiferal stable isotopic variability. *Earth and Planetary Science Letters* **201**, 383-396.

Oppo, D. W., and Lehman, S. J. (1995). Suborbital timescale variability of North Atlantic Deep Water during the past 200,000 years. *Paleoceanography* **10**, 901-910.

Peterson, L. C., Haug, G. H., Hughen, K. A., Röhl, Ursula. (2000). Rapid changes in the hydrologic cycle of the tropical Atlantic during the last glacial. *Science* **290,** 1947-1951.

Peterson, R. G., and Stramma, L. (1990). Upper-level circulation in the South Atlantic Ocean. *Progress in Oceanography* **26**, 1-73.

Piotrowski, A. M., Goldstein, S. L., Hemming, S. R., Fairbanks, R. G. (2005). Temporal relationships of carbon cycling and ocean circulation at glacial boundaries. *Science* **307**, 1933-1938.

Rahmstorf, S. (2002). Ocean circulation and climate during the past 120,000 years. *Nature* **419**, 207-214.

Rhein, M., Schott, F., Fischer, J., Send, U., and Stramma, L. (1996). The deep water regime in the equatorial Atlantic. *In "The South Atlantic: Present and past Circulation"* (edited by G. Wefer, W. H. Berger, G. Siedler and D. J. Webb), pp. 261-271. Springer-Verlag, Berlin.

Röhl, U., and Abrams, L. J. (2000). High-resolution, downhole, and nondestructive core measurements from sites 999 and 1001 in the Caribbean Sea: Application to the Late Paleocene Thermal Maximum. *In "Proceedings of the Ocean Drilling Program, scientific results **165**"* (edited by R. M. Leckie, H. Sigurdsson, G. D. Acton, and G. Draper), pp. 191-203.

Rühlemann, C., Mulitza, S., Müller, P. J., Wefer, G., and Zahn, R. (1999). Warming of the tropical Atlantic Ocean and slowdown of thermohaline circulation during the last deglaciation. *Nature* **402**, 511-514.

Schmidt, M. W., Spero, H. J., and Lea, D. W. (2004). Links between salinity variation in the Caribbean and North Atlantic thermohaline circulation. *Nature* **428**, 160-163.

Schott, F. A., Fischer, J., and Stramma, L. (1998). Transports and pathways of the upper-layer circulation in the western tropical Atlantic. *Journal of Physical Oceanography* **28**, 1904-1928.

Schulz, H., von Rad, U., and Erlenkeuser, H. (1998). Correlation between Arabian Sea and Greenland climate oscillations of the past 110,000 years. *Nature* **393**, 54-57.

Shackleton, N. J., Fairbanks, R. G., Chiu, T.-C., and Parrenin, F. (2004). Absolute calibration of the Greenland time scale: Implications for Antarctic time scales and for $\delta^{14}C$. *Quaternary Science Reviews* **23,** 1513-1522.

Stocker, T. F. (1998). The seasaw effect. *Science* **282**, 61-62.

Thompson, L. G., et al. (1998). A 25,000-Year tropical climate history from Bolivian ice cores. *Science* **282,** 1858-1864.

Thompson, L. G., Mosley-Thompson, E., Davis, M. E., Lin, P.-N., Henderson, K. A., Cole-Dai, J., Bolzan, J. F., and Liu, K.-B. (1995). Late glacial stage and Holocene tropical ice core records from Huascarán, Peru. *Science* **269,** 46-50.

Vidal, L., Labeyrie, L., Cortijo, E., Arnold, M., Duplessy, J. C., Michel, E., Becque, S., and van Weering, T. C. E. (1997). Evidence for changes in the North Atlantic Deep Water linked to meltwater surges during the Heinrich events. *Earth and Planetary Science Letters* **146**, 13-27.

Voelker, A. H. L. (2002). Global distribution of centennial-scale records for Marine Isotope Stage (MIS) 3: A database. *Quaternary Science Reviews* **21**, 1185-1212.

Wang, X., Auler, A. S., Edwards, R. L., Cheng, H., Cristalli, P. S., Smart, P. L., Richards, D. A., and Shen, C.-C. (2004). Wet periods in northeastern Brazil over the past 210 kyr linked to distant climate anomalies. *Nature* **432,** 740-743.

Wang, Y. J., Cheng, H., Edwards, R. L., An, Z. S., Wu, J. Y., Shen, C.-C., and Dorale, J. A. (2001). A high-resolution absolute-dated Late Pleistocene monsoon record from Hulu Cave, China. *Science* **294,** 2345-2348.

Weninger, B., Danzeglocke, U., and Jöris, O. (2005). "Comparison of dating results achieved using different radiocarbon-age calibration curves and data."

4.4 Manuscript 3: Extent of high northern latitude temperature forcing on millennial-scale precipitation changes in eastern South America

Gerrit M. N. Heil[1*], Helge W. Arz[2], Hermann Behling[3] and Gerold Wefer[1]

1 DFG Research Center Ocean Margins, Universität Bremen, P.O. Box 330440, D-28334 Bremen, Germany (gerrit.heil@uni-bremen.de)

2 GeoForschungZentrum Potsdam, Telegrafenberg C322, D-14473 Potsdam, Germany

3 Albrecht von Haller Institut für Pflanzenwissenschaften, Abteilung für Palynologie und Klimadynamik, Untere Karspüle 2, D-37033 Göttingen

* Corresponding author. Tel.: +49-421-21865680; Fax: +49-421-21865505
E-Mail: gerrit.heil@uni-bremen.de

to be submitted to *Quaternary Science Reviews*

Abstract

Millennial-scale variations in high northern latitude atmospheric and sea surface temperatures induced hemispheric-wide reorganisations of the atmospheric circulation during the last glacial, including shifts in the position of the Intertropical Convergence Zone, which, in turn, changed tropical precipitation patterns. In South America, corresponding precipitation shifts have been observed from 10°N to 22°S. The magnitude of precipitation shifts thereby decreases with distance from the modern position of the Intertropical Convergence Zone. Here, we address the question if such precipitation shifts also occurred south of the tropics by presenting precipitation records obtained from terrestrial and marine sediment records at and off the South Brazilian Atlantic coast around 28°S. We show millennial-scale precipitation changes are small and subordinate to precipitation shifts of orbital timescales, but can be related to Intertropical Convergence Zone shifts. This marks South Brazil as a transition area with respect to millennial-scale climate variability and suggests millennial-scale climate variations related to high northern latitude temperature change do not occur far south of 28°S in eastern South America.

4.4.1 Introduction

The global climate of the last glacial was dominated by quasi-cyclic variations of approximately 1,470 yrs duration, called Dansgaard/Oeschger (D/O) cycles (Grootes and Stuiver, 1997). These have been reported from many parts of the northern hemisphere, including the high to mid-latitudes (Bond et al., 1993; Cacho et al., 1999; Dansgaard et al., 1993; Hendy and Kennett, 1999) as well as the tropics (Arz et al., 1998; Schulz et al., 1998; Wang et al., 2001). Whereas D/O cycles are mainly expressed as temperature shifts in the high and mid-latitudes, they primarily show up as variations in precipitation regimes in the low latitudes (Broecker and Hemming, 2001). The climatic teleconnection between these regions thereby is provided by global reorganizations of the atmospheric wind systems (Broecker, 2003).

Some D/O stadials are associated with so-called Heinrich (H) events, which are associated with stronger disruptions of the oceanic THC than D/O cycles, and therefore show stronger variations in temperature and precipitation in many records (Arz et al., 1998; Bard, 2002; Peterson et al., 2000; Schulz et al., 1998; Wang et al., 2001). For example, in the semiarid region of Northeast Brazil, which is lying close to the equator, corresponding precipitation shifts have been observed during H events and D/O cycles (Arz et al., 1998, 1999; Auler et al., 2004; Behling et al., 2000; Heil et al., submitted-a; Jennerjahn et al., 2004; Wang et al., 2004). In contrast, in Southeast Brazil, around 20 to 22°S, significant millennial-scale precipitation shifts have been found to occur only during H events (Behling et al., 2002). Both in Northeast and Southeast Brazil, these precipitation shifts are coupled to changes in the position of the Intertropical Convergence Zone (ITCZ), which, in turn, is defined by the temperature gradient between the high latitude North Atlantic and the tropical Atlantic (Heil et al., submitted-a). As this temperature gradient is mainly governed by high latitude North Atlantic temperatures, the ITCZ provides the linkage mechanism between tropical precipitation and high northern latitude temperature.

Combined, the Northeast and Southeast Brazilian records suggest millennial-scale climate variability may be confined to the region directly or indirectly influenced by ITCZ shifts. To specify the spatial extent of this region, we extended the compilation of sub-millennial-scale precipitation records further southward. We analyzed changes in precipitation patterns in the South Brazilian catchment area of the Rio Itajaí (27 to 28°S) based on Fe/Ca ratios of sediment core GeoB 2107 from the subtropical western Atlantic. We demonstrate the amount of precipitation did not change significantly on millennial timescales in the Rio Itajaí's catchment area during the last 74 kyr. Rather, the precipitation record is predominantly governed by variations of orbital timescales. However, millennial-scale changes in the proportion of summer versus winter precipitation can be deduced from another South Brazilian climate record (Cruz et al., 2005). This suggests millennial-scale climate variability related to high northern latitude temperature change is still present in the Rio Itajaí's catchment area, but is dominated by climate variability of orbital timescales.

4.4.2 Study Area

4.4.2.1 Geographic Setting

The study area extends from the catchment area of the Rio Itajaí in southern Brazil to the continental slope off the east coast of South Brazil (Fig. 22). The Rio Itajaí drains a large part of Santa Catarina State in southern Brazil. To the west, its catchment area is confined by the Planaltos Residuais Sertanejos, a large mountain system belonging to the Brazilian Highlands. The northern and southern borders of this catchment area are formed by smaller mountain chains, whereas the Atlantic lies at its eastern margin.

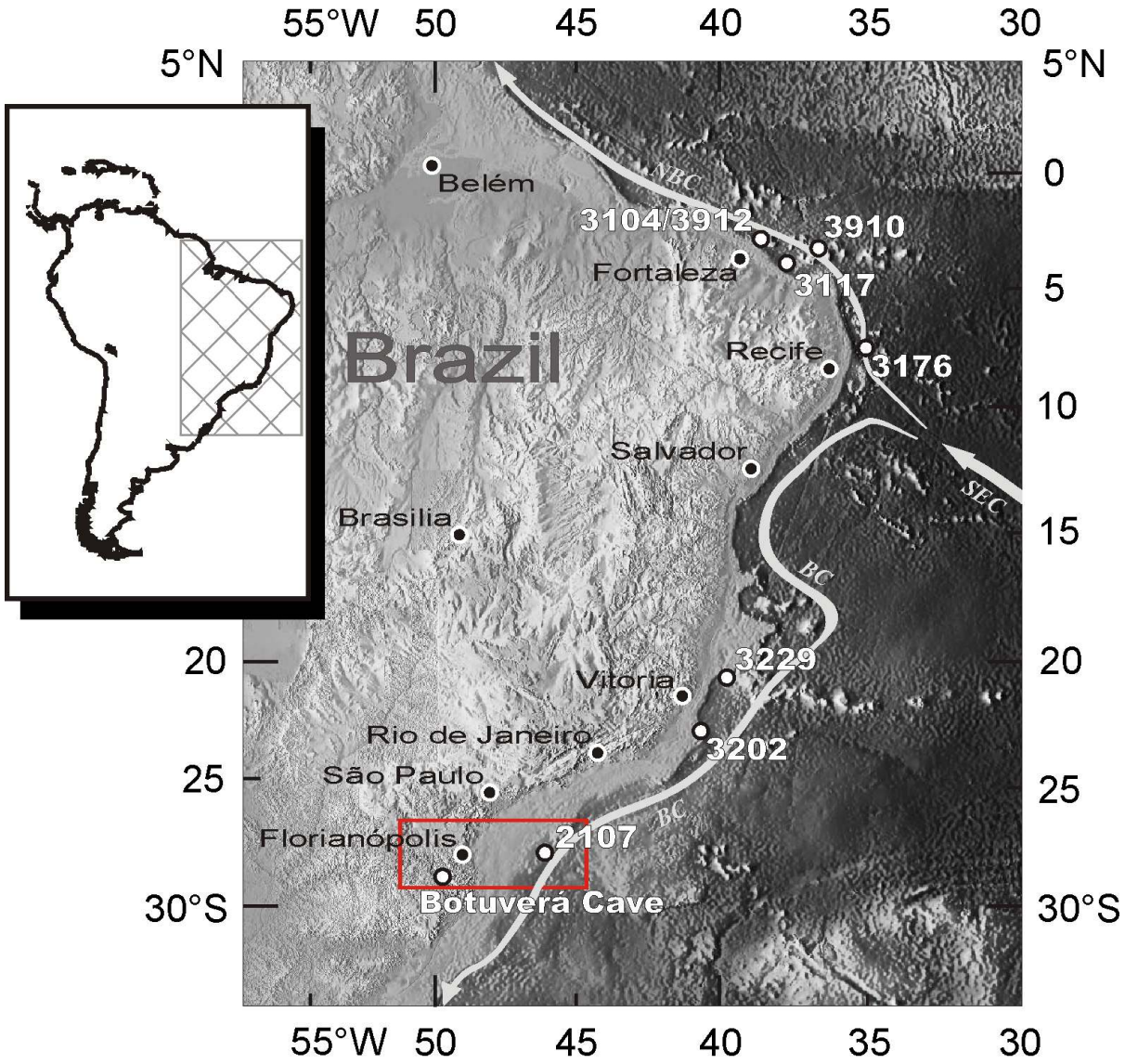

Figure 22: Sitemap of sediment archives used in this study and major ocean currents off the Brazilian coast

NBC denotes the North Brazil Current, BC the Brazil Current, and SEC the South Equatorial Current. The red rectangle marks the focus investigation area in South Brazil and the adjacent western subtropical Atlantic. Numbers from 2107 to 3912 mark the respective GeoB sediment cores (Table 6).

The lowlands and the coastal mountain chains of the Rio Itajaí's catchment area are made up by Precambrian granitoids and silt- to sandstones which are covered by siliceous sands in the fluvial and near-shore areas (Rachwal and Curcio, 1994; Schobbenhaus et al., 1995). The mountain chains in the western part of the catchment area consist of Carboniferous to Permian sand- to siltstones and cherts with small limestone deposits (Schobbenhaus et al., 1995). Altogether, the catchment area of the Rio Itajaí is mainly made up by siliceous material and does not contain significant amounts of carbonaceous material.

The continental shelf off eastern South Brazil has an average width of about 100 km (Viana et al., 1998). The shelf break is located at about 110 m water depth and marks the beginning of the continental slope, which extends over 30-40 km with an average gradient of 2.5° (Viana et al., 1998). From the base of the continental slope at 2000 m depth, the Sao Paulo Plateau, a low-gradient (< 0.5°) area, extends down to 3500 m depth and leads over into the deep sea (Viana et al., 1998).

Five main water bodies fill the western subtropical South Atlantic. The continental shelf and the upper continental slope lie in the zone of the southward flowing Tropical Water, which extends from the water surface down to about 300 m depth (Viana et al., 1998). Between 300 and 550 m depth, South Atlantic Central Water flows northward (Viana et al., 1998). Antarctic Intermediate Water (AAIW) irrigates the middle continental slope between 550 and 1200 m depth (Reid, 1989). Below the AAIW, North Atlantic Deep Water (NADW) extends from 1200 to 3500 m depth (Reid, 1989). Antarctic Bottom Water (AABW) occurs beneath NADW, far away from the outer limit of the study area (Reid, 1989).

The oceanic sediment transport is dominated by downward sea bottom currents in the study area (Xavier et al., 1993). However, upper ocean sediment transport may be influenced by the Brazil Current, eddies, tide-related bottom currents and storm waves down to 500 m depth (Viana et al., 1998). Antarctic Intermediate Water reaches its peak velocities at 800 m depth, where it may partly influence sedimentation regimes (Xavier et al., 1993).

Modern sedimentation on the continental shelf and the upper continental slope is dominated by siliciclastic to bioclastic sands (Viana et al., 1998). The middle slope (500 to 1200 m depth) shows a transgression from sand-dominated to mud-dominated sediments, and the lower slope is characterized by nanoforaminiferal ooze (Viana et al., 1998). The sediment core analyzed in this study was retrieved from the mud-dominated part of the middle slope (1048 m water depth), a relatively calm sedimentation regime with generally well-preserved sediments (Xavier et al., 1993).

4.4.2.2 Climate

Today, the climate system of the Rio Itajaí's catchment area is marked by a humid, warm (subtropical) climate without a distinct dry season (Fig. 23; Nimer, 1989). Average annual precipitation is over 2000 mm, and the mean annual temperature is 14.5 °C (Nimer, 1989). The high precipitation rates result from the topography of the Rio Itajaí's catchment area. The mountain chains form an orographic barrier for northerly, easterly and southerly winds. This induces high precipitation rates in the catchment area.

Although distinct wet and dry seasons are not observed, winter and summer precipitation are related to different atmospheric circulation systems (Carvalho et al., 2002; Xie and Arkin, 1997). During austral winter and early spring, the southern polar fronts reach their northernmost position and trigger equator ward incursions of mid- to high-latitude cold air. This results in cyclonic wind systems, which transport large amounts of moisture from the Atlantic Ocean to the continent (Vera et al., 2002). Over southern Brazil, these cold air masses meet the warm tropical air masses, resulting in strong precipitation (Hastenrath, 1991; Nimer, 1989).

During austral summer and early autumn, the ITCZ reaches its southernmost position and gives rise to the South American Summer Monsoon (SASM), which transports huge amounts of moisture from the Atlantic onto the continent (Gan et al., 2004; Zhou and Lau, 1998). This induces high precipitation rates in the Rio Itajaí's catchment area during January and February (Fig. 23). Therefore, although not being directly beneath the centre of tropical convectivity, summer precipitation in the Rio Itajaí's catchment area is linked to the ITCZ. Strength and position of the SASM are dynamically coupled to the position of the ITCZ, i.e. the more southward the ITCZ is located during austral summer, the stronger is the SASM and the higher are the resulting summer precipitation rates (Zhou and Lau, 1998).

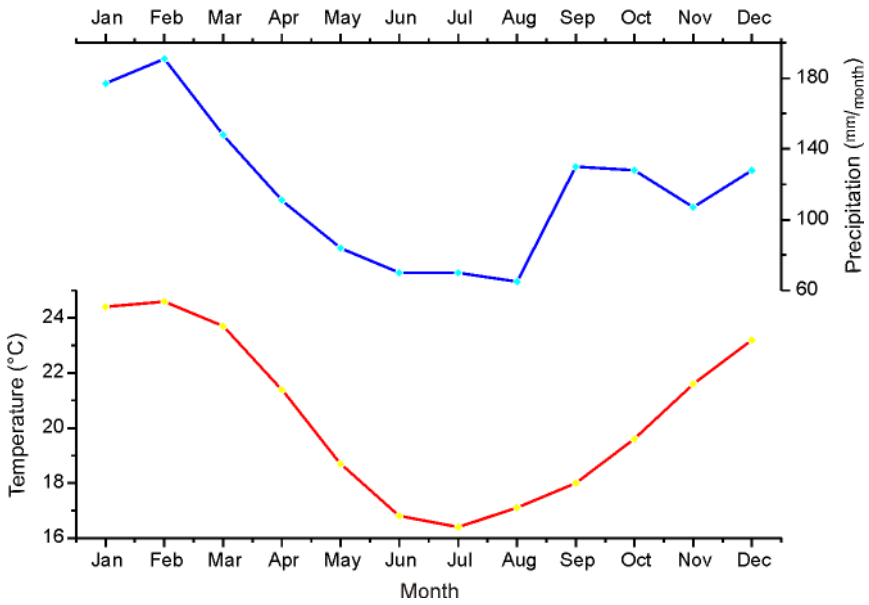

Figure 23: Climate diagram of Florianopolis (South Brazil). Note the precipitation maximum in January and February.

4.4.3 Material and Methods

4.4.3.1 Material

We analyzed sediment core GeoB 2107 (27°10,6' S, 46°27,1' W, 1048 m water depth), raised from the continental slope off the east coast of South Brazil with RV Meteor (Fig. 22; Bleil et al., 1993). GeoB 2107 consists of homogeneous dark grey nannofossil-bearing silt with two small sandy silt layers. The core offers a 783 cm long sediment sequence of which the upper 6 m show minor signs of bioturbation. The two small sandy silt layers occur at 0.8 and 3.5 m depth and have been removed from the sedimentary record. Except for these layers, the core shows a continuous and undisturbed sediment sequence.

GeoB 2107 was retrieved from approximately 270 km off the river mouth of the Rio Itajaí. The sediments transported into the Atlantic by this river are partly trapped on the narrow continental shelf, but a significant part of these sediments is transported down to the continental slope. Riverine sediments deposited there make up the terrestrial fraction of GeoB 2107. Therefore, GeoB 2107 provides information on both the western subtropical South Atlantic and the hydroclimatic regime in the Rio Itajaí's catchment area.

In addition to GeoB 2107, we included results from other sediment archives from the Southeast Brazilian coast in our study. These archives are shown in Fig. 22 and their location is given in Table 6.

Table 6: Sediment archives used in this study (see Fig. 22 for location of archives)

Sediment archive	Type of archive	Latitude	Longitude	Water depth (m bsl) / altitude (m asl)
GeoB 2107	marine sediment core	27°10,6' S	46°27,1' W	1048
GeoB 3104	marine sediment core	3°40,0' S	37°43,0' W	767
GeoB 3117	marine sediment core	4°11,1' S	37°08,0' W	930
GeoB 3176	marine sediment core	7°00,7' S	34°26,5' W	1385
GeoB 3202	marine sediment core	21°37,0' S	39°58,1' W	1090
GeoB 3229	marine sediment core	19°38,1' S	38°43,0' W	780
GeoB 3910	marine sediment core	4°14,7' S	36°20,7' W	2362
GeoB 3912	marine sediment core	3°40,0' S	37°43,0' W	772
Botuverá Cave	stalagmite	27°13,4' S	49°09.3' W	230

4.4.3.2 Bulk sediment chemistry

At intervals of 1 cm (average time resolution of 120 yrs), we analyzed GeoB 2107 for bulk sediment chemistry by X-ray fluorescence (XRF) on the XRF core scanner of the University of Bremen. This method allows the non-destructive analysis of split sediment cores regarding

the XRF intensities of the chemical elements from atomic number 19 (potassium) to 38 (strontium; Röhl and Abrams, 2000). The XRF intensities give an estimate of the concentrations of the respective elements in the sediment cores. Here, we report Ti, Fe, K, Ca and Sr XRF intensities.

4.4.3.3 Stable oxygen isotopes

For stratigraphic correlation of GeoB 2107 to the Specmap $\delta^{18}O$ record (Imbrie et al., 1984), stable oxygen isotope ratios ($\delta^{18}O$) of the benthic foraminifer *Uvigerina perigrina (U.peregr.)* were determined for every cm of GeoB 2107. We picked 4 well-preserved specimens for each sample, processed them with an automatic carbonate preparation system (Carbo type Bremen) and analyzed them on a Finnigan MAT 251 mass spectrometer (values reported in ‰ $\delta^{18}O$ versus VPDB). Every tenth sample was analyzed in duplicate. The average reproducibility was ± 0.4 ‰ and the analytical internal long-time precision better than ± 0.07 ‰.

4.4.3.4 Stratigraphy

The stratigraphy of GeoB 2107 (Fig. 24) is based on 14 calibrated and linearly interpolated radiocarbon ages spanning the last 50 cal. kyrs (Table 7). Radiocarbon dating was performed on mainly monospecific (*Globigerinoides sacculifer*, 600 - 800 specimens sized between 200 and 450 µm) carbonate samples at the Leibniz Laboratory for Radiometric Dating and Isotope Research of the University of Kiel, Germany. Radiocarbon ages were uniformly corrected for a reservoir age of 400 years (Bard, 1988) and calibrated (cal.) with CalPal (Weninger et al., 2005) using the CalPal_SFCP_2005 calibration curve, which is based on the radiocarbon calibration presented by Fairbanks et al. (2005). For the part of the core lying beyond the range of the radiocarbon method (50 cal. kyr and older), we tuned the $\delta^{18}O$ record of *U. peregrina* to the Specmap $\delta^{18}O$ record (Imbrie et al., 1984).

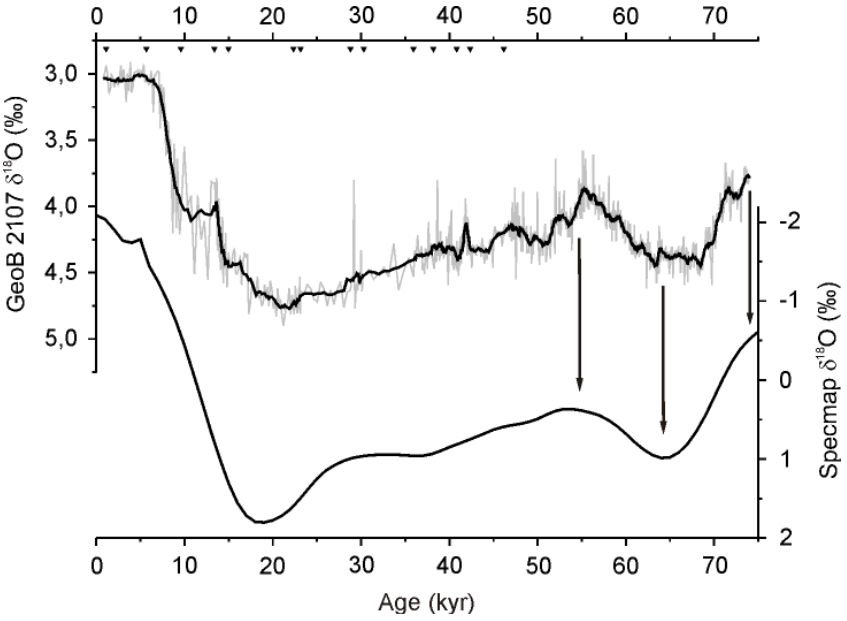

Figure 24: Age model of GeoB 2107: Combination of calibrated radiocarbon ages (black triangles on top) and correlation of GeoB 2107 benthic foraminiferal (*Uvigerina peregrina*) $\delta^{18}O$ to Specmap $\delta^{18}O$ (indicated by black arrows)

Table 7: Age model of sediment core GeoB 2107

Accelerator mass spectrometry (AMS) radiocarbon (^{14}C) ages were obtained from monospecific (*Globigerinoides sacculifer*, 600 - 800 specimens sized between 200 and 450 µm) carbonate samples. Radiocarbon ages were uniformly corrected for a reservoir age of 400 years (Bard, 1988) and calibrated (cal.) with CalPal (Weninger et al., 2005) using the CalPal_SFCP_2005 calibration curve, which is based on the radiocarbon calibration of Fairbanks et al. (2005). Correlations to Specmap are based on tuning the benthic foraminiferal $\delta^{18}O$ record of GeoB 2107 to Specmap $\delta^{18}O$ (Fig. 24).

Core depth (cm)	^{14}C-age (yr)	+error (yr)	-error (yr)	Cal. age (yr)	±error (yr)	Type of dating	Lab ID
3	1590	30	30	1120	40	AMS ^{14}C dating	KIA 14534
33	5340	40	40	5670	40	AMS ^{14}C dating	KIA 14533
63	8995	55	55	9580	50	AMS ^{14}C dating	KIA 14532
73	11890	80	80	13390	130	AMS ^{14}C dating	KIA 14530
103	13030	80	80	14990	300	AMS ^{14}C dating	KIA 14528
148	19100	130	120	22340	280	AMS ^{14}C dating	KIA 22409
163	19810	150	150	23160	350	AMS ^{14}C dating	KIA 14525
178	24250	200	200	28790	380	AMS ^{14}C dating	KIA 22408
193	25750	240	240	30310	320	AMS ^{14}C dating	KIA 22407
203	31180	460	430	35950	430	AMS ^{14}C dating	KIA 16166
223	33380	580	540	38200	820	AMS ^{14}C dating	KIA 16164
253	35990	870	780	40840	1000	AMS ^{14}C dating	KIA 16165
298	37600	1250	1080	42360	640	AMS ^{14}C dating	KIA 14524
338	42760	1940	1560	46170	1750	AMS ^{14}C dating	KIA 22404
472				56000		Correlation to Specmap	
660				64120		Correlation to Specmap	
783				74000		Correlation to Specmap	

4.4.4 Results

The XRF intensities give estimates of the concentrations of the analysed elements, but they do not allow calculations of these concentrations. Therefore, only relative changes in XRF element intensities (and therewith in element concentration) are significant. The XRF intensities of Fe, Ti, K, Ca and Sr show coincident multi-millennial changes (Fig. 25). Whereas the intensities of Fe, Ti and K correlate positively to one another, both Ca and Sr intensities correlate negatively to Fe, Ti and K intensities.

Fe, Ti and K intensities decrease from 74.0 to 37.0 kyr BP, whereas Ca and Sr intensities increase during this time (except for a sharp decrease in Ca and Sr intensities from 74.0 to 70.0 kyr BP). From 37.0 to about 25.7 kyr BP, Fe, Ti and K intensities increase again and are relatively stable from 25.7 to 18.1 kyr BP. Ca and Sr intensities show the opposite trend, decreasing first from 37.0 to 25.7 kyr BP and being relatively stable from 25.7 to 18.1 kyr BP. Thereafter, there is a strong decrease in Fe, Ti and K intensities until 13.0 kyr BP and a strong

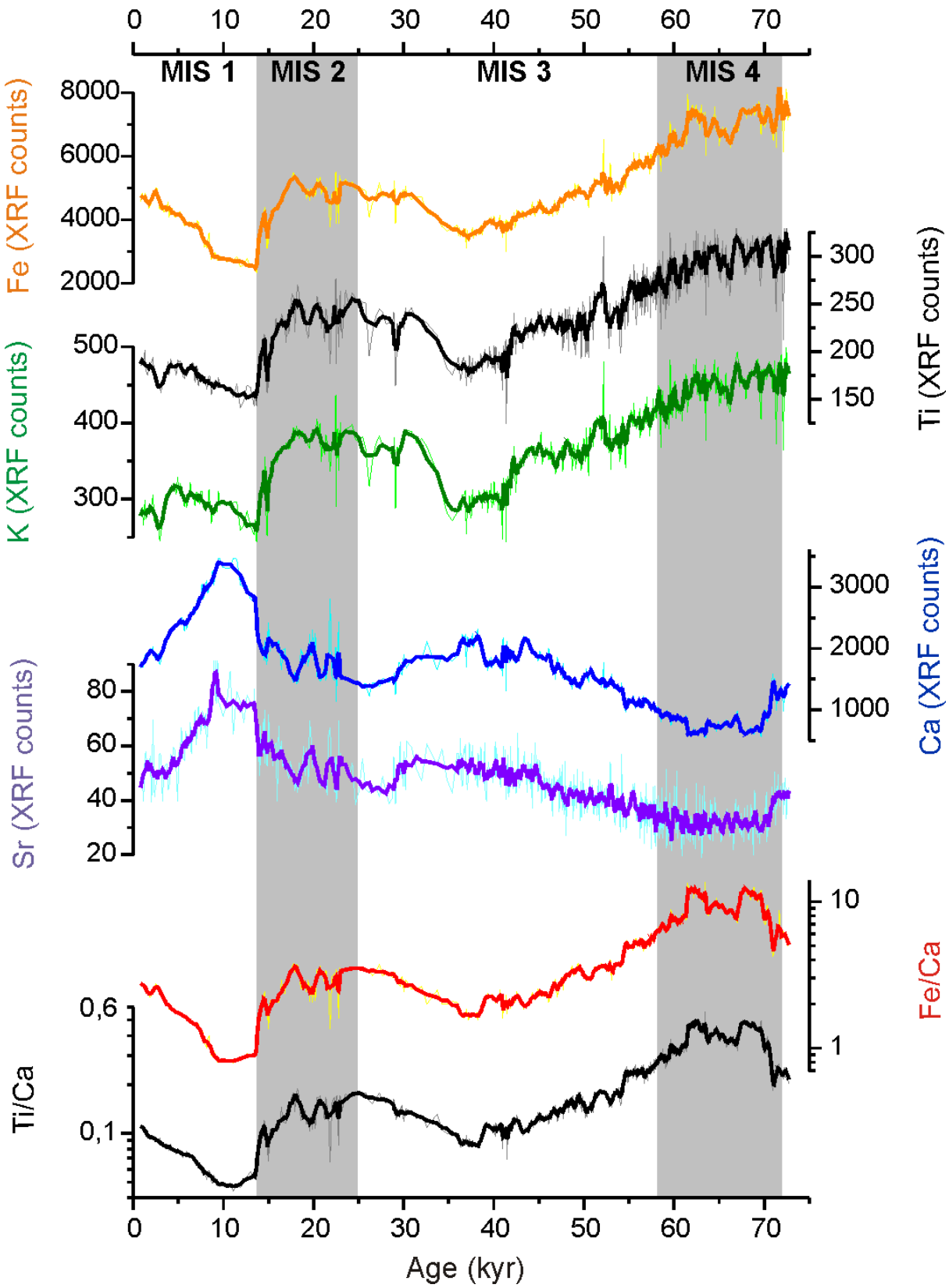

Figure 25: XRF Data of elements bound to the terrestrial (Fe, Ti, K) and marine (Ca, Sr) sediment fraction of GeoB 2107 (see Fig. 22 for location) and calculated Fe/Ca and Ti/Ca ratios

Note the similar trends in Fe, Ti and K XRF counts as well as in Ca and Sr XRF counts. Furthermore, note the opposite signal of coincident changes in the terrestrial and the marine sediment fraction. Note also the similarity between the Fe/Ca and the Ti/Ca record.

increase in Ca and Sr intensities until 9.1 kyr BP. During the Holocene, Fe intensities increase distinctly, Ti and K intensities slightly, and Ca and Sr intensities decrease strongly. Consequently, modern Fe, Ca and Sr intensities approach MIS 2 values, whereas Ti and K intensities are lower than their MIS 2 counterparts.

For further analysis, we chose Fe as representative for the group of Alkali and Transition Metals (Fe, Ti, K) and Ca for the Alkaline Earth Metals (Ca, Sr). As the XRF intensities of Fe and Ca are an order of magnitude higher than those of the other analyzed elements, Fe and Ca XRF intensities allow the most reliable analysis of changes in GeoB 2107 sediment composition. Fe (as well as Ti and K) derives from the humid weathering of tropical soils (Blume et al., 2002) and therefore represents the terrestrial (siliciclastic) sediment fraction of GeoB 2107 (Arz et al., 1998). In contrast, Ca (as well as Sr) mainly occurs in foraminiferal shells, pteropods and coccoliths in GeoB 2107. Due to the absence of significant Ca sources in the catchment area of the Rio Itajaí (Schobbenhaus et al., 1995), the terrestrial sediment fraction does not contain significant amounts of Ca.

As Fe represents the terrestrial and Ca the marine source material, the Fe/Ca ratio is suitable for analysing the ratio of terrestrial versus marine sediment input. The Fe/Ca ratio varies between 0.8 and 12.3 ($^{\text{Fe counts}}/_{\text{Ca counts}}$). As it is unlikely that marine productivity varied by a factor of 15, a significant part of the variability in Fe/Ca must be due to changes in the amount of terrestrial sediment input. Therefore, we use Fe/Ca as proxy for the amount of terrestrial sediment input here. This is supported by Ti/Ca ratios from the same archive, which show the same pattern as Fe/Ca ratios and therefore indicate that variations in terrestrial sediment influx govern changes in the sediment composition of GeoB 2107. Furthermore, as terrestrial sediments in GeoB 2107 mainly derive from riverine sediment influx of the Rio Itajaí, Fe/Ca ratios are related to the amount of precipitation in its catchment area (e.g. Arz et al., 1998; Peterson et al., 2000).

At the oldest part of the record (74.0 kyr BP), the Fe/Ca record starts with a Fe/Ca ratio of 5.1, which increases sharply to 11.0 until 70.0 kyr BP. This is followed by minor millennial-scale oscillations until 61.5 kyr BP with minimum Fe/Ca values of 7.6 at 67.2 kyr BP and maximum Fe/Ca values of 12.3 at 67.8 and 62.1 kyr BP. From 62.1 to 38.0 kyr BP, Fe/Ca ratios decrease continuously to 1.7 with minor millennial-scale oscillations. Thereafter, Fe/Ca ratios increase again to 3.5 until 24.9 kyr BP. Relatively stable Fe/Ca ratios with minor millennial-scale oscillations characterize the period from 25 to 18.1 kyr BP. From 18.1 to 12.9 kyr BP, Fe/Ca ratios decrease sharply from 3.6 to 0.8. Fe/Ca values stay at these lowest values recorded in GeoB 2107 until 9.2 kyr BP. Thereafter, they increase continuously to 2.7 at the top of the core (0.8 kyr BP).

4.4.5 Discussion

4.4.5.1 Forcing of changes in South Brazilian precipitation

Forcing mechanisms for South Brazilian precipitation are related to two different atmospheric circulation systems (see section 2.2). Summer precipitation is mainly dependent on the intensity of the SASM and may therefore be modulated by regional insolation and the position of the ITCZ (Zhou and Lau, 1998). Winter precipitation, however, is governed by the northward extent of the southern polar fronts and may therefore be influenced by changes in southern high latitude climate (Vera et al., 2002). Earlier studies demonstrated millennial- to multi-millennial changes in South Brazilian precipitation patterns are dominated by variations in regional insolation (Cruz et al., 2005). This conclusion derives from a stalagmite $\delta^{18}O$ record from the South Brazilian Botuverá Cave, lying approximately 50 km south of the Rio Itajaí's catchment area. This record shows variations coincident with changes in February insolation at 30°S for the last 120 kyr, which are superposed by minor millennial-scale $\delta^{18}O$ shifts coincident with Greenland D/O cycles (Fig. 26; Cruz et al., 2005). These changes in precipitation patterns derive from variations in the relative contribution of summer versus winter rainfall (Cruz et al., 2005). However, they are not necessarily associated with shifts in the amount of precipitation (Cruz et al., 2005).

Other South Brazilian paleoclimate records also provide sparse information about possible changes in precipitation rates during the last glacial. Although there is a compilation of pollen records covering an extensive area in the South Brazilian states of Paraña (Behling, 1997), Santa Catarina (Behling, 1993; Behling, 1995; Behling and Negrelle, 2001) and Rio Grande do Sul (Behling et al., 2004; Roth and Lorscheitter, 1993), none of these records provides sufficient information on the South Brazilian hydrologic regime during the last glacial. The pollen records consistently indicate a widespread dominance of grassland vegetation in South Brazil from the early last glacial to the early Holocene, which is related to low temperatures rather than to low precipitation rates, as cold conditions with repeated frost events and minimum winter temperatures below -10°C did not permit the growth of trees then (e.g. Behling and Lichte, 1997). However, some of these pollen records allow a qualitative evaluation of precipitation changes during the last glacial and indicate relatively wet conditions from 43 to 27 kyr BP and relatively dry conditions during the LGM and the late-glacial period (e.g. Behling et al., 2004). Furthermore, during warmer deglacial and Holocene times the pollen records allow reconstructing changes in South Brazilian precipitation rates. They consistently indicate continuous dry conditions during the deglacial and the early Holocene and wetter conditions towards the late Holocene (e.g. Behling et al., 2004). As the stalagmite $\delta^{18}O$ record of Cruz et al. (2005) indicates a trend towards a higher proportion of

summer precipitation during the Holocene, South Brazilian precipitation rates seem to be related to the relative proportion of summer rainfall during the Holocene. As this is probably dependent on local summer insolation (Cruz et al., 2005), insolation seems to govern South Brazilian precipitation rates during the Holocene.

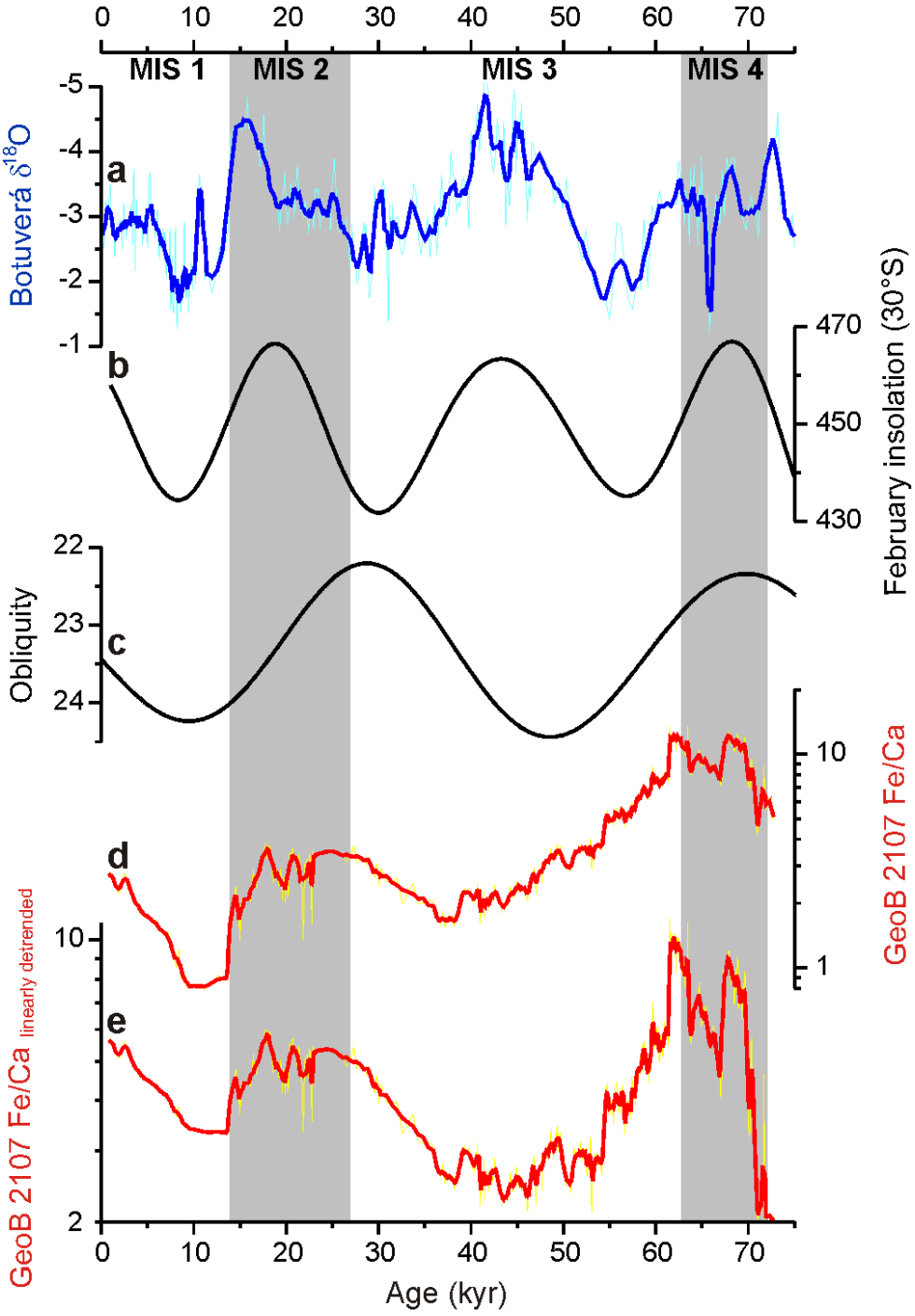

Figure 26: Dominance of orbital-timescale variations in South Brazilian precipitation records **a)** stalagmite $\delta^{18}O$ record from Botuverá Cave (Cruz et al., 2005); **b)** February insolation at 30°S (Berger and Loutre, 1991); **c)** earth's obliquity; **d)** Fe/Ca record from the marine sediment core GeoB 2107 (this study); **e)** linearly detrended Fe/Ca record of GeoB 2107 (linear detrending was performed for correcting GeoB 2107 Fe/Ca for dissolution effects); see Fig. 22 for location of sediment archives

The data presented in this study suggest the linkage between the relative contribution of summer versus winter rainfall and the absolute amount of precipitation is confined to the Holocene and the deglacial. GeoB 2107 Fe/Ca ratios provide a proxy for the amount of precipitation in the Rio Itajaí's catchment area for the Holocene and the last glacial. Like Botuverá stalagmite $\delta^{18}O$ and South Brazilian pollen records, GeoB 2107 Fe/Ca ratios indicate changes in the absolute amount of precipitation coincident with variations in February (summer) insolation at 30°S during the Holocene and the deglacial (Fig. 26). During the last glacial, however, this correlation breaks down. Instead, the Fe/Ca record shows some similarity to the record of earth's obliquity (Fig. 26). This correlation between Fe/Ca ratios and obliquity is present throughout the whole Fe/Ca record (from 0 to 74 kyr BP). Maxima in Fe/Ca ratios thereby lag corresponding peaks in obliquity by 4 to 8 kyr.

These reconstructed changes in South Brazilian precipitation partly agree with those implied by the pollen records, as both pollen and Fe/Ca indicate dry conditions before approximately 40 kyr BP and a wettening towards the early LGM as well as dry deglacial conditions and a wettening throughout the Holocene. In contrast to the pollen records, however, GeoB 2107 Fe/Ca indicates wet conditions during the LGM. This may be an artifact resulting from the global sea level lowstand during the LGM. As large parts of the eastern South American continental shelf were exposed during the LGM, terrigenous sediment input onto the continental slope increased dramatically due to shifting of the river mouths towards the shelf break and reworking of terrigenous matter trapped on the shelf during sea level highstands (Arz et al., 1999). Therefore, GeoB 2107 Fe/Ca may be biased towards higher values during the LGM.

Fe/Ca ratios of GeoB 2107 are probably not only influenced by the amount of terrestrial sediment input. Benthic foraminifers show significant signs of dissolution in the lower part of the core (the parts of the core aged 40 kyr and older). The grade of dissolution thereby increases continuously with depth/age. Dissolution of the calcareous foraminifers decreases the Ca concentration in the core and, consequently, increases Fe/Ca ratios. In order to correct Fe/Ca ratios for this dissolution effect, we subtracted the linear trend in Fe/Ca from the original dataset. Even better than the original Fe/Ca dataset, the corrected Fe/Ca record shows predominant variations on orbital timescales (Fig. 26). The lag between extrema in the filtered Fe/Ca record and the obliquity cycle, however, still constitutes between 4 and 8 kyr.

The direct climate forcing effect of obliquity on low- to mid-latitude regions is rather small (Huybers and Wunsch, 2005). In the high latitudes, however, variations in obliquity may

change the mean annual insolation significantly (Huybers and Wunsch, 2003; Rubincam, 1994; Sachs et al., 2001). The coupling between obliquity and high southern latitude insolation is positive, i.e. an obliquity increase results in increased insolation and vice versa (Gallimore and Kutzbach, 1995). The variations in high southern latitude insolation trigger corresponding changes in high southern latitude temperatures, which, in turn, induce changes in Southern Ocean sea ice volume (Gallimore and Kutzbach, 1995; Khodri et al., 2001). During periods of decreasing insolation, feedback mechanisms between expansion of Southern Ocean sea ice and cooling atmospheric temperatures may help to magnify temperature changes and sea ice expansion (Sachs et al., 2001). Furthermore, feedbacks between Sea ice expansion and Agulhas Current leakage may accentuate the southern high latitude temperature change induced by variations in obliquity (Peeters et al., 2004). Changes in Southern Ocean sea ice volume, in turn, are associated with shifts in the position of the southern hemisphere polar fronts (Gallimore and Kutzbach, 1995). Analogous to the mechanism triggering South Brazilian winter rains in the modern climate system (see section 2.2), a northward shift of the polar fronts may trigger more equatorward incursions of mid- to high-latitude cold air masses. These, in turn, would result in an increase in moisture transport from the Atlantic to the continent, resulting in increased winter precipitation in South Brazil.

Although modern South Brazilian precipitation is dominated by summer precipitation (Fig. 23), GeoB 2107 Fe/Ca ratios indicate obliquity-related variations in winter precipitation may have driven changes in the amount of South Brazilian precipitation during the last glacial. This may be due to different glacial climatic boundary conditions, which probably increased the influence of winter precipitation on the South Brazilian precipitation regime. Glacial South Brazilian winter temperatures regularly were below -10°C (Behling and Lichte, 1997), indicating a massive increase in the influence of mid- to high latitude southern air masses on the atmospheric circulation over South Brazil during the last glacial. This is probably related to the larger extension of circum-Antarctic sea ice during the last glacial (Kunz-Pirrung et al., 2002), which generally shifted the polar fronts northwards. Therefore, changes in sea ice extent driven by variations in obliquity probably had a more pronounced influence on South Brazilian precipitation.

Millennial-scale changes in GeoB 2107 Fe/Ca are an order of magnitude smaller than orbital-scale variations (Fig. 26). For analyzing these small-scale changes, we filtered the original Fe/Ca record with a 1.5-kyr-smooth record of GeoB 2107 Fe/Ca, which accentuates variations with frequencies higher than 3 kyr. This filtered record shows minor non-regular millennial-

scale variations in Fe/Ca, which cannot clearly be related to D/O cycles registered in Greenland ice cores (e.g. Grootes and Stuiver, 1997; data not shown). Therefore, we conclude the absolute amount of precipitation did not change significantly on millennial timescales in South Brazil.

4.4.5.2 Predominance of millennial-scale precipitation changes in tropical Brazil and multi-millennial-scale precipitation shifts in subtropical Brazil

Greenland D/O cycles are accompanied by precipitation changes in Northeast Brazil (Heil et al., submitted-a). These millennial-scale precipitation shifts are the dominant feature of precipitation records there (Arz et al., 1998; Jennerjahn et al., 2004). As shown before, South Brazilian precipitation records are dominated by variations of orbital timescales (Behling et al., 2004; Cruz et al., 2005; this study). D/O cycles, if observable, are subordinate to these multi-millennial precipitation changes (Cruz et al., 2005). In order to confine the region influenced by millennial-scale precipitation shifts, we compare records from along the tropical/subtropical eastern South American coast (Fig. 22, Table 6).

In Fig. 27, we show Fe/Ca and pollen records from marine sediment cores retrieved from off the Northeast Brazilian coast between 4 and 8°S. These records cover the last 70 kyr and indicate significantly increased precipitation during Greenland stadials. These precipitation increases arise from southward shifts of the ITCZ (Arz et al., 1999). These, in turn, are triggered by increased temperature gradients between the high latitude North Atlantic and the tropical Atlantic during Greenland stadials, which mainly arise from lowered high northern latitude temperatures (Heil et al., submitted-a). The increased temperature gradient between the high latitude North Atlantic and the tropical Atlantic results in an increase in northern hemisphere atmospheric circulation intensity (Chiang et al., 2003; Chiang and Bitz, 2005). This includes an increase in Northeast trade wind intensity and a subsequent cooling of the middle and low northern latitudes (Chiang et al., 2003; Chiang and Bitz, 2005). Cooled northern tropics combined with unchanged temperatures in the southern tropics lead to a southward shift of the ITCZ, which changes tropical precipitation patterns accordingly (Chiang et al., 2003; Chiang and Bitz, 2005). Therefore, millennial-scale changes are the dominant feature in precipitation records from Northeast Brazil. Additionally, all Northeast Brazilian records indicate subordinate shifts between wetter glacial and dryer interglacial conditions.

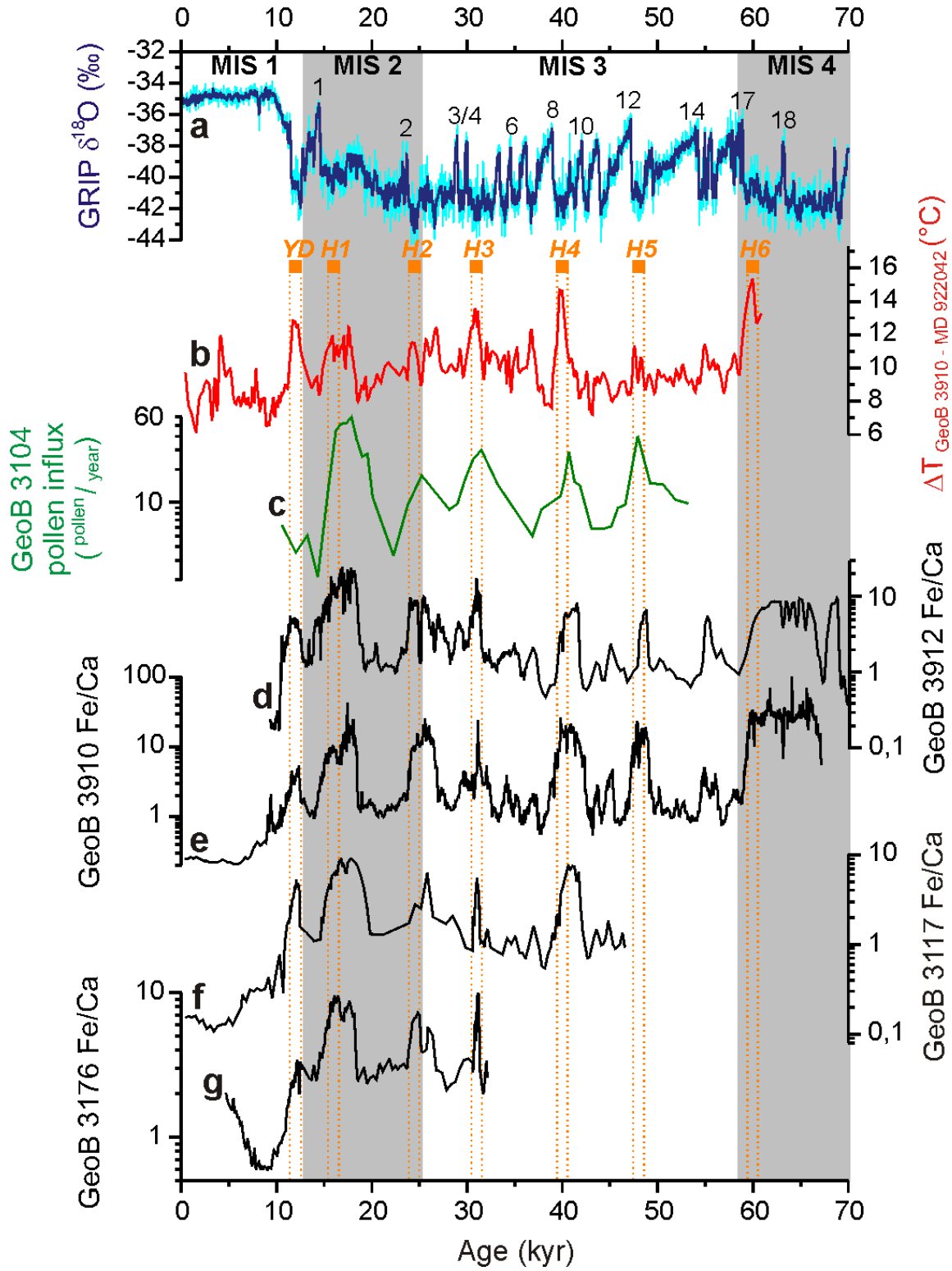

Figure 27: Dominance of millennial-scale precipitation shifts in Northeast Brazil coupled to shifts of the Intertropical Convergence Zone

a) $\delta^{18}O$ record from Greenland ice core GRIP (Grootes and Stuiver, 1997); **b)** temperature gradient between the tropical and the mid-latitude north Atlantic (Heil et al., submitted-a), YD and H1 to H6 denote the Younger Dryas and Heinrich events 1 to 6, respectively; **c)** pollen influx into marine sediment core GeoB 3104 (Behling et al., 2000); **d-g)** Fe/Ca records of western tropical Atlantic marine sediment cores **d)** GeoB 3912 (Heil et al., submitted-b); **e)** GeoB 3910 (Heil et al., submitted-a); **f)** GeoB 3117 (Arz et al., 1999); **g)** GeoB 3176 (Arz et al., 1999); see Fig. 22 for location of GeoB cores

Fig. 29 shows Fe/Ca and pollen records from marine sediment cores retrieved from off the Southeast Brazilian coast at 20 and 22°S. These Fe/Ca records are dominated by multi-millennial variability, indicating Southeast Brazilian precipitation changed primarily on these rather than on millennial timescales between 20 and 22°S. Fe/Ca ratios show some similarity to November insolation at 20°S during the last glacial, indicating the amount of Southeast Brazilian precipitation may primarily be governed by austral summer precipitation on multi-millennial timescales. This agrees with modern Southeast Brazilian climatic conditions, which show maximum precipitation in November and December (Fig. 28). In contrast to the glacial, the Holocene part of the Fe/Ca records does not show any similarity to November insolation. Rather, Holocene Fe/Ca ratios are lower than late glacial ones and show only minor millennial-scale variability. The difference between Holocene and glacial Fe/Ca ratios may be related to sea level variations. During the glacial, large parts of the relatively wide Southeast Brazilian shelf were above sea level, leading to sediment discharge further offshore than during the Holocene. This accounts for increased terrestrial sediment input onto the continental slope and for a higher sensitivity of the sedimentation regime of the continental slope to precipitation variations in Southeast Brazil during the last glacial. As the sediment cores were retrieved from the upper continental slope (water depths of 780 and 1090 m, respectively; Pätzold et al., 1996), this explains the variations in Fe/Ca ratios.

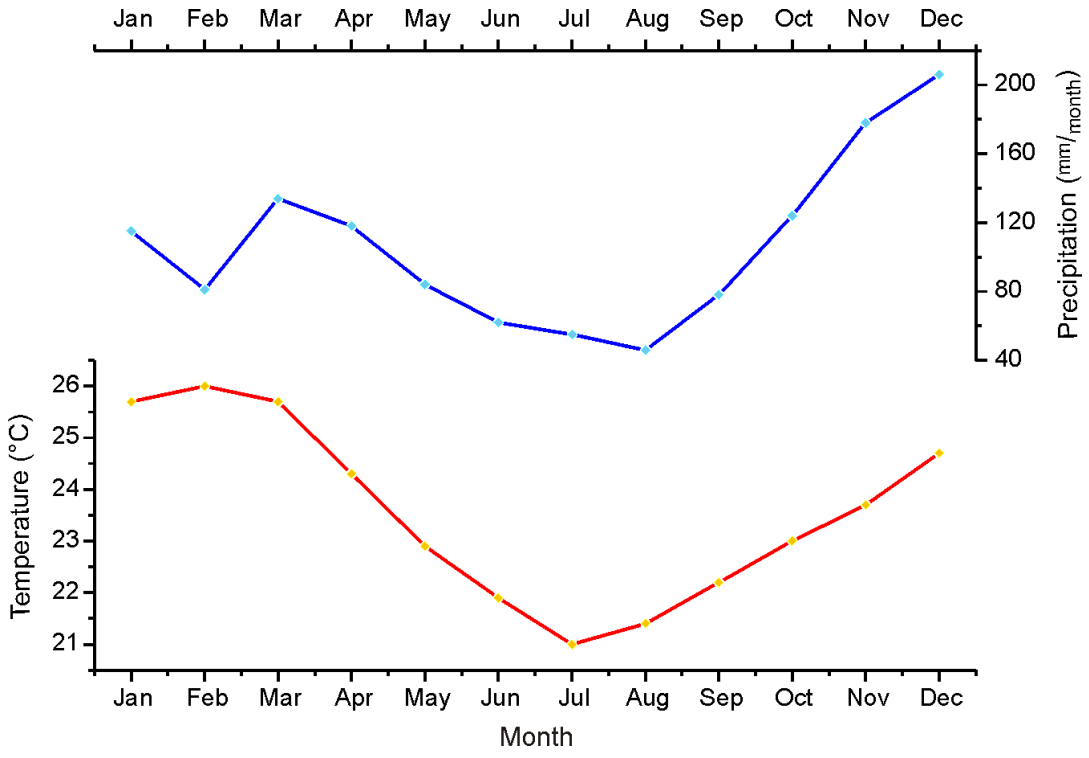

Figure 28: Climate diagram of Vitória (Southeast Brazil). Note the precipitation maximum in November and December.

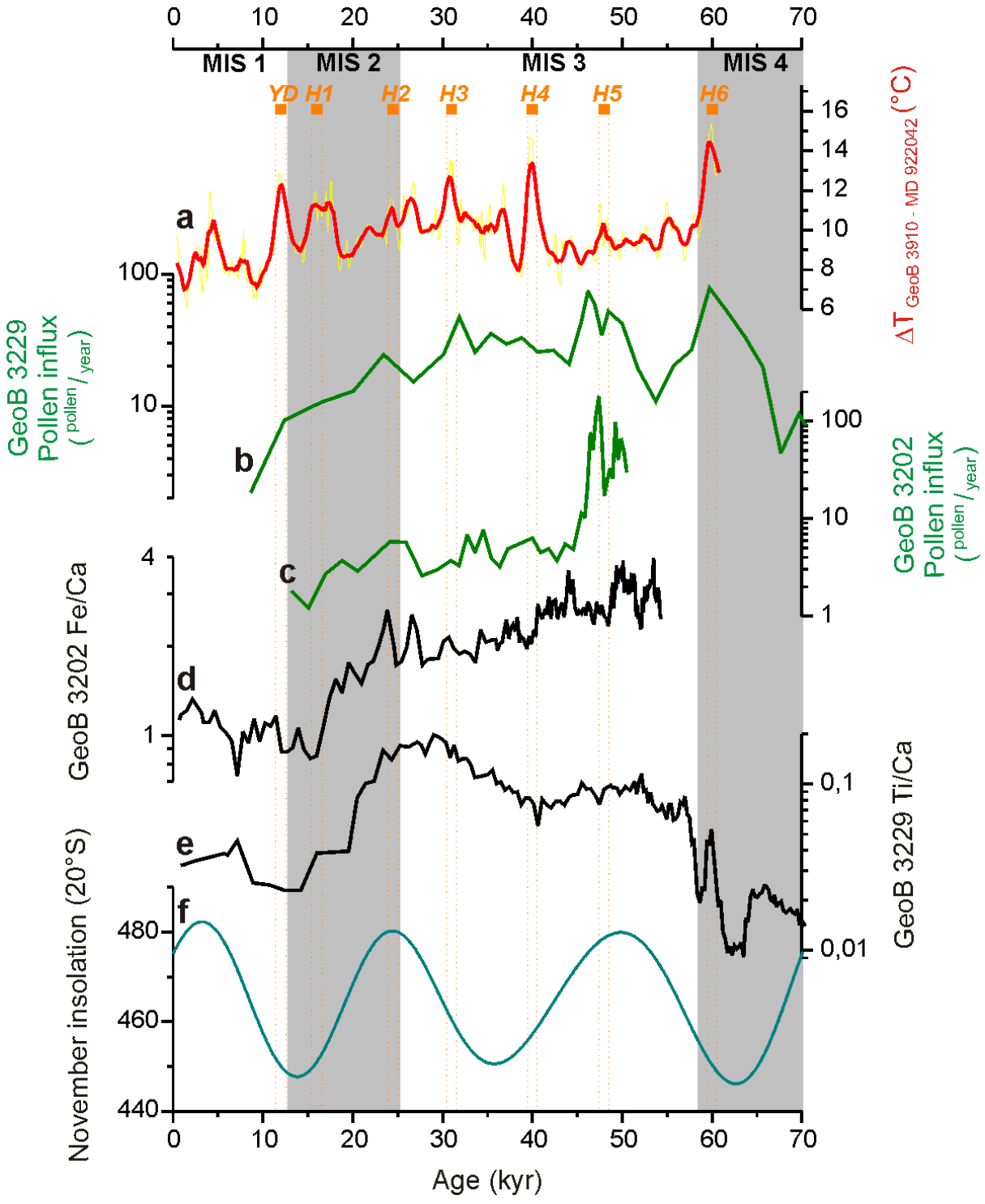

Figure 29: Combined orbital-timescale and millennial-scale precipitation shifts in Southeast Brazil

a) temperature gradient between the tropical and the mid-latitude north Atlantic (Heil et al., submitted-a); **b)** pollen influx into marine sediment core GeoB 3229 (Behling et al., 2002); **c)** pollen influx into marine sediment core GeoB 3202 (Behling et al., 2002); **d)** Fe/Ca records marine sediment core GeoB 3202 (Behling et al., 2002); **e)** Fe/Ca records marine sediment core GeoB 3229 (Behling et al., 2002); **f)** November insolation at 20°S (Berger and Loutre, 1991); see Fig. 22 for location of GeoB cores

Pollen influx records from these sediment cores show a pattern different from that observed in Fe/Ca ratios. On glacial-interglacial timescales, the pollen records primarily indicate relatively cold and dry conditions during the last glacial and relatively warm and humid conditions during the Holocene. This supports our interpretation of glacial-interglacial changes in Fe/Ca ratios to mainly reflect sea level changes. Maximum pollen influx rates occurred during H events, indicating increased Southeast Brazilian precipitation during these events (Behling et al., 2002). This suggests millennial-scale precipitation variability related to ITCZ shifts occurs in Southeast Brazil. However, not all H events show maxima in pollen influx rates. Therefore, we conclude that multi-millennial precipitation changes dominate the Southeast Brazilian climate records, although millennial-scale variability can clearly be detected.

As discussed before, the South Brazilian precipitation records are dominated by changes of orbital timescales. Additionally, they indicate small millennial-scale variations in precipitation patterns (Cruz et al., 2005). Although not directly caused by the ITCZ, these millennial-scale variations are linked to changes in the intensity of the SASM, which, in turn, are related to shifts of the ITCZ (Cruz et al., 2005).

The precipitation records from Northeast, Southeast and South Brazil (Fig. 30) allow assessing the extent of high northern latitude influence on the climate system on millennial timescales. In the Northeast Brazilian precipitation records, millennial-scale changes are the dominant signal. In Southeast Brazil, millennial-scale precipitation shifts still occur, but are dominated by variations of orbital timescales. South Brazilian precipitation records are also dominated by millennial-scale variability and show only small millennial-scale changes. Therefore, we suppose millennial-scale precipitation variability may be confined to the region influenced by the ITCZ and atmospheric systems directly coupled to it (like the SASM) in South America.

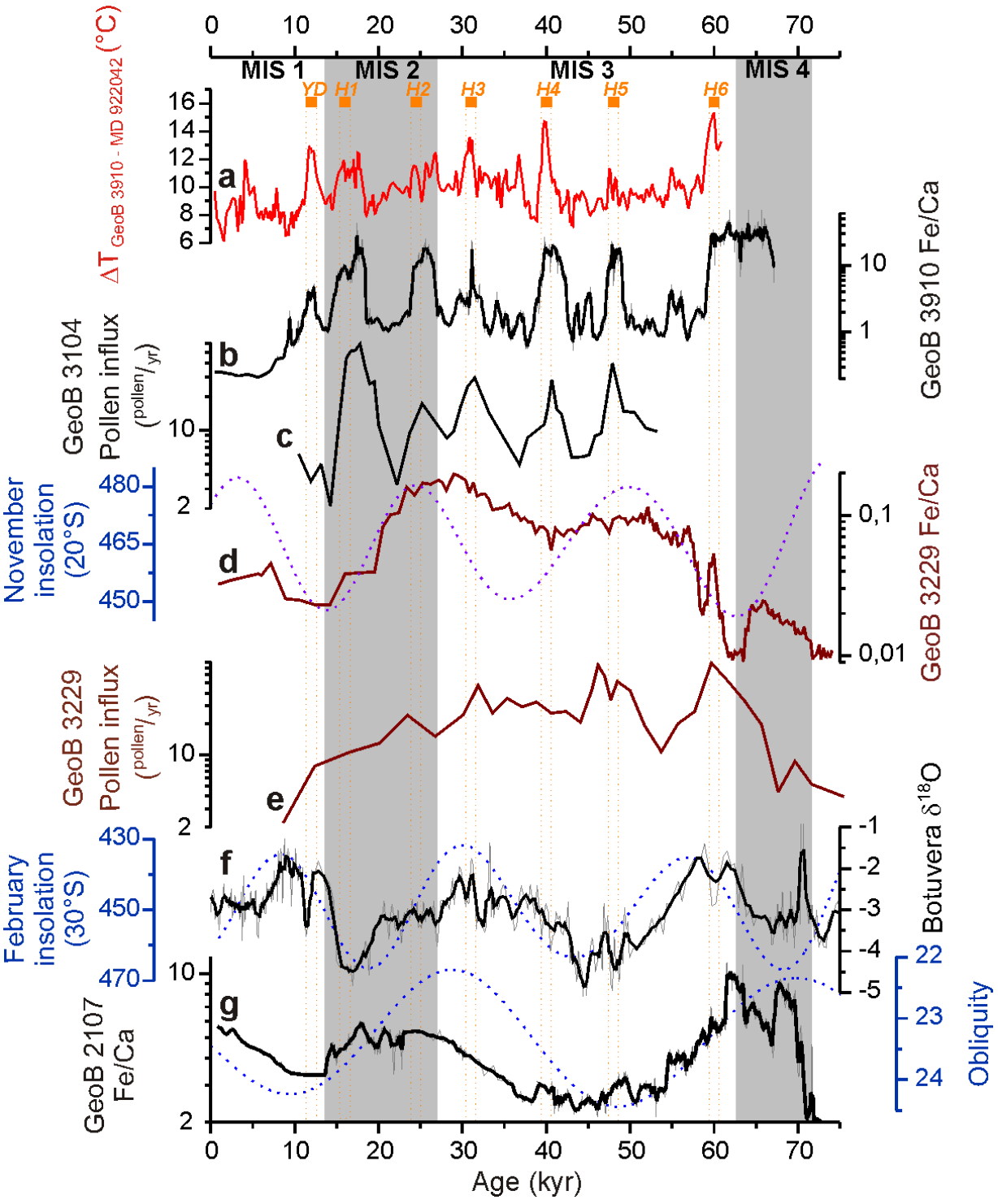

Figure 30: Forcing mechanisms of precipitation changes in tropical to subtropical Brazil

a-c) coincident changes in **a)** the meridional North Atlantic temperature gradient (Heil et al., submitted-a); **b)** Fe/Ca ratios of marine sediment core GeoB 3910; **c)** pollen influx into marine sediment core GeoB 3104 (Behling et al., 2000); **d)** insolation-related variations in Fe/Ca ratios of marine sediment core GeoB 3229 (Behling et al., 2002); **e)** Heinrich event maxima in pollen influx into GeoB 3229 (Behling et al., 2002); **f)** insolation-dominated changes in Botuverá Cave stalagmite $\delta^{18}O$ (Cruz et al., 2005); **g)** obliquity-dominated variations in GeoB 2107 Fe/Ca ratios

4.4.6 Conclusions

South Brazilian precipitation records around 28 to 29°S are governed by variations of orbital timescales. During the Holocene, multi-millennial precipitation changes are related to variations in summer rainfall and are driven by summer insolation at 30°S. During the last glacial, precipitation changes also relate to changes in winter rainfall, which are triggered by variations in earth's obliquity.

In precipitation records from more northern parts of eastern South America, millennial-scale shifts are more dominant. In Northeast Brazil (4 to 8°S), millennial-scale precipitation variability related to ITCZ shifts dominate the precipitation records. In Southeast Brazil (20 to 22 °S), precipitation records are dominated by variations of orbital timescales, but millennial-scale variations still occur.

Our results demonstrate high northern latitude millennial-scale temperature shifts still influence precipitation patterns in eastern South America at 28 to 29°S. However, the resulting precipitation variations are small and not detectable for every D/O cycle. Therefore, this region represents a transition zone between areas clearly affected by high northern latitude millennial-scale temperature shifts (tropical South America) and regions not directly affected by these changes (subtropical South America).

Acknowledgements

We thank Carsten Rühlemann for providing some radiocarbon datings of GeoB 2107 and Rik Tjallingii and Cristiano Chiessi for discussions. This work was generously supported by the Gary Comer Foundation.

4.4.7 References

Arz, H. W., Pätzold, J., and Wefer, G. (1998). Correlated millennial-scale changes in surface hydrography and terrigenous sediment yield inferred from last glacial marine deposits off northeastern Brazil. *Quaternary Research* **50**, 157-166.

Arz, H. W., Pätzold, J., and Wefer, G. (1999). Climatic changes during the last deglaciation recorded in sediment cores from the northeastern Brazilian Continental Margin. *Geo-Marine Letters* **19**, 209-218.

Auler, A. S., Wang, X., Edwards, R. L., Cheng, H., Cristalli, P. S., Smart, P. L., and Richards, D. A. (2004). Quaternary ecological and geomorphic changes associated with rainfall events in presently semi-arid northeastern Brazil. *Journal of Quaternary Science* **19**, 693-701.

Bard, E. (1988). Correction of accelerator mass spectrometry ^{14}C ages measured in planktonic foraminifera: Paleoceanographic implications. *Paleoceanography* **3**, 635-645.

Bard, E. (2002). Abrupt climate changes over millennial time scales: Climate shock. *Physics Today* **55**, 32-38.

Behling, H. (1993). "Untersuchungen zur spätpleistozänen und holozänen Vegetations- und Klimageschichte der tropischen Küstenwälder und der Araukarienwälder in Santa Catarina (Südbrasilien)." *Dissertationes Botanicae* **206**, 149 pp, J. Cramer, Berlin.

Behling, H. (1995). Investigations into the Late Pleistocene and Holocene history of vegetation and climate in Santa Catarina (South Brazil). *Vegetation History and Archaeobotany* **4**, 127-152.

Behling, H. (1997). Late Quaternary vegetation, climate and fire history from the tropical mountain region of Morro de Itapeva, Southeast Brazil. *Palaeogeography, Palaeoclimatology, Palaeoecology* **129**, 407-422.

Behling, H., Arz, H. W., Pätzold, J., and Wefer, G. (2000). Late Quaternary vegetational and climate dynamics in northeastern Brazil, inferences from marine core GeoB 3104-1. *Quaternary Science Reviews* **19**, 981-994.

Behling, H., Arz, H. W., Pätzold, J., and Wefer, G. (2002). Late Quaternary vegetational and climate dynamics in southeastern Brazil, inferences from marine cores GeoB 3229-2 and GeoB 3202-1. *Palaeogeography, Palaeoclimatology, Palaeoecology* **179**, 227-243.

Behling, H., dePatta Pillar, V., Orlóci, L., and Bauermann, S. G. (2004). Late Quaternary Araucaria forest, grassland (Campos), fire and climate dynamics, studied by high-resolution pollen, charcoal and multivariate analysis of the Cambará do Sul core in southern Brazil. *Palaeogeography, Palaeoclimatology, Palaeoecology* **203**, 277-297.

Behling, H., and Lichte, M. (1997). Evidence of dry and cold climatic conditions at glacial times in tropical southeastern Brazil. *Quaternary Research* **48**, 348-358.

Behling, H., and Negrelle, R. R. B. (2001). Tropical rain forest and climate dynamics of the Atlantic Lowland, southern Brazil, during the Late Quaternary. *Quaternary Research* **56**, 383-389.

Berger, A., and Loutre, M. F. (1991). Insolation values for the climate of the last 10 million years. *Quaternary Science Reviews* **10**, 297-317.

Bleil, U., et al. (1993). Report and preliminary results of Meteor Cruise 23/2. *Berichte, Fachbereich Geowissenschaften, Universität Bremen* **76**, 133 pp., Bremen.

Blume, H.-P., Brümmer, G., Schwertmann, U., and Horn, R. (2002). "Scheffer/Schachtschabel: Lehrbuch der Bodenkunde." Spektrum Akademischer Verlag, Heidelberg.

Bond, G. C., Broecker, W. S., Johnsen, S., McManus, J., Labeyrie, L., Jouzel, J., and Bonani, G. (1993). Correlations between climate records from North Atlantic sediments and Greenland ice. *Nature* **365**, 143-147.

Broecker, W. S. (2003). Does the trigger for abrupt climate change reside in the ocean or in the atmosphere? *Science* **300**, 1519-1522.

Broecker, W. S., and Hemming, S. (2001). Climate swings come into focus. *Science* **294**, 2308-2309.

Cacho, I., Grimalt, J. O., Pelejero, C., Canals, M., Sierro, F. J., Flores, J. A., and Shackleton, N. (1999). Dansgaard-Oeschger and Heinrich event imprints in the Alboran Sea paleotemperatures. *Paleoceanography* **14**, 698-705.

Carvalho, L., Jones, C., and Liebmann, B. (2002). Extreme precipitation events in southeastern South America and large-scale convective patterns in the South Atlantic convergence zone. *Journal of Climate* **15**, 2377-2394.

Chiang, J. C. H., Biasutti, M., and Battisti, D. S. (2003). Sensitivity of the Atlantic Intertropical Convergence Zone to Last Glacial Maximum boundary conditions. *Paleoceanography* **18**, doi:10.1029/2003PA000916.

Chiang, J. C. H., and Bitz, C. M. (2005). Influence of high latitude ice cover on the marine Intertropical Convergence Zone. *Climate Dynamics* **25**, 477-496.

Cruz, F. W., Burns, S. J., Karmann, I., Sharp, W. D., Vuille, M., Cardoso, A. O., Ferrari, J. A., Silva Dias, P. L., and Viana, O. (2005). Insolation-driven changes in atmospheric circulation over the past 116,000 years in subtropical Brazil. *Nature* **434**, 63-66.

Dansgaard, W., et al. (1993). Evidence for general instability of past climate from a 250-kyr ice-core record. *Nature* **364**, 218-220.

Fairbanks, R. G., Mortlock, R. A., Chiu, T.-C., Cao, L., Kaplan, A., Guilderson, T. P., Fairbanks, T. W., Bloom, A. L., Grootes, P. M., and Nadeau, M.-J. (2005). Radiocarbon calibration curve spanning 10,000 to 50,000 years BP based on paired $^{230}Th/^{234}U/^{238}U$ and ^{14}C Dates on pristine Corals. *Quaternary Science Reviews* **25**, 1781-1796.

Gallimore, R. G., and Kutzbach, J. E. (1995). Snow cover and sea ice sensitivity to generic changes in Earth's orbital parameters. *Journal of Geophysical Research* **100**, 1103-1120.

Gan, M. A., Kousky, V. E., and Ropelewski, C. F. (2004). The South American monsoon circulation and its relationship to rainfall over West-Central Brazil. *Journal of Climate* **17**, 47-66.

Grootes, P. M., and Stuiver, M. (1997). Oxygen 18/16 variability in Greenland snow and ice with 103- to 105-year time resolution. *Journal of Geophysical Research* **102**, 26,455-26,470.

Hastenrath, S. (1991). "Climate Dynamics of the Tropics." Kluwer, Dordrecht.

Heil, G. M. N., Arz, H. W., deMenocal, P. B., and Wefer, G. (submitted-a). Forcing of tropical South American precipitation during the last 63,000 years. *Nature*.

Heil, G. M. N., Arz, H. W., and Wefer, G. (submitted-b). Last glacial millennial-scale changes in Atlantic thermohaline circulation and Northeast Brazilian precipitation. *Paleoceanography*.

Hendy, I. L., and Kennett, J. P. (1999). Latest Quaternary North Pacific surface-water responses imply atmosphere-driven climate instability. *Geology* **27**, 291-294.

Huybers, P., and Wunsch, C. (2003). Rectification and precession-period signals in the climate system. *Geophysical Research Letters* **30**, doi: 10.1029/2003GL017875.

Huybers, P., and Wunsch, C. (2005). Obliquity pacing of the Late Pleistocene glacial terminations. *Nature* **434**, 491-494.

Imbrie, J., Hays, J. D., Martinson, D. G., McIntyre, A., Mix, A. C., Morley, J. J., Pisias, N. G., Prell, W. L., and Shackleton, N. J. (1984). The orbital theory of pleistocene climate: Support from a revised chronology of the marine $\delta^{18}O$ record. *In "Milankovitch and climate, part I"* (edited by Berger, A.I. et al.), pp. 269-305.

Jennerjahn, T. C., Ittekkot, V., Arz, H. W., Behling, H., Pätzold, J., and Wefer, G. (2004). Asynchronous terrestrial and marine signals of climate change during Heinrich events. *Science* **306**, 2236-2239.

Khodri, M., Leclainche, Y., Ramstein, G., Braconnot, P., Marti, O., and Cortijo, E. (2001). Simulating the amplification of orbital forcing by ocean feedbacks in the last glaciation. *Nature* **410**, 570-574.

Kunz-Pirrung, M., Gersonde, R., and Hodell, D. A. (2002). Mid-Brunhes century-scale diatom sea surface temperature and sea ice records from the Atlantic sector of the Southern Ocean (ODP Leg 177, Sites 1093, 1094 and core PS2089-2). *Palaeogeogr. Palaeoclimatol. Palaeoecol.* **182**, 305-328.

Nimer, E. (1989). "Climatologia do Brasil." IBGE, Rio de Janeiro.

Pätzold, J., et al. (1996). Report and preliminary results of RV Victor Hensen cruise JOPS II, leg 6 Fortaleza - Recife, 13.03. - 26.03.95 and Leg 8 Vitória - Vitória, 10.04. - 23.04.95. *Berichte Fachbereich Geowissenschaften Universität Bremen* **76**, 87 pp., Bremen.

Peeters, F. J. C., Acheson, R., Brummer, G.-J. A., de Ruijter, W. P. M., Schneider, R. R., Ganssen, G. M., Ufkes, E., and Kroon, D. (2004). Vigorous exchange between the Indian and Atlantic oceans at the end of the past five glacial periods. *Nature* **430**, 661-665.

Peterson, L. C., Haug, G. H., Hughen, K. A., and Röhl, U. (2000). Rapid changes in the hydrologic cycle of the tropical Atlantic during the last glacial. *Science* **290**, 1947-1951.

Rachwal, M. F. G., and Curcio, G. R. (1994). Principais tipos de solos do Estado do Paraná, suas características e distribuição na paisagem. *In A vegetação natural do estado do Paraná*. Instituto Paranense de Desenvolvimento Econômico e Social, 20 pp., Curitiba.

Reid, J. L. (1989). On the total geostrophic circulation of the South Atlantic Ocean: flow patterns, tracers, and transports. *Progr. Oceanogr.* **23**, 149-244.

Röhl, U., and Abrams, L. J. (2000). High-resolution, downhole, and nondestructive core measurements from sites 999 and 1001 in the Caribbean Sea: Application to the Late Paleocene Thermal Maximum. *In "Proceedings of the Ocean Drilling Program, scientific results **165**"* (edited by R. M. Leckie, H. Sigurdsson, G. D. Acton, and G. Draper), pp. 191-203.

Roth, L., and Lorscheitter, M. L. (1993). "Palynology of a bog in Parque Nacional de Aparados da Serra, East Plateau of Rio Grande do Sul, Brazil." A.A. Balkema, Brookfield.

Rubincam, D. (1994). Insolation in terms of earth's orbital parameters. *Theoretical and applied climatology* **48**, 195-202.

Sachs, J. P., Anderson, R. F., and Lehman, S. J. (2001). Glacial surface temperatures of the Southeast Atlantic Ocean. *Science* **294**, 2077-2079.

Schobbenhaus, C., de Almeida Campos, D., Derze, G. R., and Asmus, H. E. (1995). Mapa geológico do Brasil. Serviço Geológico do Brasil, Rio de Janeiro.

Schulz, H., von Rad, U., and Erlenkeuser, H. (1998). Correlation between Arabian Sea and Greenland climate oscillations of the past 110,000 years. *Nature* **393**, 54-57.

Vera, C. S., Vigliarolo, P. K., and Berbery, E. H. (2002). Cold season synoptic-scale waves over subtropical South America. *Mon. Weath. Rev.* **130**, 684–699.

Viana, A. R., Faugères, J. C., Kowsmann, R. O., Lima, J. A. M., Caddah, L. F. G., and Rizzo, J. G. (1998). Hydrology, morphology and sedimentology of the Campos continental margin, offshore Brazil. *Sedimentary Geology* **115**, 133-157.

Wang, X., Auler, A. S., Edwards, R. L., Cheng, H., Cristalli, P. S., Smart, P. L., Richards, D. A., and Shen, C.-C. (2004). Wet periods in northeastern Brazil over the past 210 kyr linked to distant climate anomalies. *Nature* **432**, 740-743.

Wang, Y. J., Cheng, H., Edwards, R. L., An, Z. S., Wu, J. Y., Shen, C.-C., and Dorale, J. A. (2001). A high-resolution absolute-dated Late Pleistocene monsoon record from Hulu Cave, China. *Science* **294**, 2345-2348.

Weninger, B., Danzeglocke, U., and Jöris, O. (2005). Comparison of dating results achieved using different radiocarbon-age calibration curves and data.

Xavier, A. G., Martinez, M. B., and Lima, J. A. M. (1993). Analise preliminar de dados de corrente de fundo na Bacia de Campos. Petrobras/Cenpes/Diprex, *Internal Report Sepron 016/93*, Rio de Janeiro, 17 pp.

Xie, P., and Arkin, P. A. (1997). Global precipitation: A 17-year monthly analysis based on gauge observations, satellite estimates, and numerical model outputs. *Bull. Amer. Meteor. Soc.* **78**, 2539-2558.

Zhou, J., and Lau, K. M. (1998). Does a monsoon climate exist over South America? *Journal of Climate* **11**, 1020-1040.

5 Discussion

Paleoprecipitation records from tropical South America providing millennial-scale resolution consistently indicate tropical South American precipitation patterns primarily depend on the position of the ITCZ on millennial timescales (Manuscript 1 and 2). The ITCZ position is coupled to the meridional temperature gradient in the North Atlantic on millennial timescales, which, in turn, is largely defined by temperatures in the high northern latitudes (Manuscript 1). During Greenland stadials, pronounced high northern latitude cooling increased the meridional temperature gradient in the North Atlantic, which induced an intensification of the northern hemisphere atmospheric circulation and subsequently cooled the northern middle to low latitudes (Chiang and Bitz, 2005). Due to cooler northern tropics, the ITCZ shifted southward and changed the tropical atmospheric circulation, leading to dryer conditions in the northern tropics and wetter ones in the southern tropics. During interstadials, the North Atlantic meridional temperature gradient was similar to the modern one. Therefore, it supported a similar northern ITCZ position like in the modern climate system and correspondingly caused wet conditions in the northern tropics and relatively dry conditions in the southern tropics.

The dependency of tropical precipitation patterns on the North Atlantic meridional temperature gradient is contrasting to observations of the modern climate system. Like during the last glacial, modern tropical South American precipitation patterns are largely governed by the position of the ITCZ (Hastenrath and Heller, 1977; see Chapter 2.2.3). This, however, depends on the temperatures in the tropics themselves and the temperature contrast between the northern and southern tropics in the modern climate system (Hastenrath, 1990). The repeated significant southward shifts of the ITCZ during periods of an increased North Atlantic meridional temperature gradient are unique to the last glacial. This is probably due to the different amplitudes of variations in this temperature gradient during the Holocene and the last glacial. During the last glacial, the huge high northern latitude temperature shifts associated with Dansgaard/Oeschger cycles (Bard, 2002; Bond et al., 1993; Grootes and Stuiver, 1997) triggered large changes in this temperature gradient (Manuscript 1). During the Holocene, however, high northern latitude temperature variations were much smaller than during the last glacial (Bond et al., 1997). Consequently, the amplitude of changes in the North Atlantic's meridional temperature gradient also was much smaller in the Holocene. The resulting shifts in the position of the ITCZ were not large enough to cause significant variations in Northeast Brazilian precipitation during the Holocene. However, recent high-resolution analyses of terrestrial sediment influx into the Cariaco Basin indicate such

millennial-scale precipitation variations occurred in Venezuela during the late Holocene, although they were much less pronounced than during the last glacial (Haug et al., 2003). Furthermore, model studies of Chiang and Bitz (2005) also suggest minor variations in the temperature gradient between the high northern latitudes and the tropics may cause shifts in the position of the ITCZ. Therefore, millennial-scale ITCZ shifts complementary to those from the last Glacial probably occurred during the Holocene, but were more limited in spatial extent.

As high latitude North Atlantic SST largely define the North Atlantic meridional temperature gradient and this, in turn, governs tropical precipitation patterns, there is a close coupling between tropical precipitation patterns and North Atlantic SST on millennial timescales. Furthermore, as North Atlantic SST are closely linked to variations in the oceanic THC (e.g. Keigwin and Jones, 1994), changes in tropical precipitation patterns are also related to reorganisations of the oceanic THC (Manuscript 2). This study provides a reconstruction of changes in deep tropical Atlantic conditions, which is based on the same archive (sediment core GeoB 3910) as the tropical Atlantic SST record and one of the Northeast Brazilian precipitation records presented in this study (Manuscript 2). The changes in deep tropical Atlantic conditions indicate variations in NADW production intensity which coincide with temperature variations observed in the GRIP ice core from central Greenland. Therefore, the record of deep tropical Atlantic conditions provides an excellent independent validation of the stratigraphy of sediment core GeoB 3910 with respect to GRIP. As changes in Greenland temperatures are closely coupled to variations in North Atlantic SST (e.g. Bond et al., 1993), this allows to stratigraphically validate the coupling of tropical South American precipitation patterns to high latitude North Atlantic SST.

The various South American precipitation records reported in this study allow investigating the spatial extent of ITCZ shifts during the last glacial. A terrigenous sediment influx record from the Southeast Caribbean Cariaco Basin e.g. suggests significant precipitation changes caused by shifts in the position of the ITCZ occurred in Venezuela during Dansgaard/Oeschger cycles (Peterson et al., 2000). Venezuelan precipitation rates were high during Greenland interstadials and low during stadials. This study (Manuscript 1 and 2) provides a high-resolution reanalysis of terrigenous sediment influx records from the western tropical Atlantic (Arz et al., 1998, 1999) which indicates coastal Northeast Brazilian precipitation patterns also varied during Dansgaard/Oeschger cycles. In contrast to Venezuelan precipitation rates, however, Northeast Brazilian precipitation rates were high during Greenland stadials and low during interstadials as Northeast Brazil is situated at the

southern border of the modern ITCZ. Further south, a stalagmite dating record from central Northeast Brazil indicates precipitation changes during H events and the YD only (Wang et al., 2004). Furthermore, high-resolution ice core and lake sediment records from the Bolivian and Peruvian Andes also suggests precipitation changes associated with ITCZ southward shifts during H events and the YD only (Baker et al., 2001a, 2001b; Thompson et al., 1995, 1998).

As Venezuela and coastal Northeast Brazil are situated directly at the modern (and probably interstadial) border of the ITCZ, small shifts in the position of the ITCZ are sufficient to cause variations in precipitation patterns there. However, the North Atlantic meridional temperature gradient was not high enough during Dansgaard/Oeschger cycles to induce changes in precipitation patterns in the Bolivian to Peruvian Andes and central Northeast Brazil (Fig. 31). As these regions are not located directly at the modern (and probably interstadial) border of the ITCZ, a significant ITCZ southward shift is needed to induce a precipitation increase there. This only occurred during H events, when extreme cooling of the high northern latitudes strongly increased the North Atlantic meridional temperature gradient, which ultimately caused a significant southward shift of the ITCZ associated with precipitation increases in these regions (Fig. 31, Manuscript 1 and 2).

The impact of high northern latitude cooling during Dansgaard/Oeschger stadials and H event stadials on tropical precipitation patterns does not only differ by the spatial extent, as suggested by Broecker and Hemming (2001), but also by the amplitude of precipitation changes. Northeast Brazilian and Venezuelan precipitation records indicate precipitation changes during both Dansgaard/Oeschger cycles and H events, but these changes are an order of magnitude larger during H events. This is due to the dynamic coupling of the ITCZ to the North Atlantic meridional temperature gradient, which was much larger during H events than during other stadials. Therefore, the spatial extent of ITCZ shifts and the amplitude of corresponding precipitation changes are coupled to each other (Manuscript 2).

Precipitation records from subtropical South America suggest precipitation patterns of these regions still changed on millennial timescales due to ITCZ shifts. However, the ITCZ is not the dominant factor governing precipitation rates in these regions. Subtropical South American precipitation records rather show variations of orbital frequency, which points to precipitation forcing mechanisms originating in the southern hemisphere subtropical to polar regions (Manuscript 3).

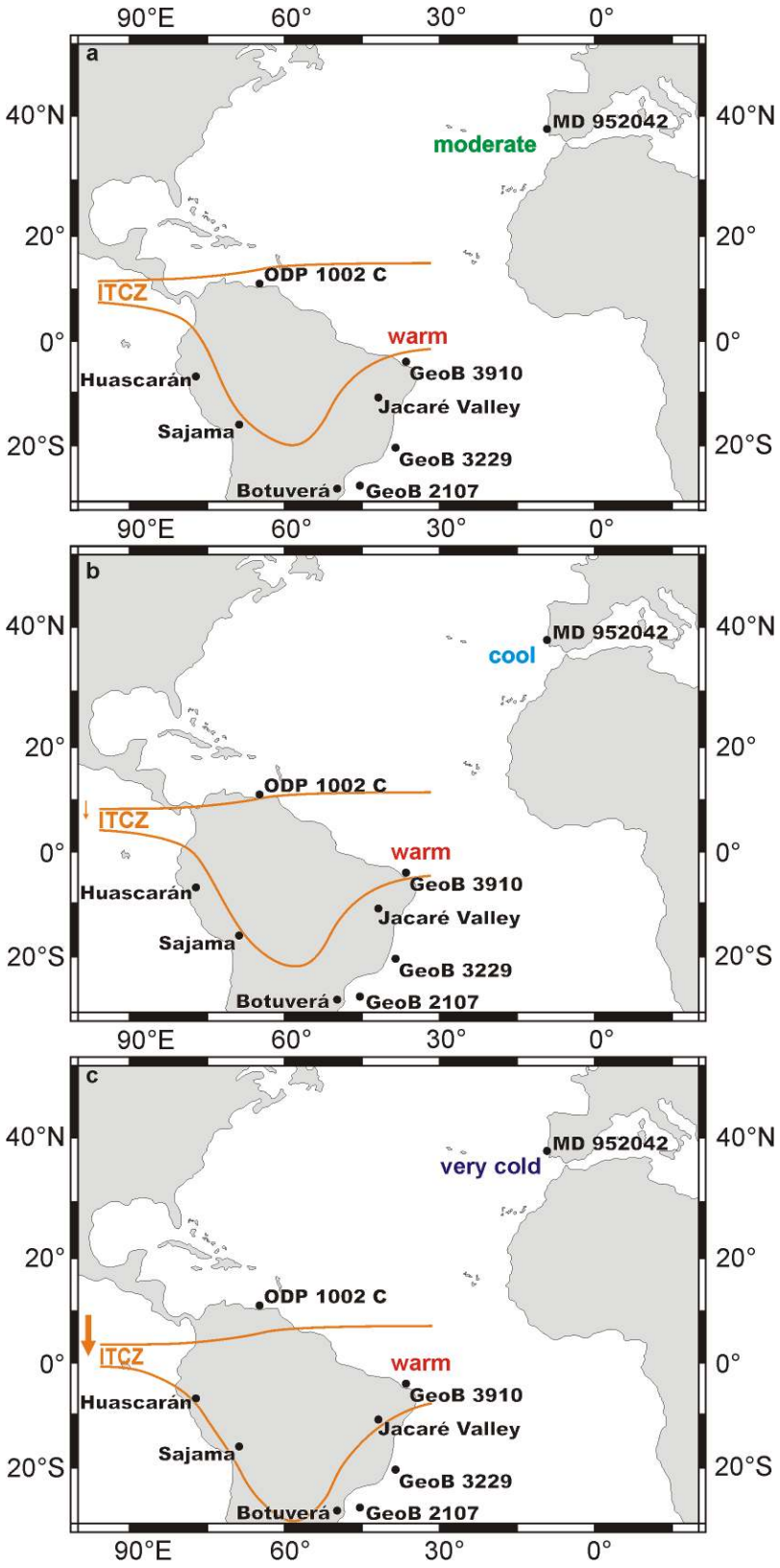

Figure 31: Setting of the ITCZ in South America in **a)** the modern climate system and implied ITCZ shifts during **b)** Dansgaard/Oeschger stadials and **c)** Heinrich events

Black dots with labels represent South American precipitation archives mentioned in the text and temperature records from sediment cores off Portugal (MD 952042; Bard, 2002) and Northeast Brazil (GeoB 3910, this study), which were used to calculate the Atlantic meridional temperature gradient typical of **a)** the modern climate, **b)** Dansgaard/Oeschger stadials and **c)** Heinrich events

A stalagmite oxygen isotope record from South Brazil indicates precipitation pattern changes which are coincident with variations in regional (subtropical) February insolation (Cruz et al., 2005). This record also suggests subordinate variations in precipitation patterns coincident with H events, the YD and some other Dansgaard/Oeschger cycles. These millennial-scale precipitation pattern shifts arose from changes in the proportion of local summer versus winter rainfall which were probably driven by ITCZ shifts (Cruz et al., 2005). However, they do not indicate variations in the total amount of precipitation (Cruz et al., 2005). This study provides a terrigenous sediment influx record from the western subtropical Atlantic which indicates changes in the total amount of precipitation also primarily occurred on orbital timescales in South Brazil (Manuscript 3). However, it does not indicate any significant millennial-scale variations in precipitation that might relate to ITCZ shifts. In contrast to the insolation-driven precipitation pattern changes derived from the stalagmite oxygen isotope record, this terrigenous sediment influx record suggests shifts in South Brazilian precipitation patterns coincide with variations in earth's obliquity. The direct influence of changes in obliquity on the tropical to subtropical climate system is clearly subordinate to the influence of variations in tropical to subtropical insolation (Huybers and Wunsch, 2005). In the high southern latitudes, however, shifts in obliquity may cause prominent changes in Southern ocean sea ice extent through feedback mechanisms between southern high latitude temperatures and sea ice extent (Khodri et al., 2001; Rubincam, 1994; Sachs et al., 2001). These variations in sea ice extent are associated with shifts in the position of the southern polar fronts (Gallimore and Kutzbach, 1995). As the northward shift of the polar fronts during austral winter triggers abundant winter precipitation in South Brazil in the modern climate system, variations in the position of the southern polar fronts on orbital timescales probably also induce changes in South Brazilian precipitation patterns (Fig. 32). This provides a mechanism for coupling variations in earth's obliquity to changes in South Brazilian precipitation.

This study cannot provide a final explanation for the discrepancy between the implications for changes in precipitation patterns on orbital timescales derived from the stalagmite oxygen isotope record (Cruz et al., 2005) and the terrigenous sediment influx record (GeoB 2107; Manuscript 3). Whereas the oxygen isotope record indicates the proportion of summer versus winter rainfall primarily varied with regional summer insolation, changes in the total amount of precipitation, as derived from the terrigenous sediment influx record, coincide with shifts in earth's obliquity. It is not likely that changes in the total amount of South Brazilian precipitation are not related to variations in the proportion of summer versus winter rainfall.

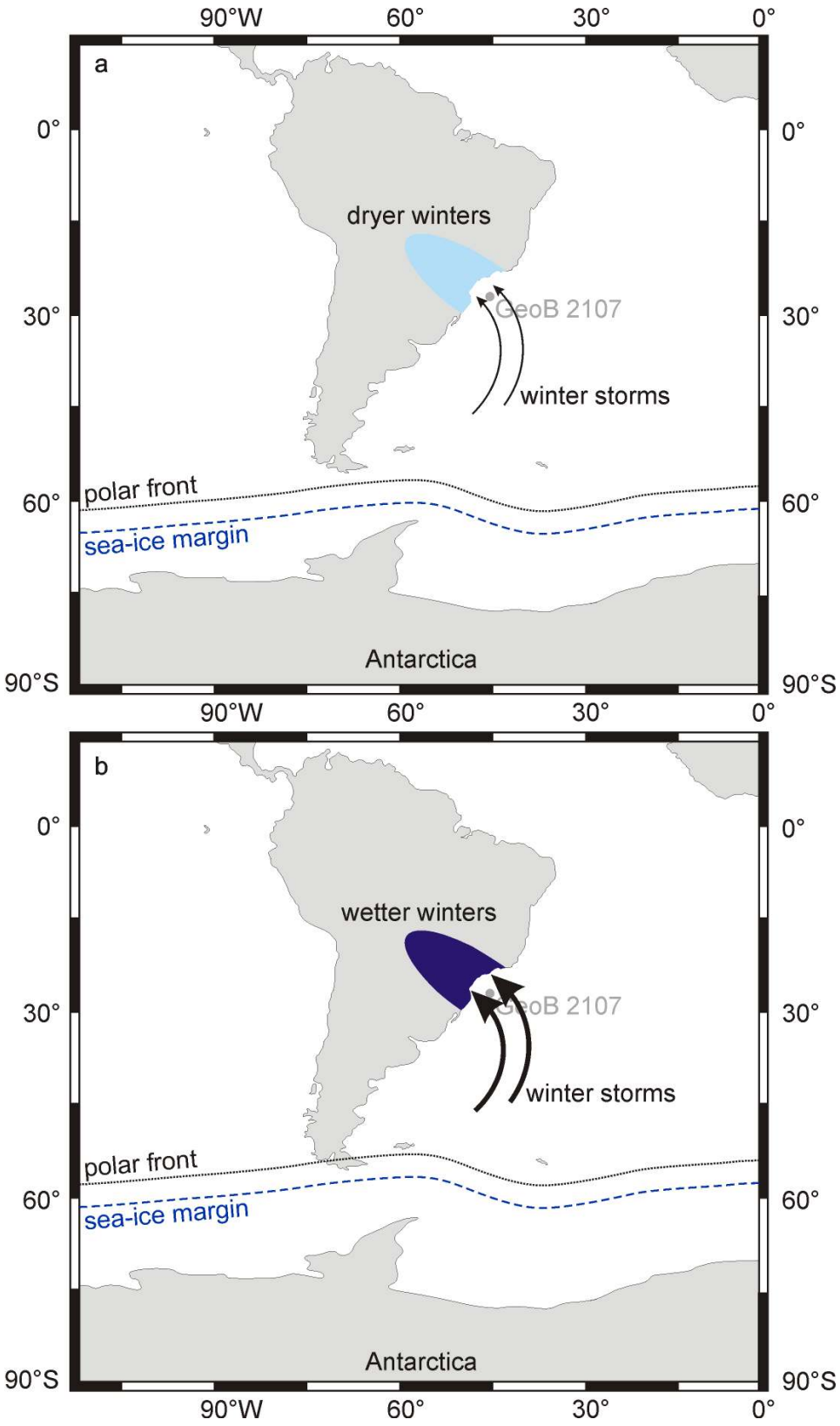

Figure 32: Generalized description of the influence of circum-Antarctic winter sea ice extent on associated South Brazilian winter precipitation rates during periods of **a)** high obliquity and **b)** low obliquity

Note the northward shift of the circum-Antarctic sea ice margin (blue dashed line) and the associated polar front (black dotted line) during periods of low obliquity and the associated increase in western subtropical South Atlantic winter storm intensity (marked by the thicker arrows) and South Brazilian precipitation rates (marked by the dark blue shaded area).

However, we suppose changes in winter precipitation might have a bigger impact on erosion rates in South Brazil than variations in summer precipitation, because lower vegetation cover might support higher erosion rates during winter. Therefore, the terrigenous sediment influx record from the subtropical western South Atlantic might be biased towards winter precipitation. Although this does not allow evaluating whether South Brazilian precipitation patterns primarily changed coincidently with variations in regional insolation or earth's obliquity, both the stalagmite oxygen isotope and the terrigenous sediment influx record indicate millennial-scale variations in precipitation patterns are clearly subordinate to those on orbital timescales.

5.1 References Chapter 5

Arz, H. W., Pätzold, J., and Wefer, G. (1998). Correlated millennial-scale changes in surface hydrography and terrigenous sediment yield inferred from last-glacial marine deposits off northeastern Brazil. *Quaternary Research* **50**, 157-166.

Arz, H. W., Pätzold, J., and Wefer, G. (1999). Climatic changes during the last deglaciation recorded in sediment cores from the northeastern Brazilian continental margin. *Geo-Marine Letters* **19**, 209-218.

Baker, P. A., Rigsby, C. A., Seltzer, G. O., Fritz, S. C., Lowenstein, T. K., Bacher, N. P., and Veliz, C. (2001a). Tropical climate changes at millennial and orbital timescales on the Bolivian Altiplano. *Nature* **409**, 698-701.

Baker, P. A., Seltzer, G. O., Fritz, S. C., Dunbar, R. B., Grove, M. J., Tapia, P. M., Cross, S. L., Rowe, H. D., and Broda, J. P. (2001b). The history of South American tropical precipitation for the past 25,000 years. *Science* **291**, 640-643.

Bard, E. (2002). Abrupt climate changes over millennial timescales: Climate shock. *Physics Today* **55**, 32-38.

Bond, G., Showers, W., Cheseby, M., Lotti, R., Almasi, P., deMenocal, P., Priore, P., Cullen, H., Hajdas, I., and Bonani, G. (1997). A pervasive millennial-scale cycle in North Atlantic Holocene and glacial climates. *Science* **278**, 1257-1266.

Bond, G. C., Broecker, W. S., Johnsen, S., McManus, J., Labeyrie, L., Jouzel, J., and Bonani, G. (1993). Correlations between climate records from North Atlantic sediments and Greenland ice. *Nature* **365**, 143-147.

Broecker, W. S., and Hemming, S. (2001). Climate swings come into focus. *Science* **294**, 2308 - 2309.

Chiang, J. C. H., and Bitz, C. M. (2005). Influence of high latitude ice cover on the marine Intertropical Convergence Zone. *Climate Dynamics* **25**, 477-496.

Cruz, F. W., Burns, S. J., Karmann, I., Sharp, W. D., Vuille, M., Cardoso, A. O., Ferrari, J. A., Silva Dias, P. L., and Viana, O. (2005). Insolation-driven changes in atmospheric circulation over the past 116,000 years in subtropical Brazil. *Nature* **434**, 63-66.

Gallimore, R. G., and Kutzbach, J. E. (1995). Snow cover and sea ice sensitivity to generic changes in Earth's orbital parameters. *Journal of Geophysical Research* **100**, 1103–1120.

Grootes, P. M., and Stuiver, M. (1997). Oxygen 18/16 variability in Greenland snow and ice with 103- to 105-year time resolution. *Journal of Geophysical Research* **102**, 26455-26470.

Hastenrath, S. (1990). Prediction of Northeast Brazil rainfall anomalies. *Journal of Climate* **3**, 893-904.

Hastenrath, S., and Heller, L. (1977). Dynamics of climatic hazards in Northeast Brazil. *Quarterly Journal of the Royal Meteorological Society* **103**, 77-92.

Huybers, P., and Wunsch, C. (2005). Obliquity pacing of the Late Pleistocene glacial terminations. *Nature* **434**, 491-494.

Keigwin, L. D., and Jones, G. A. (1994). Western North Atlantic evidence for millennial-scale changes in ocean circulation and climate. *Journal of Geophysical Research* **99**, 12397-12410.

Khodri, M., Leclainche, Y., Ramstein, G., Braconnot, P., Marti, O., and Cortijo, E. (2001). Simulating the amplification of orbital forcing by ocean feedbacks in the last glaciation. *Nature* **410**, 570-574.

Peterson, L. C., Haug, G. H., Hughen, K. A., Röhl, Ursula. (2000). Rapid changes in the hydrologic cycle of the tropical Atlantic during the last glacial. *Science* **290**, 1947-1951.

Rubincam, D. (1994). Insolation in terms of Earth's orbital parameters. *Theoretical and applied climatology* **48**, 195-202.

Sachs, J. P., Anderson, R. F., and Lehman, S. J. (2001). Glacial surface temperatures of the Southeast Atlantic Ocean. *Science* **294**, 2077-2079.

Thompson, L. G. et al. (1998). A 25,000-year tropical climate history from Bolivian ice cores. *Science* **282**, 1858-1864.

Thompson, L. G., Mosley-Thompson, E., Davis, M. E., Lin, P.-N., Henderson, K. A., Cole-Dai, J., Bolzan, J. F., and Liu, K.-B. (1995). Late glacial stage and Holocene tropical ice core records from Huascarán, Peru. *Science* **269**, 46-50.

Wang, X., Auler, A. S., Edwards, R. L., Cheng, H., Cristalli, P. S., Smart, P. L., Richards, D. A., and Shen, C.-C. (2004). Wet periods in northeastern Brazil over the past 210 kyr linked to distant climate anomalies. *Nature* **432**, 740-743.

6 Conclusions and Outlook

6.1 Conclusions

This thesis provides new insight into the dynamics of tropical South American precipitation. It presents new records of millennial- to multi-millennial-scale changes in Northeast and South Brazilian precipitation patterns and evaluates corresponding variations in precipitation indicated by proxy records from other sites in tropical South America. Furthermore, it analyses which mechanisms are responsible for these precipitation pattern changes. The main results of this thesis can be summarised as follows:

- Tropical precipitation patterns varied during H events and Dansgaard/Oeschger cycles. These changes in precipitation patterns were triggered by shifts of the ITCZ. The position of the ITCZ, in turn, is governed by the meridional temperature gradient in the North Atlantic. This is contrasting to seasonal to interannual variations of the ITCZ position in the modern climate system, which are largely governed by tropical Atlantic SST.
- The spatial extent of ITCZ shifts is dynamically dependent on the magnitude of changes in the North Atlantic's meridional temperature gradient. Correspondingly, a small change in this gradient results in a small shift of the ITCZ, whereas a large change causes significant ITCZ shifts. This study provides evidence for ITCZ shifts during the H events and Dansgaard/Oeschger cycles of the last glacial. Additionally, a high-resolution record of Holocene precipitation changes in North Venezuela indicates corresponding ITCZ shifts on decadal to multi-millennial timescales (Haug et al., 2001). Combined with the results of this thesis, the study of Haug et al. (2001) suggests a high sensitivity of tropical precipitation patterns to also small changes in the North Atlantic's meridional temperature gradient.
- The semiquantitative NADW production intensity record agrees with earlier findings of coincident changes in high northern latitude temperatures and NADW production intensity (e.g. Curry and Oppo, 2005). In addition, it provides a better resolution during MIS 3 than other existing deep ocean circulation records and proves that all high northern latitude Dansgaard/Oeschger temperature cycles are associated with shifts in NADW production. This study shows there furthermore is a close coupling of changes in tropical precipitation patterns to reorganisations of the oceanic THC via North Atlantic SST. Therefore, the NADW production intensity record provides an excellent stratigraphic validation of the coincidence of tropical precipitation pattern changes and both variations in North Atlantic SST and, consequently, the North Atlantic's meridional temperature gradient.

- The influence of ITCZ shifts on regional precipitation patterns diminishes from the tropics towards the southern subtropics. Subtropical South Brazilian precipitation patterns still show changes probably related to ITCZ shifts, but these are clearly subordinate to variations of orbital frequency. Changes in regional insolation and earth's obliquity seem to be the dominant forcing factors of variations in South Brazilian precipitation rather than ITCZ shifts.
- Whereas there is a direct coupling of regional summer insolation to South Brazilian summer precipitation (e.g. Curry and Oppo, 2005), changes in obliquity do not have the potential to alter subtropical precipitation rates directly (e.g. Huybers and Wunsch, 2005). This study demonstrates variations in obliquity nevertheless may influence southern hemisphere subtropical precipitation patterns by altering circum-Antarctic sea ice extent and, correspondingly, triggering changes in the influx of polar to mid-latitude cold air masses to the subtropics. As these cold air masses meet warm tropical ones in South Brazil and correspondingly trigger abundant precipitation, this provides a mechanism for coupling variations in earth's obliquity and South Brazilian precipitation.

6.2 Outlook

This study provides the first multi-archive analysis of the spatial extent of millennial-scale ITCZ shifts and associated precipitation pattern changes in tropical South America. Furthermore, it demonstrates the position of the ITCZ is dynamically dependent on the North Atlantic's meridional temperature gradient. Thereby, it provides the basis for further research on the dependency of tropical precipitation patterns to high northern latitude temperature changes. This includes the following research fields:

- Whereas variations in the hydroclimatic conditions of the Northeast (4 to 8°S), Southeast (20 to 22°S) and South Brazilian region (around 28°S) allow a general assessment of the spatial extent of millennial-scale ITCZ shifts in eastern South America, filling the large gaps between these records with new precipitation records would allow to investigate the spatial extent of these ITCZ shifts in more detail. In a first endeavour, it might be important to generate more records between 8°S and 20°S, as this might allow to better confine the southern margin of the area in northeastern Brazil that is dominated by millennial-scale variations in precipitation. This might allow a better quantitative analysis of the dependency of the spatial extent of ITCZ shifts on the magnitude of changes in the North Atlantic's meridional temperature gradient.

- The precipitation records generated in this study will be combined with further tropical South American precipitation records which partly are still in process. This joint study will focus on the extent of ITCZ shifts during the last deglacial and the Holocene and includes stalagmite oxygen isotope records from central Southeast Brazil (Xianfeng Wang, University of Minnesota) and the Peruvian Andes (Martin van Breukelen, Vrije Universiteit Amsterdam) and lake level records from Northeast Brazil (Abdelfettah Sifeddine, Institut de recherche pour le développement, Paris).
- The finding of the dynamic dependency of the ITCZ position on the North Atlantic's meridional temperature gradient will provide a new component for models which calculate the effect of variations in North Atlantic deep water production or anthropogenically induced high northern latitude warming on tropical precipitation patterns (e.g. Barnett and Pennell, 2004; Lohmann, 2003). This may be especially valuable for downscaling the results of these models, which may help to better assess regional future changes in tropical precipitation patterns.

Besides precipitation proxy records, many foraminiferal isotope records, which provide information on changes in western South Atlantic upper and deep ocean conditions related to THC reorganisations, have been generated during this study. These isotope records are mainly based on the sediment cores GeoB 3910 and 2107 and have only partly been included into this thesis. The remaining datasets open up the following research fields, which partly would require the analysis of additional datasets:

- In the western tropical Atlantic, centennial-scale resolution stable isotope records of the foraminiferal species *G. ruber*, *Globorotalia truncatulinoides (G. trunca.)* and *C. wuell.* have been generated based on sediment core GeoB 3910. These records cover the last 63 kyr and are representative for surface ocean, thermocline and deep ocean conditions of the western tropical Atlantic, respectively. Combined, the *G. ruber* and *G. trunca.* records allow analysing variations in the grade of mixing or stratification in the upper western tropical Atlantic (surface ocean to thermocline), which may be associated with THC reorganisations. Furthermore, *C. wuell.* stable isotope records from GeoB 3910 (2362 m bsl) and nearby sediment core GeoB 3912 (772 m bsl) may be combined to analyse variations in the depth level of the AAIW/NADW mixing zone during the last glacial. The record of GeoB 3912, however, only covers the time frame from 31 to 44 kyr BP yet and would have to be extended (GeoB 3912 offers material from the last 80 kyrs).

- In a joint study with Alex Piotrowski (University of Cambridge), GeoB 3910 is now analysed for Nd isotopes (δ^{144}Nd), a recently established proxy for deep ocean circulation (e.g. Piotrowski et al., 2005). Whereas leads of δ^{144}Nd to benthic foraminiferal δ^{13}C suggest that changes in the global carbon cycle preceded THC reorganisations at glacial/interglacial boundarys, the relationship between the carbon cycle and the THC is rather unclear for Dansgaard/Oeschger cycles (Piotrowski et al., 2005). As GeoB 3910 provides one of the most highly resolved deep ocean circulation records during MIS 3, it represents an ideal archive for analysing the relationship between millennial-scale changes in the carbon cycle and reorganisations of the THC.

- In the western subtropical Atlantic, centennial-resolution stable isotope records of the foraminiferal species *G. ruber, G. trunca.* and *U. peregr.* were generated based on GeoB 2107. Analogous to GeoB 3910, these records allow investigating rates of mixing or stratification in the upper ocean and evaluating changes in deep ocean conditions of the western subtropical Atlantic.

- The *C. wuell.* record of GeoB 2107 (1048 m bsl) can be combined with to-be-generated benthic foraminiferal isotope records of the nearby sediment cores GeoB 2104 (1503 m bsl), 2106 (497 m bsl) and 2109 (3011 m bsl), which provide a depth profile along the continental slope off eastern South Brazil. For future analysis of these sediment cores, preliminary stratigraphies based on correlating XRF Fe/Ca ratios of these cores to XRF Fe/Ca ratios of GeoB 2107 were established for GeoB 2104 and 2106. These preliminary stratigraphies suggest that these cores cover at least the last 60 kyrs. Therefore, a combination of these benthic foraminiferal isotope records would provide a powerful tool for analysing changes in intermediate to deep ocean conditions in the western subtropical Atlantic during the last glacial.

- The SST record of GeoB 3910 was combined with the *G. ruber* oxygen isotope record to calculate Sea Surface Salinities (SSS) of the western tropical Atlantic during the last 63 kyrs. Combined, the SST and SSS records indicate that THC reorganisations during H events and the YD were associated with large variations in NBC intensity. As the NBC provides the main heat and salt flux from the South Atlantic to the North Atlantic, variations in NBC intensity may alter the potential of deep water formation in the high latitude North Atlantic. To investigate the effect of tropical SST and SSS changes on the THC, the SST and SSS analyses of GeoB 3910 will be combined with other tropical Atlantic SST and SSS records in a joint international study with Peter deMenocal (Lamont-

Doherty Earth Observatory, New York), David Lea (University of California, Santa Barbara), Matthew Schmidt (Georgia Institute of Technology, Atlanta) and Howard Spero (University of California, Davis). Aim of this study is to map changes in tropical surface ocean currents during H events and the YD in detail and to investigate the potential of these ocean circulation changes for triggering or amplifying THC reorganisations.

- Analogous to GeoB 3910, SST and SSS records were produced and calculated for the western subtropical Atlantic based on GeoB 2107. This record covers the last 30 kyrs yet and will be extended to the base of GeoB 2107 (74 kyr BP). These records will be combined and used to assess changes in heat export from the South Atlantic to the North Atlantic during the last glacial. First results seem to prove that GeoB 3910 SST and SSS reflect changes in NBC intensity and the associated heat export to the North Atlantic.

6.3 References Chapter 6

Barnett, T.P., and Pennell, W. (2004). Impact of global warming on western US water supplies. *Climate Change* **62** (spec. Vol.).

Curry, W. B., and Oppo, D. W. (2005). Glacial water mass geometry and the distribution of $\delta^{13}C$ of ΣCO_2 in the western Atlantic Ocean. *Paleoceanography* **20**, doi:10.1029/2004PA001021.

Haug, G. H., Hughen, K. A., Sigman, D. M., Peterson, L. C., and Röhl, U. (2001). Southward migration of the Intertropical Convergence Zone through the Holocene. *Science* **293**, 1304-1308.

Huybers, P., and Wunsch, C. (2005). Obliquity pacing of the Late Pleistocene glacial terminations. *Nature* **434**, 491-494.

Lohmann, G. (2003). Atmospheric and oceanic freshwater transport during weak Atlantic overturning circulation. *Tellus* **A 55**, 438-449.

Piotrowski, A. M., Goldstein, S. L., Hemming, S. R., and Fairbanks, R. G. (2005). Temporal relationships of carbon cycling and ocean circulation at glacial boundaries. *Science* **307**, 1933-1938.